

Spring 1987

Groin-Associated Rip Currents Measured Using a New Digital Current Meter

Dennis L. Lundberg
Old Dominion University

Follow this and additional works at: https://digitalcommons.odu.edu/oeas_etds



Part of the [Oceanography Commons](#)

Recommended Citation

Lundberg, Dennis L.. "Groin-Associated Rip Currents Measured Using a New Digital Current Meter" (1987).
Doctor of Philosophy (PhD), Dissertation, Ocean & Earth Sciences, Old Dominion University, DOI:
10.25777/362r-7k58
https://digitalcommons.odu.edu/oeas_etds/144

This Dissertation is brought to you for free and open access by the Ocean & Earth Sciences at ODU Digital Commons. It has been accepted for inclusion in OES Theses and Dissertations by an authorized administrator of ODU Digital Commons. For more information, please contact digitalcommons@odu.edu.

GROIN-ASSOCIATED RIP CURRENTS
MEASURED USING A NEW
DIGITAL CURRENT METER

by

Dennis L. Lundberg
B.S. December 1972 The University of Michigan

A Dissertation Submitted to the Faculty of
Old Dominion University in Partial Fulfillment
of the Requirements
for the Degree of

DOCTOR OF PHILOSOPHY
OCEANOGRAPHY

OLD DOMINION UNIVERSITY
April, 1987

Approved by:

J. C. Ludwick (Director)

/ ~~A. F. Denell~~ \

~~C. E. Grosch~~ //

G. R. Whittier

**Copyright by Dennis L. Lundberg 1987
All Rights Reserved**

ABSTRACT

GROIN-ASSOCIATED RIP CURRENTS MEASURED USING A NEW DIGITAL CURRENT METER

Dennis L. Lundberg
Old Dominion University, 1987
Director: Dr. John C. Ludwick

Rip currents have often been noted in physical model studies of groins and their effectiveness. Nevertheless, detailed field investigations of rip currents along a groin wall have not been heretofore conducted. A new digital current meter system was designed and built to study the groin-associated rip currents in a test groin compartment at Willoughby Spit, Norfolk, VA. Six ducted impeller current meters are controlled by a data acquisition system that utilizes an onboard microprocessor and solid state memory. The new system provides high quality data on horizontal water velocities associated with wave action. The velocities stored are time mean velocities averaged over one second. The system will make possible future studies of three dimensional flow in the nearshore and coastal zones at relatively low cost.

The present study verified the existence of a groin-associated rip current in the test compartment. Measured vertical velocity profiles showed that the near bottom time mean flow was often directed onshore while the time mean flow in the upper levels was nearly always directed offshore. The presence of the rip current reduces groin effectiveness by transporting sediment from the compartment seawards beyond the groin ends. The complex vertical structure of the time mean flow makes the use of depth-averaged velocities to estimate sediment transport in a groin compartment ques-

tionable. The flow intensity for both the near bottom flow and the upper flow was directly proportional to the wave breaker height and reflects the low wave energy input to this estuarine beach site. Eddies that rotate clockwise were observed at the upstream groin wall relative to the tidal current. The action of these eddies may contribute significantly to sediment scour near the groin ends.

Dedicated to my wife, Jane

ACKNOWLEDGEMENTS

Over the years, I have received the support and encouragement from many friends and faculty within the Oceanography Department.

I am deeply grateful to Dr. John C. Ludwick, my dissertation advisor. Over the years and through many long discussions, he has taught me to be a better scientist. But, his influence extended beyond the realm of science. My association with him has also made me a better and wiser person.

I am indebted to Drs. George F. Oertel and G. Richard Whittecar for their critiques of the manuscript. Dr. Chester E. Grosch taught me much about data and spectral analysis.

A special thanks to the ODU Science Shop. The help of Thurmond Gardner, Bobby Powell, and Bob Kizear was invaluable. They were cheerful in their assistance and always offered encouragement.

Dr. Ron Johnson was always there with a word of encouragement and his friendship. Dr. Don Johnson helped in the early phases of the instrumentation and offered many helpful suggestions.

There were many of my fellow students who assisted in the field work. They are Chris Krahforst, David Velinsky, Mark Byrnes, and Kathy Gingerich. My warmest thanks and appreciation go to Hyo Jin Kang and Neville Reynolds who spent many long hours in the field during each of the four experiments. Their assistance

and friendship will be treasured.

The members of the Naval Oceanographic Reserve Activity 2186 helped in the shakedown field experiment. They have also provided friendship and encouragement throughout my doctoral work.

Finally, and most importantly, I want to thank my wife, Jane. There are not words to express the importance of her love, support, and encouragement during this long endeavor. This work is dedicated to her.

PREFACE

A two-fold research project was conducted, first to design and construct a data acquisition system that would monitor and control up to six ducted impeller current meters. The data acquisition system utilized a microprocessor and solid state memory for data storage, and second to employ the new and unique system to study the wave and current dynamics of a groin system and determine the nature and structure of the seaward directed return flow from a groin compartment. In so doing, a field evaluation of the system was also accomplished.

Part I of this dissertation deals with the development of the data acquisition system and the calibration of the current meters. Part II concerns the the field experiments and the analysis of that data.

TABLE OF CONTENTS

	Page
LIST OF TABLES	vii
LIST OF FIGURES	viii
PART I	
Chapter	
1. INTRODUCTION	1
DESIGN REQUIREMENTS	2
2. DESIGN	7
MECHANICAL DESIGN	7
ELECTRONIC DESIGN	11
MICROPROCESSOR BOARD	19
PROGRAMMING FOR THE FIELD SYSTEM	21
DATA AQUISITION TO COMPUTER INTERFACING	30
3. CALIBRATION FACILITY	33
MECANICAL DESIGN AND CONSTRUCTION	33
CALIBRATION FACILITY ELECTRONICS	36
4. CALIBRATION METHOD	39
PENDULUM MOTION	39
GAIN AND PHASE LAG	42
COSINE RESPONSE	51
5. SUMMARY AND CONCLUSIONS	55
REFERENCES	58

PART II

1. INTRODUCTION	60
RECENT WORK AT WILLOUGHBY SPIT	60
PREVIOUS GROIN STUDIES	62
PHYSICAL SETTING	67
PURPOSE OF STUDY	68
2. EXPERIMENTAL PROCEDURES	71
FIELD PROCEDURES	71
ANALYTICAL PROCEDURES	72
2. RESULTS	75
SHAKE DOWN EXPERIMENT	75
EXPERIMENT I	76
EXPERIMENT II	78
EXPERIMENT III	81
EXPERIMENT IV	87
DATA SUMMARY	96
4. DISCUSSION	98
RIP CURRENT ALONG THE GROIN WALL	98
WAVE-CURRENT INTERACTIONS	109
TIDAL EFFECTS	122
5. SUMMARY AND CONCLUSIONS	126
REFERENCES	129
APPENDICES	
A. DETAILED CIRCUIT DIAGRAMS	132
B. SELECTED PROGRAMS	147

LIST OF TABLES

Table	Page
Part I	
I. Summary of the Gain and Threshold Values of Each Current Meter for the Forward and Reverse Directions.....	50
Part II	
I. Data Summary for Experiment I, 23 May, 1986	77
II. Data Summary for Experiment II, 17 June, 1986.....	79
III. Data Summary for Experiment III, 19 June, 1986	82
IV. Data Summary for Experiment IV, 27 June, 1986.....	88

LIST OF FIGURES

Figure		Page
Part I		
1. Schematic of the Ducted Impeller Current Meters.....		8
2. Timing Diagram of an Event.....		14
3. Timing Diagram to Illustrate Problem if There is No Time Overlap Between Channel A and B.....		15
4a. Flow Chart of the Main Program of the Data Acquisition System.....		25
4b. Flow Chart of the Data Read Subroutine.....		26
4c. Flow Chart of the 1 Sec. Averaging Subroutine.....		28
4d. Flow Chart of the Data Transfer Subroutine		29
5. Schematic of the Calibration Tank and Cradle.....		35
6. Pendulum Arm Used in the Calibration Facility		41
7. Ideal Time Series of $\Theta(t)$, $\theta(t)$, and $u(t)$		43
8. Example of the Raw Pendulum Data Plotted Against the Fitted Curve for the Pendulum Motion		44
9. Example of the Raw Data Output from a Current Meter		45
10. Calibration Curve of the Gain for Current Meter 1, Run A.....		47
11. Calibration Curve of the Gain for Current Meter 2, Run A.....		48

12. Calibration Curve of the Gain for Current Meter 3, run A.....	49
13. Pooled Time Lag Data for All Current Meters ans All Runs	52
14. Cosine Response of the Current Meters Plotted Against the Ideal Cosine Response	54

Part II

1. Geographic Location of the Study Area	61
2. Location of the Terminal Spit	63
3. Diagram of the Test Compartment Showing the Approximate Location of the Current Meter Array.....	69
4. Diagram of the General Location of the Eddies and the Current Meter Array	84
5. Velocity Data for Run 38 Showing the Velocities Associated with the Eddy.....	85
6. Velocity Data from Run 39	86
7. Velocity Data from Run 46 Current Meter 1	90
8. Velocity Data from Run 46 Current Meter 2.....	91
9. Velocity Data from Run 46 Current Meter 3	92
10. Velocity Data from Run 56 Current Meter 1.....	93
11. Velocity Data from Run 56 Current Meter 2.....	94
12. Velocity Data from Run 56 Current Meter 3.....	95

13. Diagram of the Rip Current Generated as a Result of Mass Transport into the Compartment.....	99
14. Velocity Profiles of the Mass Transport Due to Waves for a Stokes Wave (a) and for Longuet-Higgins (1953) (b).....	101
15. Diagram of the Rip Current Generated by Wave Diffraction Around the Groin End.....	107
16. Velocity Data for the Bottom Meter (CM 1), Run 50	112
17. Velocity Data for the Top Meter (CM 3), Run 50	113
18. Energy Spectrum for Bottom Meter (CM 1), Run 50	114
19. Energy Spectrum for Top Meter (CM 3), Run 50	115
20. Velocity Data for the Bottom Meter (CM 1), Run 25	116
21. Velocity Data for the Mid Depth Meter (CM 3), Run 25	117
22. Energy Spectrum for Bottom Meter (CM 1), Run 25	118
23. Energy Spectrum for the Mid Depth Meter (CM 3), Run 25	119
24a. Diagram of the Current Gyre during the Flood Current.....	123
24b. Diagram of the Current Gyre that forms during the Ebb Current.....	124

CHAPTER 1

INTRODUCTION

The purpose of Part I of this dissertation is to describe the development of the data acquisition system and the calibration of the ducted impeller current meters used in this study. Current meters of this type have been used by a number of investigators to measure currents in the nearshore and coastal environments (Meadows, 1977; Smith, 1978; Sonu, 1973; Bradshaw et al, 1978; Wood, 1970). The measured phenomena ranged from turbulence (Smith, 1978) to wave orbital velocities (Meadows, 1977; Bradshaw et al, 1978) to quasi-steady currents such as shore-normal and shore-parallel currents generated by waves and tides (Meadows, 1977).

The most common method of acquiring data from these meters is to convert a pulse repetition frequency from the meter to an analog voltage which is then converted to digital data by an analog to digital converter (ADC) for storage on magnetic tape. The pulses from the meter are often generated by magnets attached to the impeller blades which rotate past a Hall effect switch where the direction of rotation is determined by which pole of the magnet first passes the sensor.

Another method utilized by Meadows is to measure the elapsed time of rotation of the impeller between a pair of optical sensors, the direction of rotation determined by which sensor is first shaded. The method employed by Meadows is used in this

study. The data acquisition system developed in this study used complementary metal oxide semiconductor (CMOS) solid state digital electronics to measure this elapsed time for up to six current meters simultaneously. A microprocessor monitored and controlled the system with the resultant data stored onboard in solid state memory.

1.1. DESIGN REQUIREMENTS

The design requirements for the proposed data acquisition system can be summarized as follows:

1. Low cost.
2. Rugged construction for deployment in the nearshore coastal environment.
3. Ease of deployment/retrieval.
4. A frequency response that would allow measurement of wave orbital velocities.
5. A flexible, easily upgraded data acquisition system.
6. Easily interfaced to a computer(s) for data transfer.
7. Able to monitor, control, and record several

sensors simultaneously.

8. Adequate internal data storage.

9. Low power consumption

There were several options considered to meet the above requirements. One was the procurement of electromagnetic (EM) current meters. They are rugged and have been successfully used in numerous studies. They are, however, very costly particularly when several are to be deployed.

Another option is consideration of the acoustic doppler current meter. Unfortunately, the physical size of these meters make them unsuitable for shallow water studies. Also, they are relatively expensive.

Many investigators have chosen mechanical devices such as the ducted impeller current meter. These are rather simple devices that are easy to construct at reasonable cost and are quite sturdy. Such a device meets the first three requirements given above. Most meters of this type generally use either mechanical devices or magnetic sensors to sense the rotation of the impeller. The output of these methods is typically a series of electrical pulses. The pulse repetition frequency can be converted to an analog voltage which can then be sampled using an analog to digital converter (ADC) or the pulses can be counted over some sampling interval, say 10 seconds. The output is then converted into current speed. The particular design used herein and described in more detail later, uses an optical device to sense the rotation of the impeller. The design for the current meters used in this

study was graciously provided by Dr. Guy A. Meadows of the University of Michigan.

With the type of current meter fixed, but before a data acquisition system was selected, an evaluation of how to use the output from the meters was needed. Most systems employ some variation on counting the output pulses from the current meters over some sampling interval. In so doing, the minimum error is plus or minus one count. If rotation is very slow, then it would be possible to have only two or three pulses in the sampling interval. If the count is off by one, then the possible error is 33% to 50%. The more pulses in the sampling interval, (i.e., faster rotation), the smaller the error. An alternate method compatible with Meadows' design is to measure the time it takes for the impeller to rotate between the two sensors. The count could still be off by one but percent error is now a function of the clock frequency as well as the speed of rotation. For example, if the clock frequency is 1000 Hz and the event is 10 milliseconds, then there would be 10 counts and the error would be 10% to 11%. If one wants to further reduce the error, then the clock frequency can be increased. In this scheme the greatest possible error in an event occurs when there are fewer counts i.e., greater velocities. However, if one is averaging over some interval, then error is reduced because there are more events in the sampling interval and the counting error is averaged out. The later sampling scheme is used in the present design.

Given the type of current meter and sampling scheme, an appropriate data acquisition system was needed. Initially, an InterOcean model 696 data logger was

evaluated. The logger has an eight channel ADC that stores sampled data on cassette tape. The fastest sampling rate is one sample per channel per 0.5 sec when recording on up to four channels and is 1 sec. when recording on eight channels. Each current meter uses two channels, therefore, four meters could potentially be utilized with this data logger. However, each current meter channel has an output of several pulses per second. The data logger, sampling each channel once per second, clearly is inadequate to record the data from the current meters. Additionally, commercially available data loggers were neither satisfactory nor affordable.

Another possible method was to record the output from the meters on a strip chart recorder and manually extract the data and enter it into a computer. However, several recorders would be required to record data from six current meters, each with two channels. Not only would this add to the cost of the system, but it would increase the logistical problems of the field study. The data extraction and entry would also be a time consuming and laborous task. Therefore, this method was rejected.

The above requirements, and the limitations and cost of commercially available devices, prompted a decision to design a new system that would be compatible with the output from the current meters, could be easily interfaced with any computer, and that would be sufficiently flexible to allow it to be upgraded as needed or to record data from other types of sensors. To meet these goals, the logical choice would be a system that incorporated a microprocessor. This would ease

the problem of computer interfacing, but, more importantly, it gives one effectively unlimited flexibility by changing the programming of the microprocessor. A RCA CDP1802 microprocessor along with its associated design and development support systems was used to develop a compatible system. The CDP1802 microprocessor uses complementary metal-oxide semiconductor circuitry. This is a logic family that has a very low power consumption and can operate over a wide range of voltages (3V to 18V) as opposed to transistor to transistor logic (TTL) used in most microcomputers which requires a regulated 5V power supply and consumes a great deal more power than does CMOS. The wide range of supply voltage relieves one of the requirement of a regulated power supply. This allows the potential of developing a battery operated system in the future that would permit extended deployments without shore connections. Because of these advantages, the data acquisition system is designed entirely of CMOS logic.

CHAPTER 2

DESIGN

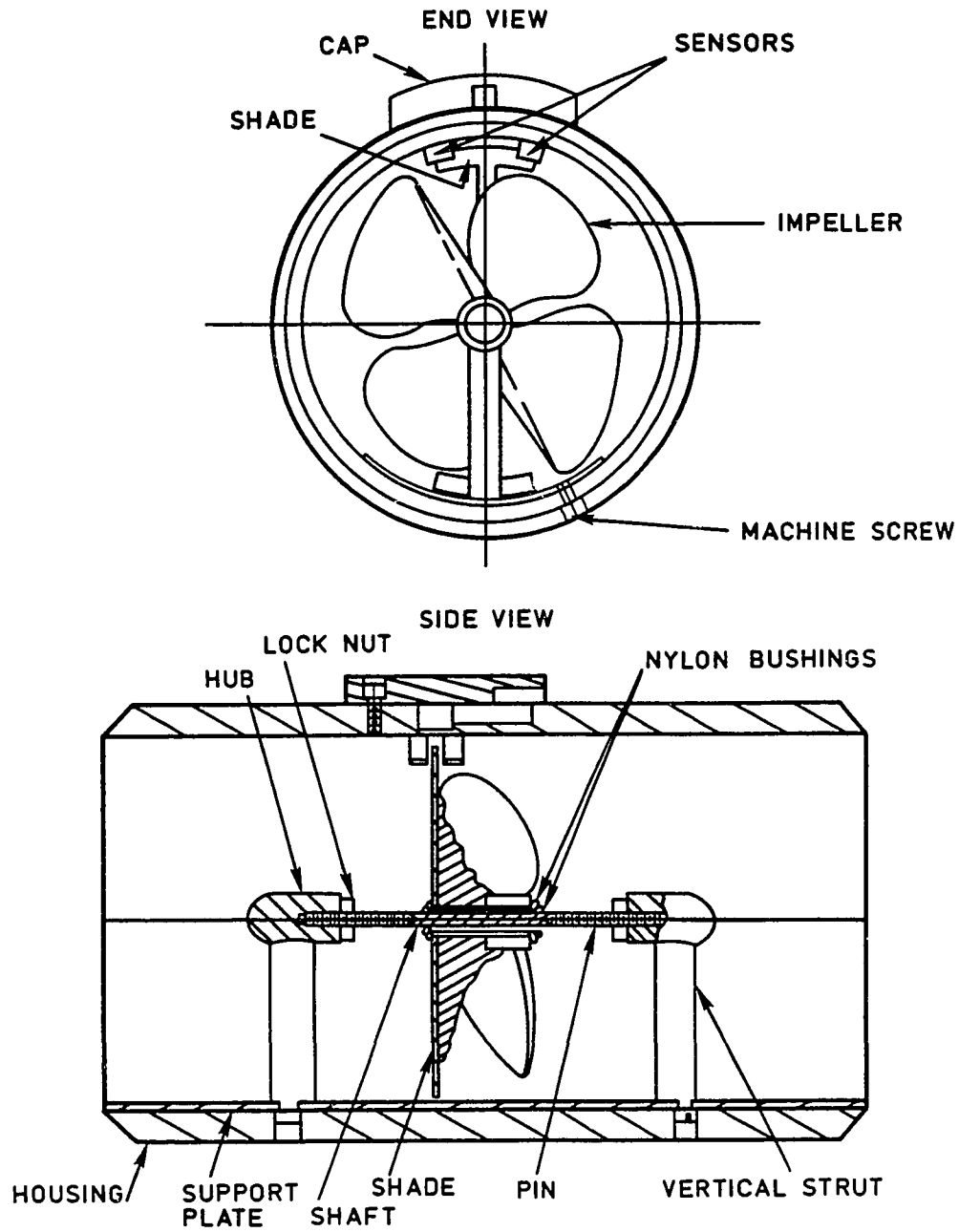
2.1. MECHANICAL DESIGN

The mechanical design of the ducted impeller current meter system, as mentioned earlier, was provided by Dr. Guy A. Meadows of the University of Michigan and is a design for which he holds a patent (Meadows, 1981 pers comm.). Figure 1 diagrams the main features of the current meter. The details of the design are summarized below.

The description of the current meter can be divided into three basic categories; the housing, the impeller and mounting assemblies, and the sensor assembly. The housing is constructed of polyvinyl chloride (PVC) pipe six inches long with an inside diameter of three inches. The inside of the pipe was planed smooth on a lathe. The wall thickness is 1/4 inch and is of sufficient thickness and strength to serve as the foundation for mounting the impeller and sensor assemblies. The advantages of using PVC pipe is that it is resistant to corrosion, durable, and easily machined. The pipe can be purchased from any plumbing supplier.

The impeller assembly has very little mass which is a factor in Meadows' design that contributes to the fast response time of the meter. The assembly consists of a four bladed glass filled plastic impeller, a stainless steel shaft with nylon

Figure 1. Schematic of the ducted impeller current meter. Not drawn to scale. (Adapted from Meadows, 1981)



bushings, and a thin stainless steel shade integral to the impeller that interrupts the light beam.

The impeller is made from two, two bladed propellers manufactured by Octura models for use on high performance model boats. They are 2.6 inches in diameter with a 4.61 inch pitch. The two propellers are notched at the hub and epoxied back-to-back to make a four bladed impeller that has nearly a symmetrical response to forward and reverse flows. Any asymmetry that does exist is handled in the calibration. The shaft fits through the center of the impeller and is held firmly in place by the nylon bushings so that the impeller and shaft rotate as a unit. The shade is manufactured from a thin piece of stainless steel sheet metal. It fits over the impeller shaft and is epoxied to the leading edge of the impeller.

The impeller and shaft is held in place by two horizontal stainless steel pins. Each pin is threaded on one end while the other end is machined and polished to a point which fits into the impeller shaft and acts as a needle bearing. Each pin screws into a hub attached to a vertical strut that is mounted onto a stainless steel plate which, in turn, is attached to the current meter housing with four machine screws. The pressure on the needle bearings can be adjusted by screwing the pins in or out of the hub. One strikes a balance between minimum pressure on the bearing for free rotation and enough pressure to ensure the impeller remains in place. This balance is not difficult to attain. The plate with the entire impeller assembly can be removed by removing the machine screws.

The sensor assembly consists of two light emitting diode (LED) interrupter modules manufactured by General Electric (GE H21B1), four resistors, and a four conductor cable. These LEDs emit electromagnetic radiation in the infrared range which minimizes interference from ambient light. The LEDs and resistors are mounted in the housing. The cable is connected to the sensors and the whole assembly is then sealed into the housing with liquid rubber and silicon sealant and capped. Two of the conductors provide power and ground to the sensors while the two remaining conductors, (channels A & B), transmit the signals from the current meter to the data acquisition system. Figure 1 in Appendix A provides the details of the sensor assembly electronic circuitry. The advantage of the optical sensor is that there is no physical or magnetic coupling between the impeller and the sensor to impede the impeller's rotation. This is another important factor that improves the response time of the current meter. The LEDs are located at approximately 30 degrees from each other along the inside wall of the housing. The shade width is such that the beams from both LEDs are both broken at some point in time as the shade rotates through them. This is done so that a pulse pair or event can be identified.

A four conductor TV antenna rotor cable is used in this system. Each of the four conductors is insulated with vinyl chloride plastic and the four as a whole are enclosed by a vinyl chloride plastic jacket. Although the cable was not designed or intended to be deployed in the marine environment, it performed flawlessly during the field experiments.

2.2. ELECTRONIC DESIGN

This section will provide a general description of the data acquisition (DA) system design. A more detailed description can be found in Appendix A. Two fundamental designs were used in this project. The first is that used by the field system and the second by the calibration system. Note that system used in this context refers to both the electronics and the programming that controls the microprocessor. The control circuitry for the timers is identical for the two systems, as one would expect. The main difference is in the programming of the microprocessor. The calibration system has additional circuitry to deal with the analog to digital converter used to sense the position of the pendulum.

CMOS integrated circuits (IC) were initially designed in the late 1960's and early 1970's for application in the aerospace industry to provide reliable, low power circuits for aircraft and satellites. Since then, its use has become more widespread. Applications range from inexpensive clocks and wrist watches to the latest in portable briefcase computers.

CMOS ICs have several advantages over other logic families, most common of which is the transistor-to-transistor logic (TTL) family. CMOS ICs use very little power, usually tenths of a milliwatt. This is two to three orders of magnitude less than TTL. CMOS ICs also have short propagation delay times through a gate, typically on the order of a few tens of nanoseconds (ns). They also have a high immunity to noise, often 45% of the supply voltage. The noise is also not propagated through the system. This can be a great advantage when designing

systems for employment in the marine environment. One important advantage mentioned earlier is the wide range of supply voltages that CMOS will tolerate. The range can be as great as 1V to 20V but is usually in the range of 3V to 18V. This means that a good power supply is not needed for the operation of systems incorporating CMOS technology. A simple battery will do in most cases.

The main disadvantage of CMOS ICs is the relatively slow switching speed of the gates. The upper limit is on the order of five megahertz. However, this disadvantage is becoming less significant as newer, high speed CMOS devices are brought into production. Another, less important disadvantage, is that some caution must be exercised when interfacing CMOS to other logic families. One needs to ensure that the voltages meet the design requirements of the logic family to which it is being interfaced. An example commonly encountered is interfacing CMOS to TTL. This is not, however, a major problem. An excellent primer on CMOS ICs and digital circuit design can be found in Hunter (1978) or Lancaster (1977).

The design problem can be broken down into three broad and general categories. The first is the control circuitry for the timing devices, the second is the interfacing of the timing devices with the microprocessor, and the third is the microprocessor and its machine language programming. The description of the design process will move from the current meter end of the problem through the interface and end with the programming of the microprocessor.

As stated earlier, the sampling scheme is to measure the time it takes for the shade to rotate from one LED to the other. The essential problem then, is to design the circuitry to turn the timing devices on and off at the appropriate times and to determine the direction of rotation. An additional signal is also generated to inform the microprocessor that data is ready.

Figure 2 depicts the sequence of steps and the signals generated for one event. Initially, the system is poised for an event to start. When the shade breaks the IR beam for LED A, a signal is sent from the current meter via channel A to the control circuitry to turn on or enable the timer (fig. 2a). As the impeller continues to rotate, it interrupts LED B, as shown in fig. 2b, a signal is sent via channel B to the control circuitry. The signal from B causes the timers to be disabled and the timing of the event stops. The time Δt is inversely proportional to the rotational speed of the impeller which is, in turn, proportional to the flow speed through the current meter. Signal C is generated by the circuitry and provides half the information necessary to signal the microprocessor that data is ready. At this time, both channels A and B are high. This ensures that the one can determine an event has occurred. If this overlap did not occur, one could not readily determine if A leads B or B leads A or precisely what is an event. Figure 3 illustrates this problem. The question that arises from this diagram is which pulses are a pairs, is it a1 and b1 or b1 and a2? Do b3 and a3 go together or is it a3 and b4? The choice of pulse pairs directly determines how the direction and speed of rotation is perceived. By making the shade wide enough to block both beams the ambiguity is easily

Figure 2. Timing diagram that defines the sequence of steps comprising an event.

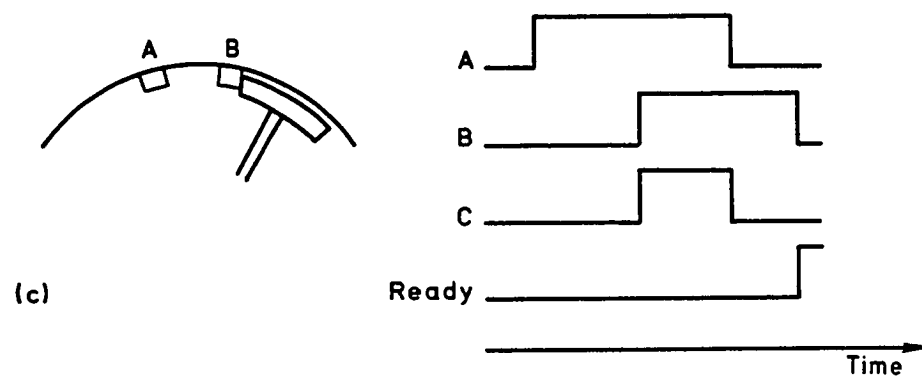
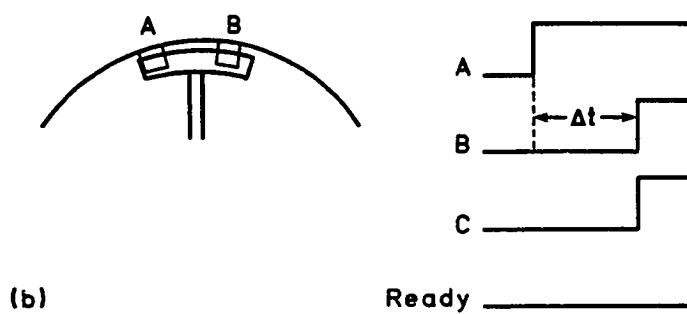
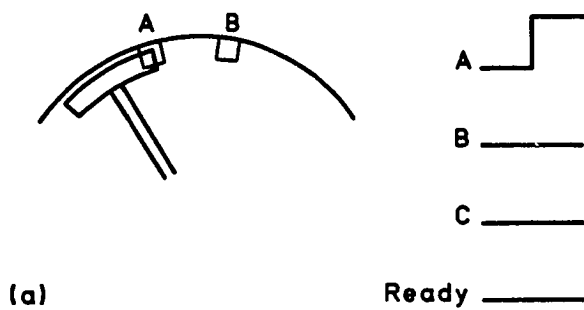
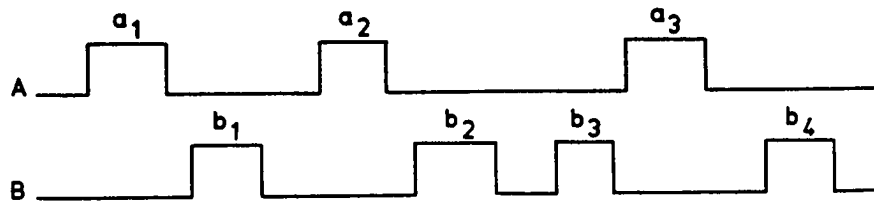


Figure 3. Timing diagram to illustrate the problem when there is no time overlap between channel A and B.



resolved. One also needs to ensure that the shade is wide enough so that signal C has a pulse width long enough to ensure it is perceived as a signal and not a noise spike.

The impeller now continues its rotation and brings the shade to the position depicted in fig. 2c. The trailing edge of the shade has just cleared the IR beam of LED B. The falling level on channel B and the information temporarily stored from signal C is passed through a logical AND gate to signal the microprocessor that a count is ready. This signal remains high until the microprocessor reads the count. After the count has been read, the microprocessor sends a signal to reset the timers and associated data registers. The system is now ready for the next event. Note that for a rotation in the opposite direction, the sequence of steps would have B leading A.

The reason why signal C alone is not used to signal the microprocessor when an event has occurred is because the speed of microprocessor operation is such that it would read the count and reset the timers before the shade could clear the trailing LED. The timer control circuitry would then sense a signal on that channel indicating that another event was starting, but with the opposite rotation. By waiting until the shade clears the trailing LED, this problem doesn't arise.

The timers are simply counting devices and in this case they count clock pulses. The clock pulses are generated on the microprocessor circuit board and sent to the clock input of the counters. Each timer consists of four, 4 bit binary counters that are cascaded together to make a single 16 bit counter. Data from the

counters are fed directly into two, 8 bit data registers for temporary storage. When ready, the microprocessor reads the data one byte (8 bits) at a time. The sixteenth bit or most significant bit (MSB) contains the sign of the count. If the MSB is 1, then the count is a negative number and the impeller was rotating in the reverse direction. After the count is read into the microprocessor, the MSB is tested to determine its sign and the appropriate action is taken.

The interface board communicates between the current meter electronics and the microprocessor communicate. If there were only two or three devices, this would not be necessary and, in fact, is not a component of the calibration system. In the case of the field system, there are six devices or current meters. The function of the interface is two fold. One, it must receive information from the current meters and present (encode) it to the microprocessor in a format that is usable. Two, it must translate or decode the control signals from the microprocessor and route them to the proper current meter.

Only one signal is transmitted from the current meter to the interface. That is the ready signal which informs the microprocessor that an event has occurred and data is ready. Herein lies one of the interfacing problems. The microprocessor cannot afford a separate ready line from each current meter. In fact, only one line is available for that purpose. Therefore, the interface must receive these signals and signal the microprocessor that an event has occurred and which current meter has that data. One could easily see that more than one current meter could have data ready at the same time. The interface must sort this out in such a manner that

data is not lost.

The problem can be solved by using what may be called a vectored interrupt. The particular design used in this system is a design modified from one found in RCA (1981a). The ready signals from each current meter are sent to a priority encoder which is capable of receiving up to eight signals. When a signal is received, it encodes it into a unique, 3 bit code for that particular current meter (CM) and puts it directly into a temporary data register. At the same time, it sends a ready signal to an external flag line on the microprocessor. When the microprocessor senses the ready signal, it reads the 3 bit code and branches to the portion of the program that handles that current meter. If two or more current meters are ready simultaneously, the priority encoder selects one that is assigned the highest priority. Each current meter is then handled in its turn. Current meter 1 is arbitrarily given highest priority and current meter 6 lowest.

Once the current meter has been decided upon, the data must be input one byte at a time, the low byte first followed by the upper byte. To do this, a unique code is sent to the interface via the output port of the microprocessor to select the low byte. The interface decodes that data and sends a signal to the low byte data register. When the data register receives the signal, it puts its data on the input data bus for the microprocessor. The microprocessor then reads the data and stores it. This procedure is repeated for the high byte. Once the data has been read and stored, reset information is sent from the microprocessor to the interface which decodes it and sends a signal to reset the current meter for the next event. To

summarize, the interface encodes signals from the current meters to the microprocessor and it decodes data sent from the microprocessor to the current meters.

2.3. MICROPROCESSOR BOARD

The microprocessor board is a RCA COSMAC Microboard Computer CDP18S604B. Details of its operation may be found in RCA (1981b). The pertinent components and features utilized in this system include the RCA CDP1802 microprocessor, 8 bit input and output ports, space for 2 kilobytes of read only memory (ROM), a 44 pin system interface connection (P1), a 34 pin input/output (I/O) connection (P2), and a user area for breadboarding small user circuits, and a 2.097152 megahertz (mhz) crystal-clock.

The CDP1802 is a CMOS, 8 bit, large scale integrated (LSI) microprocessor. Its operating voltage ranges from 4 to 10.5 volts. Internally it has sixteen, 16-bit scratch pad registers that can be used as program pointers, memory pointers or for temporary data storage. Each register is divided into a low order byte and a high order byte. The instruction set allows each register to be individually accessed by either the low or high order byte. An important advantage the 1802 has over many other microprocessors is that the user has complete control of how each register is used in a program. When the 1802 is powered on, the program counter defaults to register 0 (R0) after which any register may be designated the program pointer. Not only can any register be the program pointer, but more than one register can be designated as a program counter. This, for example, provides an efficient method to call subroutines. Note, however, that only one program pointer can be

in use at any given time. The D register is an 8 bit register that is used by many of the machine language instructions. It is used by the input commands, most of the arithmetic commands, and in transferring data to and from the scratch pad registers. The DF register is a 1 bit register that signifies if a borrow or carry has occurred in arithmetic operations and is used by the shift commands.

Another useful feature of the 1802 is the four external flags (EF1-EF4) which are used to facilitate I/O operations in this design. These are in addition to the direct-memory access (DMA) line and the interrupt line. Each EF line can be tested by conditional branch instructions in the program. EF1, EF2, and EF4 are available on the microboard and used by the present system. EF3 is used by the microboard and is not available to the data acquisition system. The EF lines are connected to both the P1 and P2 interface connections. Another important signal line on the 1802 and used by the DA system is the Q line. This is a signal that is turned on or off under program control and can be tested by conditional branch instructions. The Q line has many potential uses. In this design, it was used (along with EF4) for handshaking between a desk top computer in the data transfer process. EF1 and EF2 are used by the interface board to signal when one second has elapsed and when a current meter has data ready, respectively. There are many other features of the 1802 microprocessor not detailed herein that may be found in RCA (1979,1981c).

The P2 user interface has eight input data lines and eight output data lines that are connected to the input and output ports of the microboard, respectively.

Additionally, there are various control lines, including the EF lines and the Q line. The P2 interface connection also has power and ground lines that can be used by peripheral devices, in this case the current meters and associated electronics. In addition to the P2 connection, other timing and control signals were brought over from the microboard to the current meter subsystem via a user installed cable.

The P1 system interface contains all of the same signals as P2 as well as the address and the read/write lines for memory accessing. An additional feature of the microboard is space onboard for 2048 bytes of read-only-memory (ROM). This memory area was used to store the programming for the 1802.

2.4. PROGRAMMING FOR THE FIELD SYSTEM

The field system is a computer made up of the six current meters and associated electronics, the interface board, and the microboard and memory. While the high-level language (FORTRAN or BASIC) makes programming more efficient for the human, it does not necessarily produce machine code that is the most efficient for the microprocessor. One also does not develop a good sense of the interrelation between hardware and software when programming in a high-level language. In the vast majority of the situations one encounters, such a detailed level of understanding is neither necessary nor desired. However, in designing this particular system, it was necessary to maximize speed and efficiency of the software and to have a detailed knowledge and control of the interaction between the hardware and software of the system. The programming of the data acquisition system was, therefore, done in the machine language for the 1802 microprocessor.

The CDP1802 microprocessor has a set of 91 instructions that fall into seven general categories. Control instructions which include commands to designate the program pointer register, memory register, set/reset the Q line, and others. Memory reference commands that allow data to be brought in and out of memory. Register commands that allow one to put data into or retrieve it from the registers and to increment or decrement data in a register. Logic operations include logical OR/AND instructions, and several varieties of shift commands useful in binary arithmetic. Arithmetic operations are addition and subtraction with or without a carry or borrow. There are several add/subtract commands, the variety arises from where the data to be operated on are derived. Branch instructions included conditional testing of the EF lines, the Q line and others tests. They are essentially IF-THEN type commands. Skip instructions allow one to skip a specified number of lines and include conditional tests. Finally, there are several commands to input or output data from memory. Each I/O command generates a unique control code that can be used to control peripheral devices.

The sixteen scratch pad registers can have a great variety of uses. Multiple program counters and memory pointers are possible. The great deal of flexibility is further enhanced in that any register can be both a program pointer and a memory pointer. This allows the easy transfer of variables from the main program to a subroutine, for example. Additionally, the program pointer and the memory pointer can reside in the same register at the same time. This, for example, allowed control data to be easily output to the interface board. Examples of both can be seen

in the program for the field system given in Appendix B.

The 1802 microprocessor is capable of addressing up to 65,536 (64 kbytes) of memory directly. On the microboard, this is done via the P1 system interface connection. The memory for the field system allocates the first 2 kbytes for the erasable-programmable-read-only-memory (EPROM) and is reserved for program storage. An EPROM is a non-volatile storage medium. The second 2 kbyte block of memory is the work space for the system. Temporary data is stored here prior to final processing and storage. The remainder of the memory is reserved for storage of the processed data. The data remains here until it is transferred to a desk top computer.

In reference to the sampling scheme given for a current meter, events do not occur at regular time intervals but can be thought of as occurring randomly. This is awkward for analytical procedures such as time series analysis. Additionally, if each event with the time that it occurred were recorded, there would be insufficient memory. One of the main functions of the initial data processing, therefore, is to put the data into uniform time intervals. This is done by computing an average of the event times that occur within a 1 second time interval. One value for each current meter is then stored in memory each second. This not only puts the data into a more easily analyzed format, but also greatly reduces the required amount of memory.

The program for the field system uses four routines; the main program, the routine to calculate 1 second averages, the routine to read data from a current

meter, and the routine to transfer data to a desk top computer. Figure 4a shows the flow chart for the main program. The first operation is to initialize the system at the beginning of each data run and then to sample EF1, EF2, and EF4 in that order to determine if 1 second has elapsed, a current meter has data, or data is to be transferred, respectively.

When the system is initialized, the RAM is set to zero and the I/O ports on the microboard are then selected as the I/O ports to be used by the system. The previous step is necessitated by the factory design of the microboard. The registers that are to serve as memory pointers are set to their initial values followed by loading the starting addresses of the subroutines into the appropriate registers. Finally, the current meter timers are reset and the system is ready.

Initialization is followed by the program polling of EF1, EF2, and EF4 to determine if anything is attempting to communicate with the 1802. The program repeatedly cycles through the sequence until one of them is true.

EF2 becomes true when a current meter, via the interface board, indicates it has data. Figure 4b shows the flow chart for the data read subroutine. Once the 1802 senses the signal, it branches to the data input subroutine. The first step in this subroutine is to read the 3 bit code from the interface board that tells the 1802 which current meter is ready. This 3 bit code is put into one of the subroutine address registers and becomes part of the address code for the subroutine that handles that particular meter. The next step is to output a unique data byte to the interface board which is decoded to select the low order byte of that current meter.

Figure 4a. Flow chart of the main program of the data acquisition system.

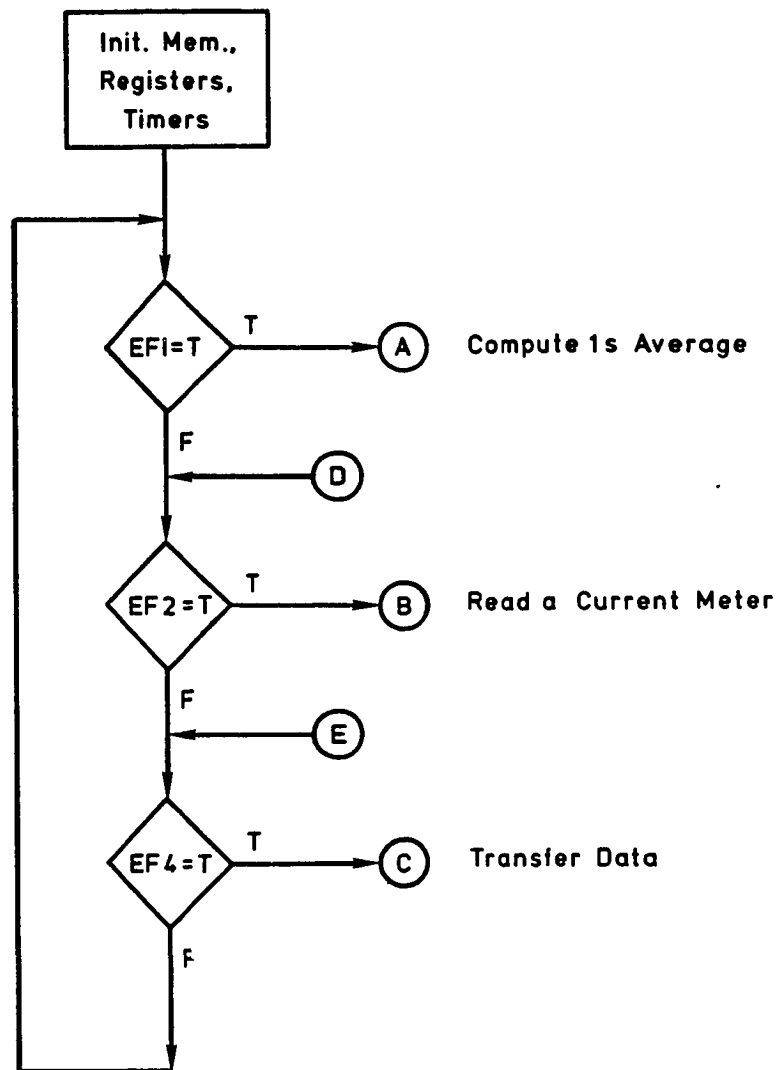
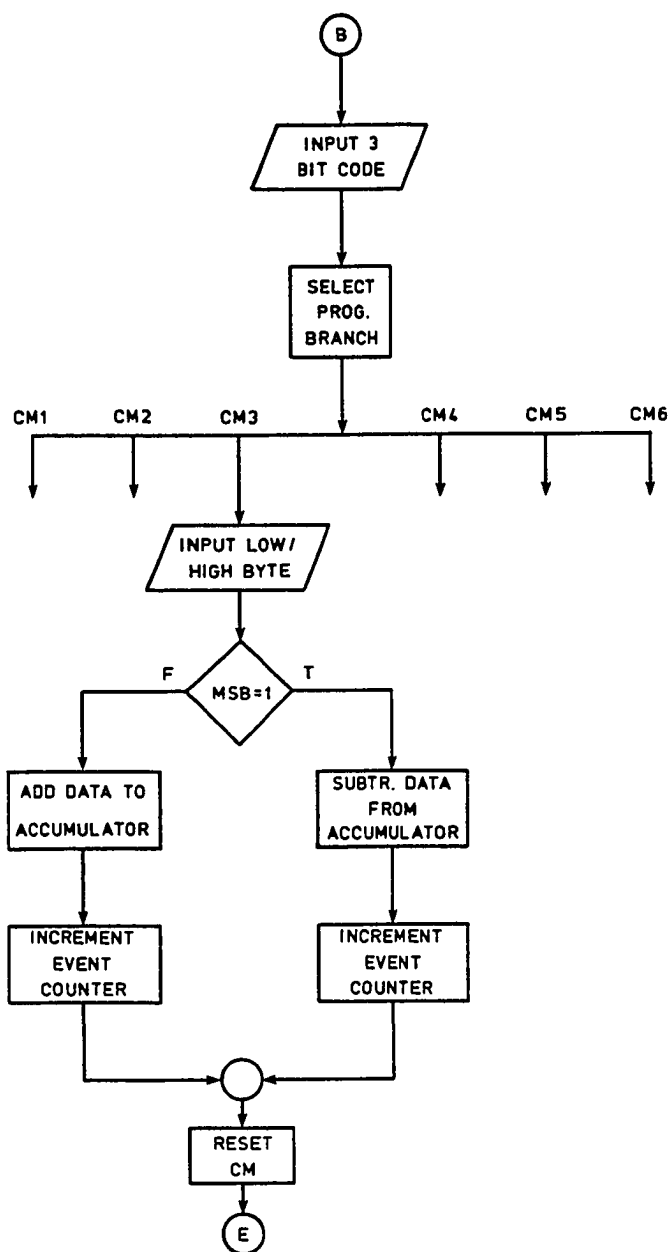


Figure 4b. Flow chart of the data read subroutine.



This data is read and stored in memory. Another data byte is output to the interface board to select the high order byte from the same meter. This byte is then read and stored. The 16th bit is tested to determine if the count is positive or negative. If negative, the input data are subtracted from the accumulator for that meter and the event counter is incremented by one. If the data are positive, they are added to the accumulator and the event counter is incremented. The final step before returning to the main program is to reset the timer for that current meter. The main program is re-entered at point E in figure 4a.

Figure 4c is the flow chart of the main features of the 1 second average subroutine. This subroutine computes the 1 second average for each of the six current meters in sequence and stores the result in the permanent storage area. If no events occurred during the 1 second interval, a large number is put into memory for that meter. A larger number implies little or no rotation of the impeller or zero velocity. The data remains here until it is transferred to the desk top computer. Two different memory pointers are used in this subroutine. One points to the work space where the event counters and accumulators for each current meter are stored. The second points to the next available memory location in permanent memory for the averaged data. After the averages are computed and stored, the event counters and accumulators are set to zero. The program then re-enters the main program at point D in figure 4a.

The data transfer subroutine is illustrated in a flow chart (figure 4d). The EF4 and Q lines provide the handshaking signals between the field system and the desk

Figure 4c. Flow chart of the 1 sec. averaging subroutine.

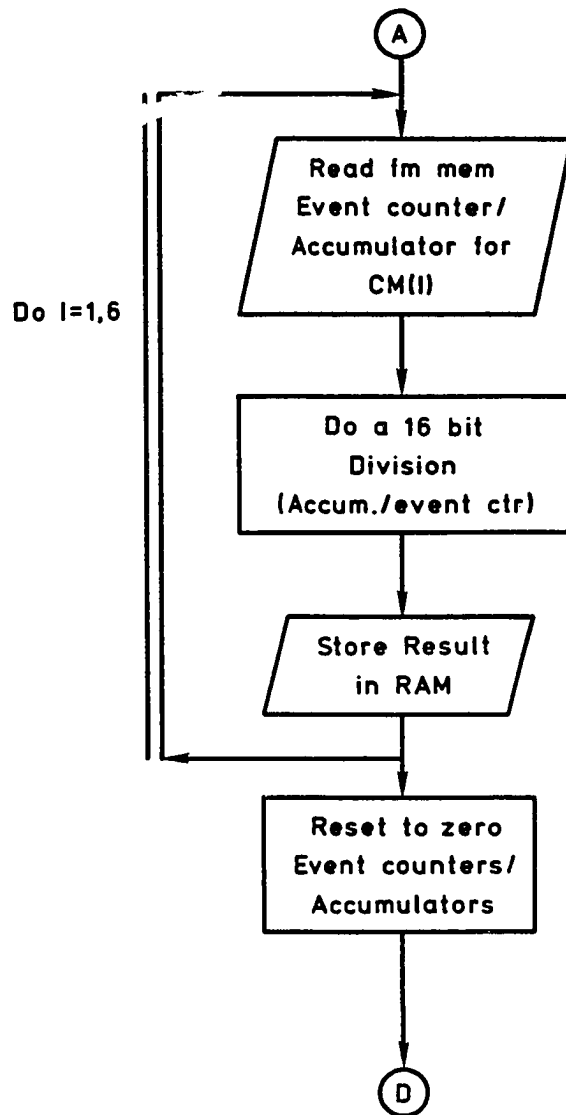
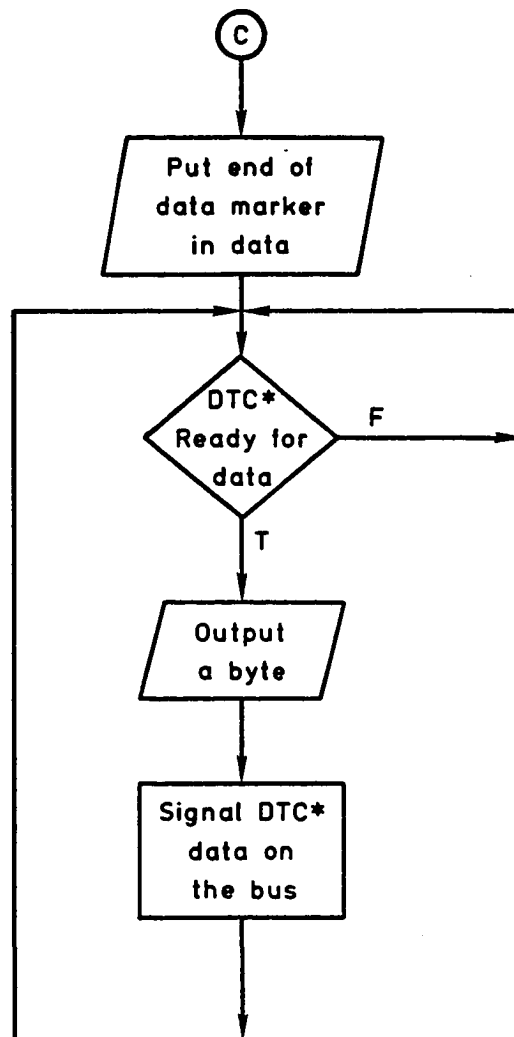


Figure 4d. Flow chart of the data transfer subroutine.



*DTC—Desk Top Computer

top computer during the transfer. The first step in this routine is to write 5 FFs (hexidecimal code for 255) at the end of the data in permanent memory to serve the function of an end-of-file marker which informs the computer receiving the data that there is no more. EF4 is sampled again to determine if the other computer is ready. If it is, the field system outputs the first data byte and then signals it is there using the Q line (Q goes from high to low). Q is reset to high thereby informing the other computer that the field system is ready to send another byte. The other computer signifies it is ready via the EF4 line and the process is repeated until the end-of-file markers are encountered.

2.5. DATA ACQUISITION TO COMPUTER INTERFACING

The ability of the data acquisition system to interface or communicate with another computer was one of the crucial aspects of this endeavor. Without this capability to transfer data for analysis, the system, as a whole, would be of little use.

To add permanent data storage (i.e., floppy disk drives or cassette tape) to the system, it was necessary to interface the field and calibration systems with another computer. Initially, the systems were configured to communicate with a Hewlett-Packard (HP)-87 desk top computer. The HP-87 is a versatile computer with many desirable options and the computer was available on loan from the University's Applied Marine Research Laboratory (AMRL). One of the features that made the HP-87 very attractive was the General Purpose Input and Output module (GPIO). This module plugged into the back of the HP-87 and provided a versatile means of

transferring data in parallel. HP (1981a) provided the necessary details on the required handshaking signals, pin connections, etc. HP (1981b) provided detailed programming guidance for the GPIO. The other end of the cable of the GPIO was wired to be compatible with the designed data acquisition system and connected to the P2 interface connection of the microboard. The HP-87 also had software features that made the data transfer easier. Among them were built in routines for binary logic operations and conversion from binary to decimal numbers. These routines could be invoked by a single programming command.

The final step in the interfacing problem was to write a short program for the HP-87 to control that end of the data transfer and convert the binary data from the data acquisition system to decimal data. The machine language programming for the 1802 microprocessor is a subroutine described in the programming section previously. This subroutine's main purpose is to output the data to the HP-87 and to provide the handshaking signals the HP-87 required. Appendix B contains both programs.

The HP-87 and HP dual disk drives were used with the calibration system when the current meters were calibrated. The HP-87 was not, however, available for the field experiments but a KAYPRO 4 portable computer was available from Dr. J. McConaughy in the Oceanography Department. One disadvantage of the KAYPRO computer was that a standard parallel I/O interface was not available. Fortunately, the KAYPRO did have an unused parallel I/O port internal to the machine. Building on the previous work of Dr. D. Johnson, formally of ODU, a

parallel I/O interface was designed and installed in the KAYPRO. The signals required by the KAYPRO and handshaking procedures were found in KAYPRO (1982). Changes were then made to the machine language program to provide the handshaking signals to the KAYPRO.

CHAPTER 3

CALIBRATION FACILITY

The calibration of the current meters was part of development of the current meters and the data acquisition system. There were three main characteristics that the calibration system needed to determine: gain, frequency response, and cosine response of the meters. The calibration also helped define the operational limitations of the instruments. The calibration facility includes both the mechanical and electronic design and concepts.

Meadows (1981) indicated that the mechanical design of the meters is quite good. His meters exhibited a linear gain up to velocities of 3 m/s, a frequency response on the order of 0.1s and a very good cosine response. The results of the present calibration are in general agreement except for the cosine response which could not be determined accurately.

3.1. MECHANICAL DESIGN AND CONSTRUCTION

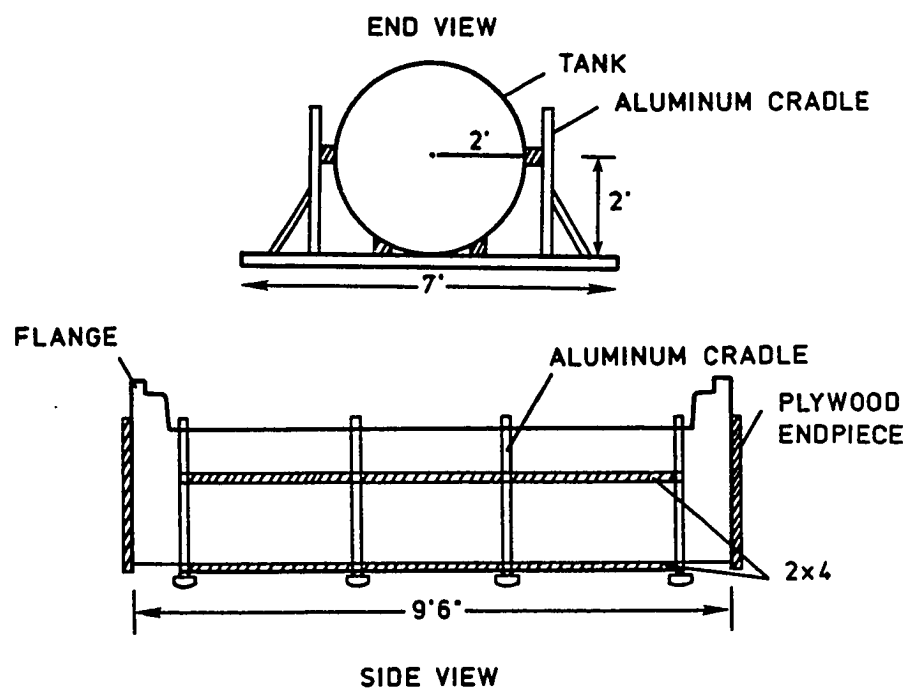
The calibration concept was patterned after that presented by Nielsen and Cowell (1981). It is a long pendulum with the current meter attached to the end which is then oscillated in a large tank filled with water. The mathematics of a damped pendulum allows one to calculate the velocity of the meter through the water. This is the standard against which the instrument is calibrated. The period of oscillation is also known which permits the frequency response of the meters to

be determined, at least for that period.

A calibration facility was designed and constructed in the warehouse area of the Oceanography Building. To accommodate the swing of the pendulum a tank was needed approximately 8 feet long and 2-3 feet deep. A large cylindrical fiberglass container 9 1/2 feet long and 4 feet in diameter was sealed by bolting 3/4 inch plywood sheets to the ends. The inside surface of the plywood had a layer of fiberglass applied to protect the wood from the water. A slot 8 feet long and 3 feet wide was cut along the length of the tank through which the pendulum would swing and a cradle was constructed of aluminum and wood to hold the tank (figure 5).

The pendulum was made of 0.84 inch diameter stainless steel boiler tubing. The length of the pendulum arm was 13.32 feet. Weights of either forty or eighty pounds were attached near the end of the arm but above the water level. A horizontal axle with either end supported by bearings was welded to one end of the pendulum. The bearings were bolted to a steel plate that was clamped to the top flange of a support beam in the ceiling of the warehouse area. A potentiometer was attached to the plate and its shaft inserted into the pendulum axle and held in place by a set screw. As the pendulum swung, the electrical resistance of the potentiometer would change as the shaft rotated. When power was applied, the output of the potentiometer was a varying voltage that indicated the position of the pendulum.

Figure 5. Schematic of the calibration tank and cradle.



NOT DRAWN TO SCALE

Tests on the potentiometer conducted in the lab showed that its response was linear. The correlation coefficient (r) was equal to 0.999. After the pendulum and potentiometer were mounted in the warehouse, another check was done and r was 0.995. The difference is attributed to the greater degree of experimental control in the laboratory than in the warehouse.

3.2. CALIBRATION FACILITY ELECTRONICS

The electronics of the calibration system is essentially identical to the field system, the core of which is the circuitry to control the timers and signal the microprocessor. Since fewer devices are sending data to the microprocessor, no interface board was required. Only two devices are connected to the 1802, one current meter and the analog to digital converter (ADC). These could easily be handled by connecting their ready signals to EF lines.

The most important modification is the addition of the electronics to handle data from the potentiometer which is an analog signal that varies from 0.2 to 0.5 volts. This is amplified by a factor of ten to take better advantage of the full operating range of the ADC (0.0 to 5.0 volts). The ADC samples this voltage at a frequency of 8Hz. After each conversion, the ADC sends a ready signal to the 1802 via the EF2 line. The 1802 then reads and stores the data in RAM. The ADC used in this study is an ADC0803. Its operating characteristics are given in National Semiconductor Corp. (1984). One of the attractive features of this ADC is that it was designed to interface directly to a microprocessor.

Initial laboratory tests of the potentiometer and the ADC were unsuccessful. Noise in the output data was traced to the input signal from the potentiometer. The noise was so great, that even a steady input voltage, as measured by a voltmeter, could not be resolved from the output. The solution was simple and straight forward. A simple RC low pass filter (Horowitz and Hill, 1983) was added to the potentiometer output that filtered out signals 60Hz and above. Following Priestley (1984), the phase lag of the filter was calculated as 0.2728 degrees and the gain as 0.967. The small difference between the input and output of the filter was ignored.

The addition of another timer was made to give the time that an event occurred during a calibration run. This was called the 'run' time. This timer operated at a frequency of 64Hz.

The differences in the calibration system and how data are treated also necessitates modifications to the machine language program. For the calibration, all of the data are required, therefore, no averaging subroutine is required. Each event time and its run time is read and stored in memory. The sequence of events for handling the current meter data is; 1) the current meter sends a signal to the 1802 via the EF1 line that a count is ready, 2) the 1802 first reads the run time timer to determine when the event occurred and stores that number in RAM, 3) the event time is then read and stored in RAM, and 4) the event timer is reset for the next event. The current meter data are stored as a data pair, the run time and the event time. Note that the run time timer runs continuously during each calibration run.

It also should be noted that the program is sampling EF2 to determine when the ADC has data which is stored in a separate memory block than the current meter data. The ADC does not need to be reset by the microprocessor since it is reset automatically at the start of each conversion (National Semiconductor Corp., 1984).

The machine language program is simpler and more straightforward than the field system's program. There are fewer devices interfacing with the microprocessor and there is no need for a 1 sec averaging subroutine. There are a few additional steps required to read the run-time timer. Since the core of the electronics of the field and calibration systems are the same, the calibration served the dual purpose of calibrating the meters and an additional test of the basic electronics package for the field system.

CHAPTER 4

CALIBRATION METHOD

4.1. PENDULUM MOTION

The calibration method presented herein is a summary of the procedure presented by Nielsen and Cowell (1981). The first piece of information needed is the angular position of the pendulum as it varies with time from which the true velocity of the current meter through water is calculated. The angular position of the pendulum is a linear function of the potentiometer output voltage, as discussed earlier. The explicit relationship can be written as

$$\theta(t) = \Theta_m \left[\frac{V(t) - V_0}{V_m - V_0} \right] \quad (1)$$

where $\theta(t)$ is the instantaneous angle of the pendulum, Θ_m is the start angle, V_m is the voltage at Θ_m , V_0 is the voltage at rest, and $V(t)$ is instantaneous voltage. To put it in terms of $y = mx + b$; y is $V(t)$, x is $\theta(t)$, b is V_0 , and m is $(V_m - V_0)/\Theta_m$ and eqn (1) is a solution for x .

The pendulum motion is assumed to have the form

$$\theta(t) = \Theta(t) \cos(\omega t) \quad (2)$$

where $\Theta(t)$ is the amplitude of the pendulum and ω is the angular frequency of the pendulum oscillation. The velocity of the current meter through the water can be given as

$$u(t) = L \frac{d\theta}{dt} \quad (3)$$

where $u(t)$ is the instantaneous velocity and L is the length from the pendulum axle to the current meter (see figure 6).

If one assumes that $\Theta(t)$ varies slowly or

$$\frac{d\Theta}{dt} \ll \omega \Theta \quad (4)$$

then

$$\frac{d\theta}{dt} = \frac{d(\Theta \cos(\omega t))}{dt} \approx \omega \Theta \sin(\omega t) \quad (5)$$

Simply, eqn 4 states that the amplitude decays slowly compared to the period of oscillation of the pendulum.

The total energy of the pendulum is

$$E(t) = \frac{1}{2} M (l \omega \Theta)^2 \quad (6)$$

where E is energy, M is the mass and l is moment arm of the pendulum measured from the axle to the center of mass. Differentiated with time, eqn 6 yields

$$\frac{dE}{dt} = \frac{1}{2} M l \omega \Theta \frac{d\Theta}{dt} \quad (7)$$

or

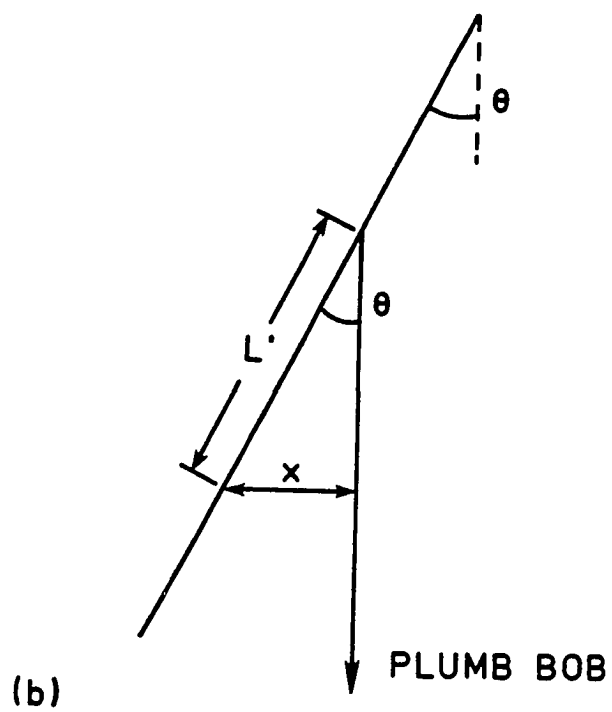
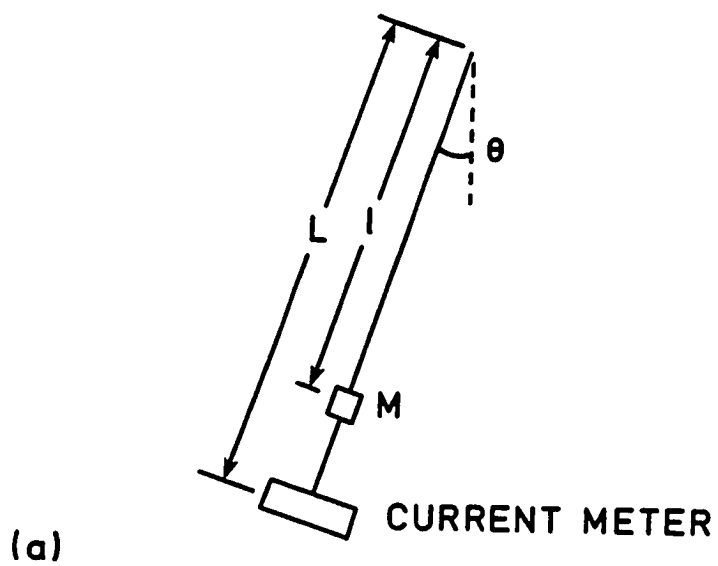
$$\frac{dE}{dt} \propto \Theta \frac{d\Theta}{dt} \quad (8)$$

The drag force is proportional to the velocity squared or

$$F_d \propto \Theta^2 |\sin(\omega t)| \sin(\omega t) \quad (9)$$

The energy dissipation rate is the drag x velocity or

Figure 6. Pendulum arm used in the calibration facility.



$$\frac{dE}{dt} \propto -\Theta^3 |\sin(\omega t)| \sin(\omega t)^2 \quad (10)$$

which averaged over one half period is

$$\frac{d\bar{E}}{dt} \propto -\Theta^3 \quad (11)$$

Equating eqns 8 and 11 and solving the differential equation yields the expression for the decay of the pendulum amplitude

$$\frac{1}{\Theta} = \frac{1}{\Theta_0} + c t \quad (12)$$

where c is the decay constant and Θ_0 is the initial amplitude. Using eqns 3 and 5 the velocity through the meter is approximated by

$$u(t) \approx L \omega \Theta \sin(\omega t) \quad (13)$$

4.2. GAIN AND PHASE LAG

Figure 7 shows the idealized time series for $\Theta(t)$, $\theta(t)$, and the measured current meter data $v(t)$. $\Theta(t)$ and ω are determined by fitting the measured pendulum data $\theta(t)$ to eqns 2 and 12. Figure 8 is an example of the result. Figure 9 depicts the raw data from the current meter.

The gain of the meter is determined by scanning the current meter data to find the local maxima values and the time they occurred. The velocity amplitude for those times are then calculated using

$$U(t) = L \omega \Theta(t) \quad (14)$$

and $\Theta(t)$ is calculated from eqn. 12. A matrix of data pairs (measured vs true) is then constructed. A linear fit of these data is accomplished. The slope of the resulting linear equation is the gain of the meter. The x intercept provides an

Figure 7. Ideal time series of $\Theta(t)$, $\theta(t)$, and $u(t)$.
(From Nielsen and Cowell, 1981)

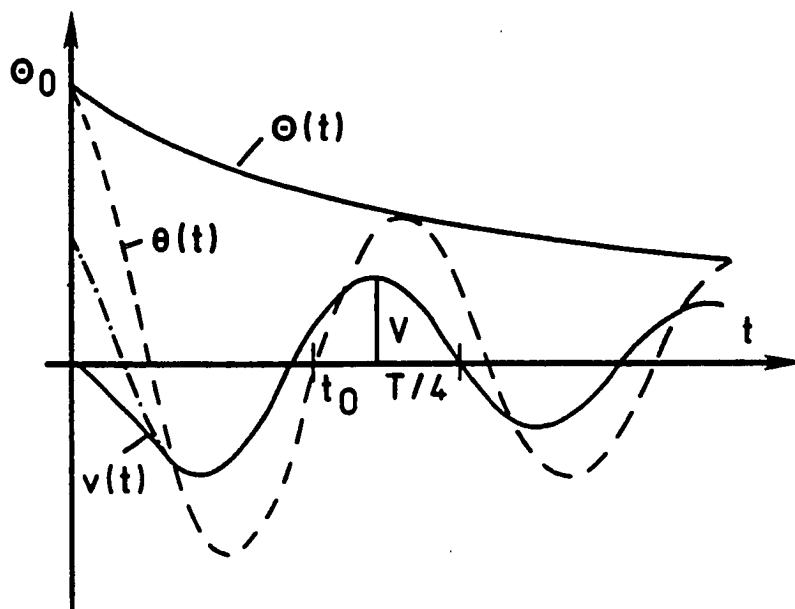


Figure 8. Example of the raw pendulum data (*) plotted against the fitted curve (solid line) for the pendulum motion.

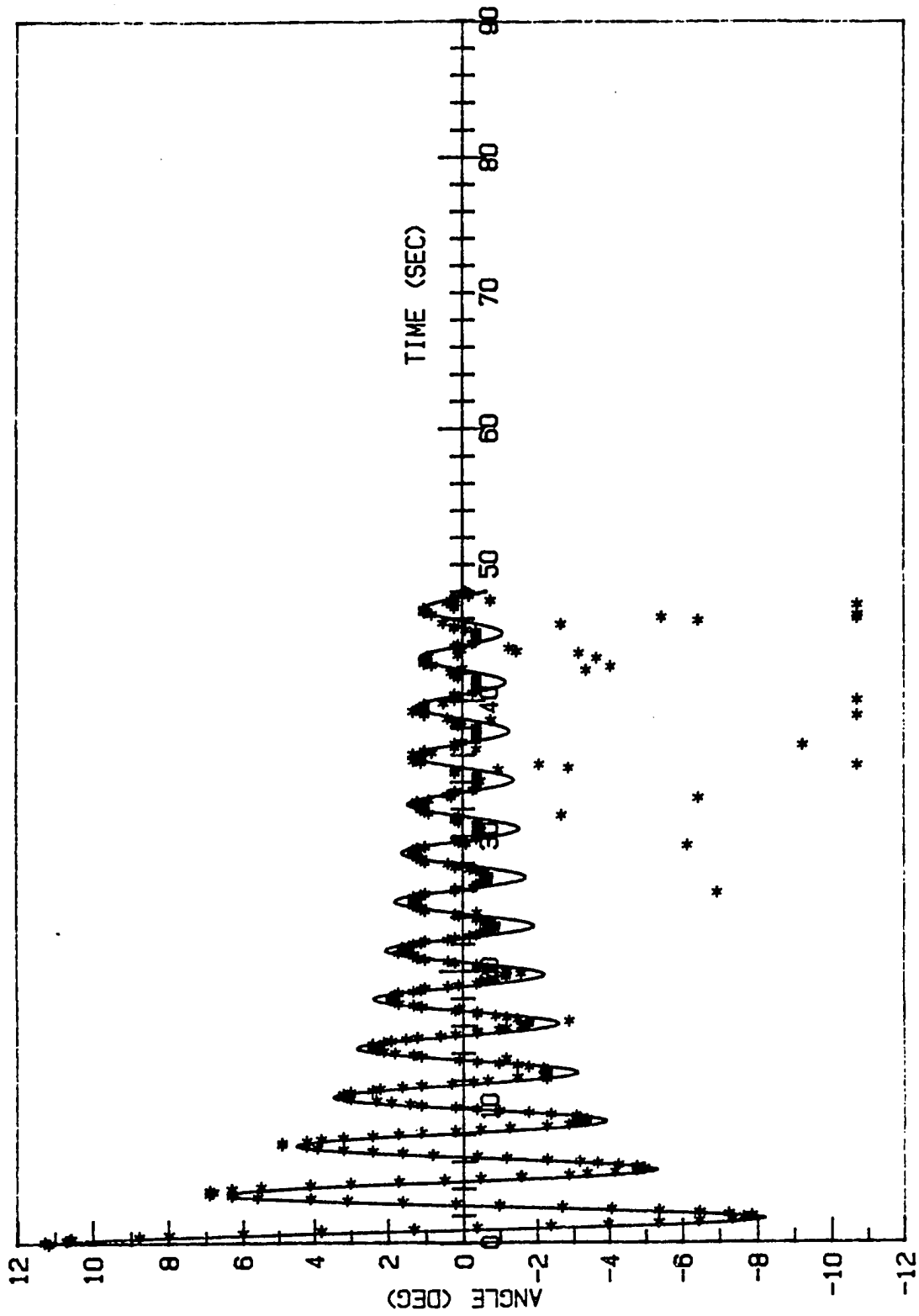
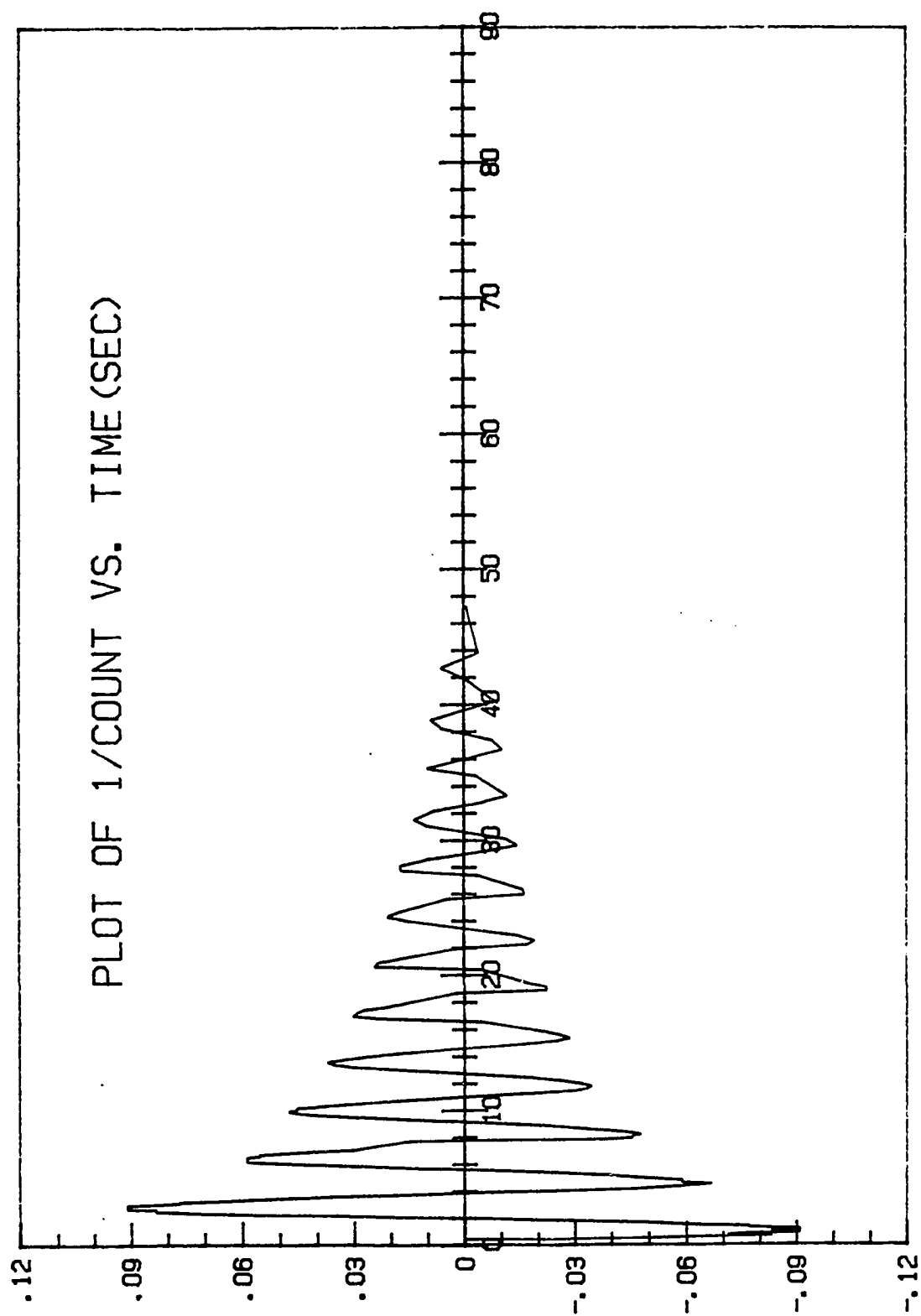


Figure 9. Example of the raw data output from a current meter.



estimate of the upper limit of the minimum or threshold velocity to which the meter will respond. The same procedure is followed for the reverse flow only the data are scanned for local minima. Figures (10 -12) show examples of the calibration curves for the current meters used in this study. Table I summarizes these results. The current meter most likely can respond to a velocity less than what the x intercept indicates. The reason is that the data used were the local maxima values from current meter data. The actual "threshold" velocity is probably less than indicated.

The gain of the meters is linear within the range they were calibrated. Figure 10 shows the calibration curves for one run for current meter (CM) 1. From Table I, it can be seen that the standard deviation for this meter is quite small, less than 0.001 for both directions. The goodness of fit is 0.993 for the forward direction and 0.996 for the reverse. CM 1 calibrated better than did the others. Figure 11 shows the calibration of CM 2 and serves to show the worst case. The goodness of fit is still quite good except for the reverse flow. For the forward flow it is 0.983 and 0.786 for the reverse. The standard deviations of the gain are 0.008 and 0.015 for the forward and reverse respectively. Figure 12 is a more typical calibration. The goodness of fit to a straight line is high, 0.996 and 0.997 for the forward and reverse flows, respectively, and the standard deviations of the gains are 0.004 for the forward flow and 0.003 for the reverse.

The time lag of the current meter is determined by comparing the time of the zero crossing of the pendulum with the following zero crossing of the current

Figure 10. Calibration curve of the gain for current meter 1, run A.

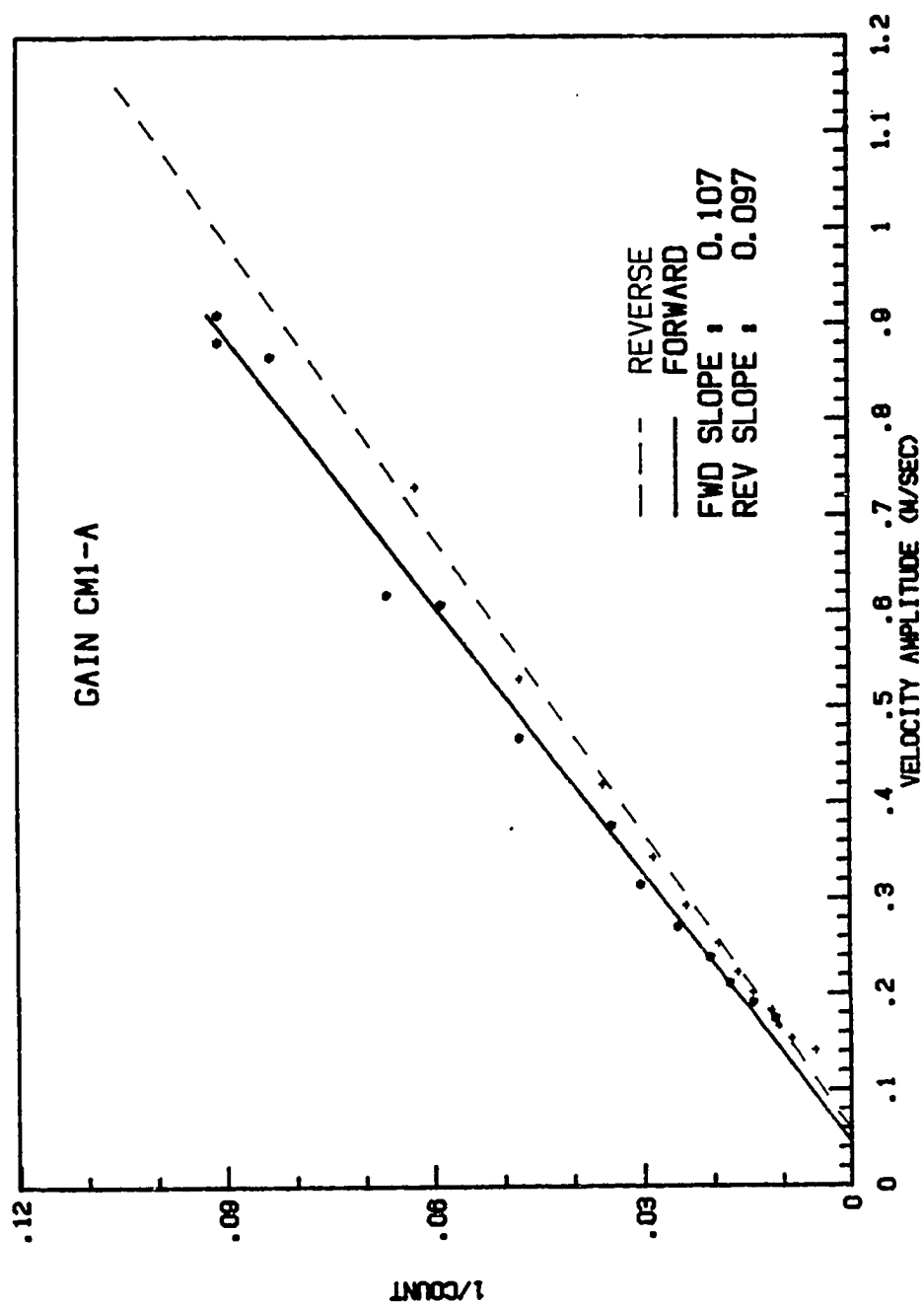


Figure 11. Calibration curve of the gain of current meter 2, run A.

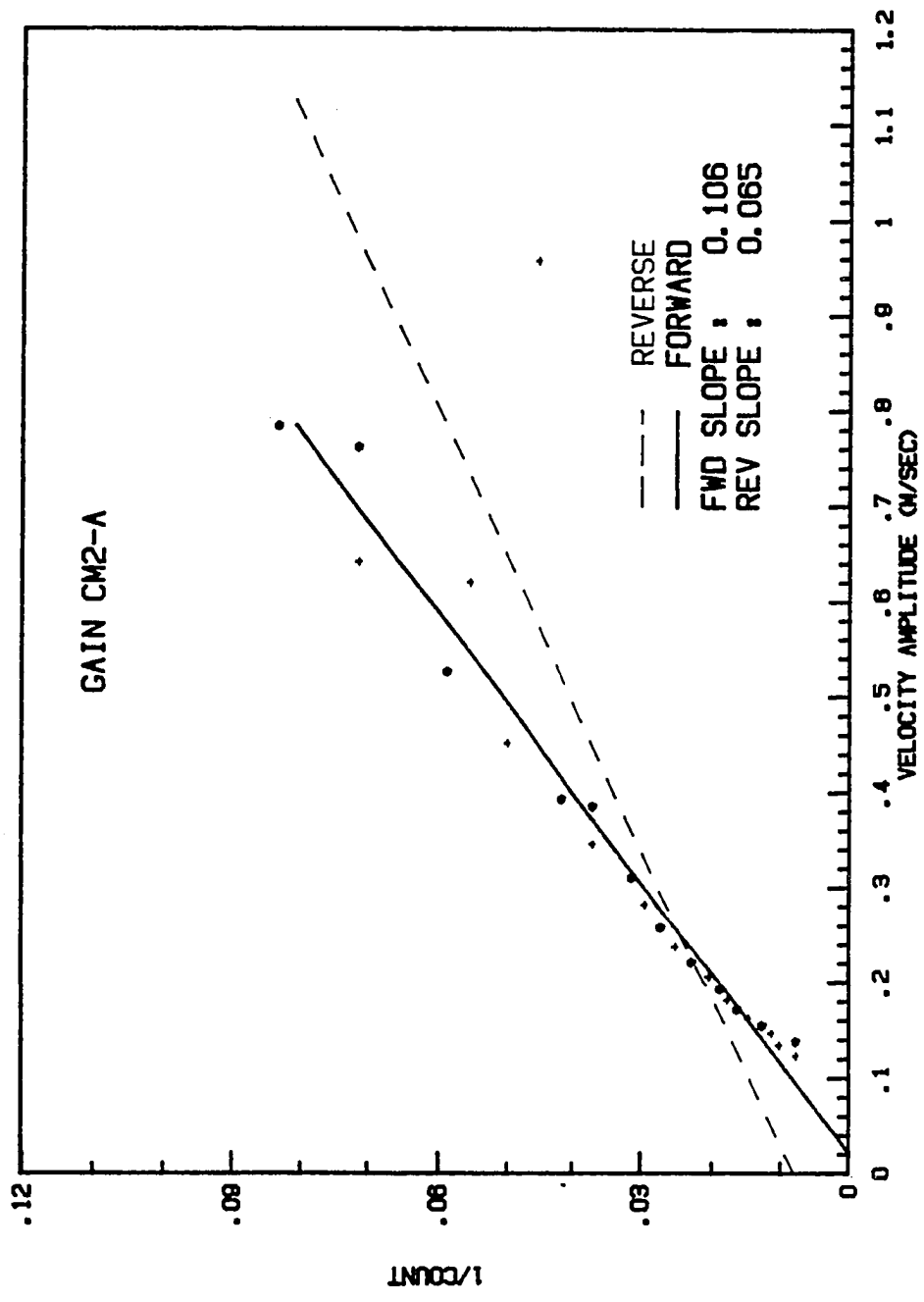


Figure 12. Calibration curve of the gain of current meter 3, run A.

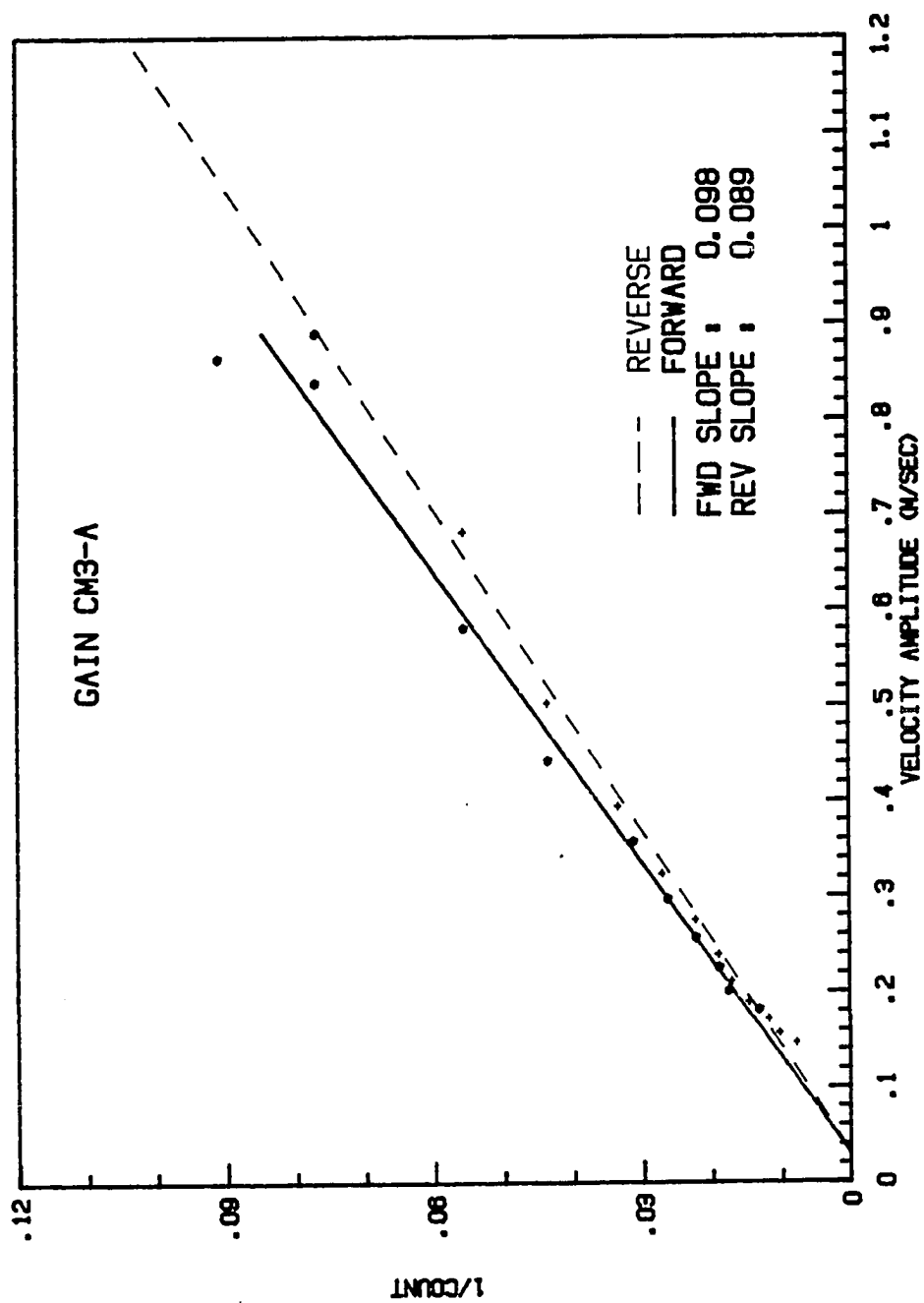


Table I. Summary of the gain and threshold values of each current meter for the forward and reverse directions.

Table I Average Current Meter Gain

Forward				Reverse		
Meter	Gain	Threshold	r	Gain	Threshold	r
1	.107+- .001	3 cm/s	.993	.097+- .002	5 cm/s	.996
2	.087+- .004	<1 cm/s	.982	.089+- .015	<1 cm/s	.789
3	.098+- .004	3 cm/s	.996	.086+- .003	2 cm/s	.997
4	.116+- .006	2 cm/s	.986	.113+- .007	2 cm/s	.910
5	.109+- .002	2 cm/s	.978	.094+- .006	<1 cm/s	.979
6	.124+- .006	6 cm/s	.993	.104+- .004	6 cm/s	.993

Note: r is the correlation coefficient

meter data. From figure 7, one can see that this time is $t_0 + T/4$ where t_0 is the time lag and T is the period of oscillation. Figure 13 shows the pooled time lag data for the current meters.

There is a large amount of scatter in the data at lower velocities. This is thought to be a function of the calibration system rather than the actual response of the meters. The amplitude of the swinging motion of the pendulum at the slower velocities is small. The impeller is responding to that motion but the shade may not be moving far enough in any one direction to trigger an event. An event may not be triggered for two or three oscillations of the pendulum. To compensate for this, the lower limit of the data are used to estimate the time lag of the meters. The time lag is estimated to be on the order of 0.11-0.12 seconds. Since this is small, no correction of the field data was necessary.

The calibration of the meters is good, over the range they were calibrated. They are linear and the time lag is very small. The calibration data clearly show that they can measure wave orbital velocities in the nearshore area. The response time of the meters indicate that these meters could be used in turbulence studies given the proper sampling scheme.

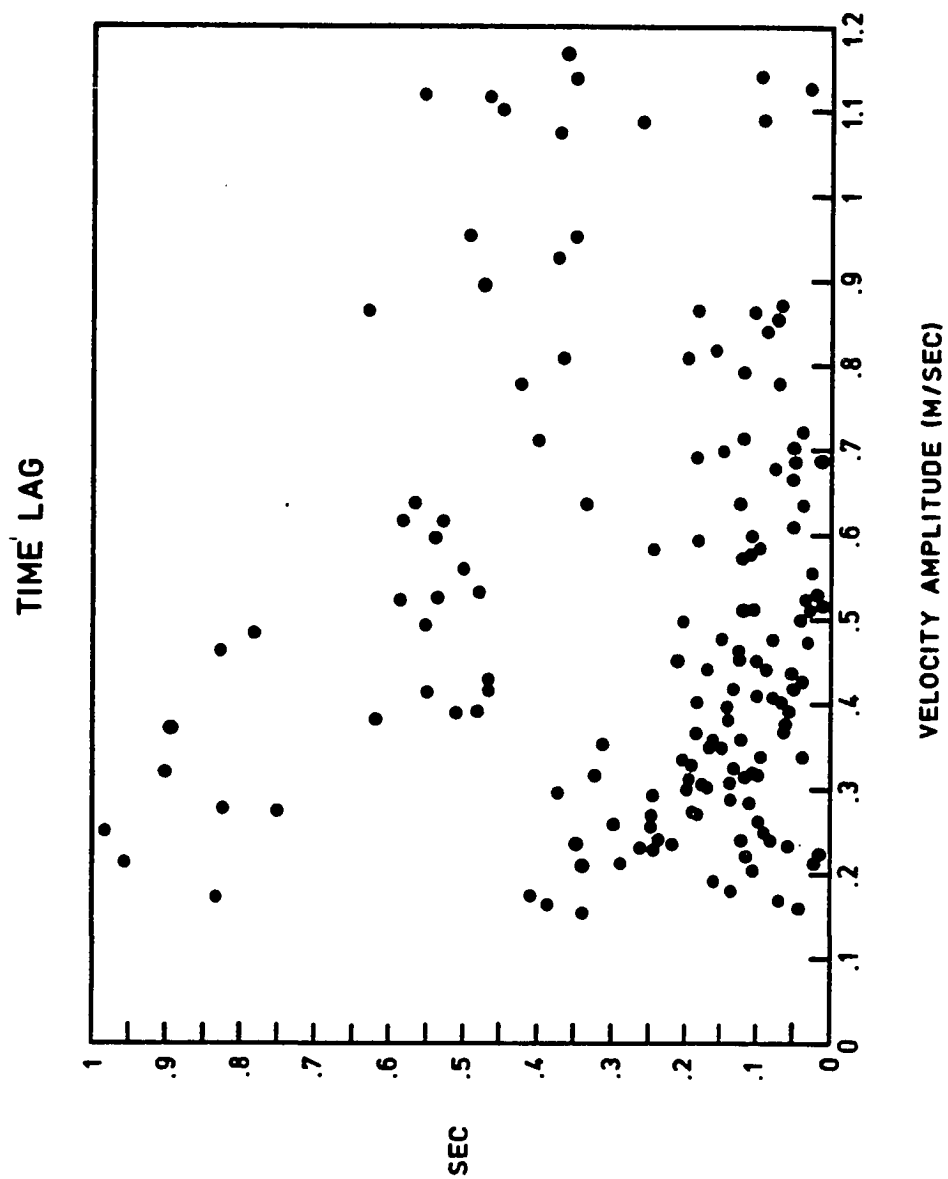
4.3. COSINE RESPONSE

The cosine response to off axis flow under ideal conditions is expected to be

$$g(\phi) = G \cos(\phi) \quad (15)$$

where ϕ is the angle between the axis of the current meter and the direction of flow, G is the gain at $\phi = 0$ and g is the gain at angle ϕ . Two current meters

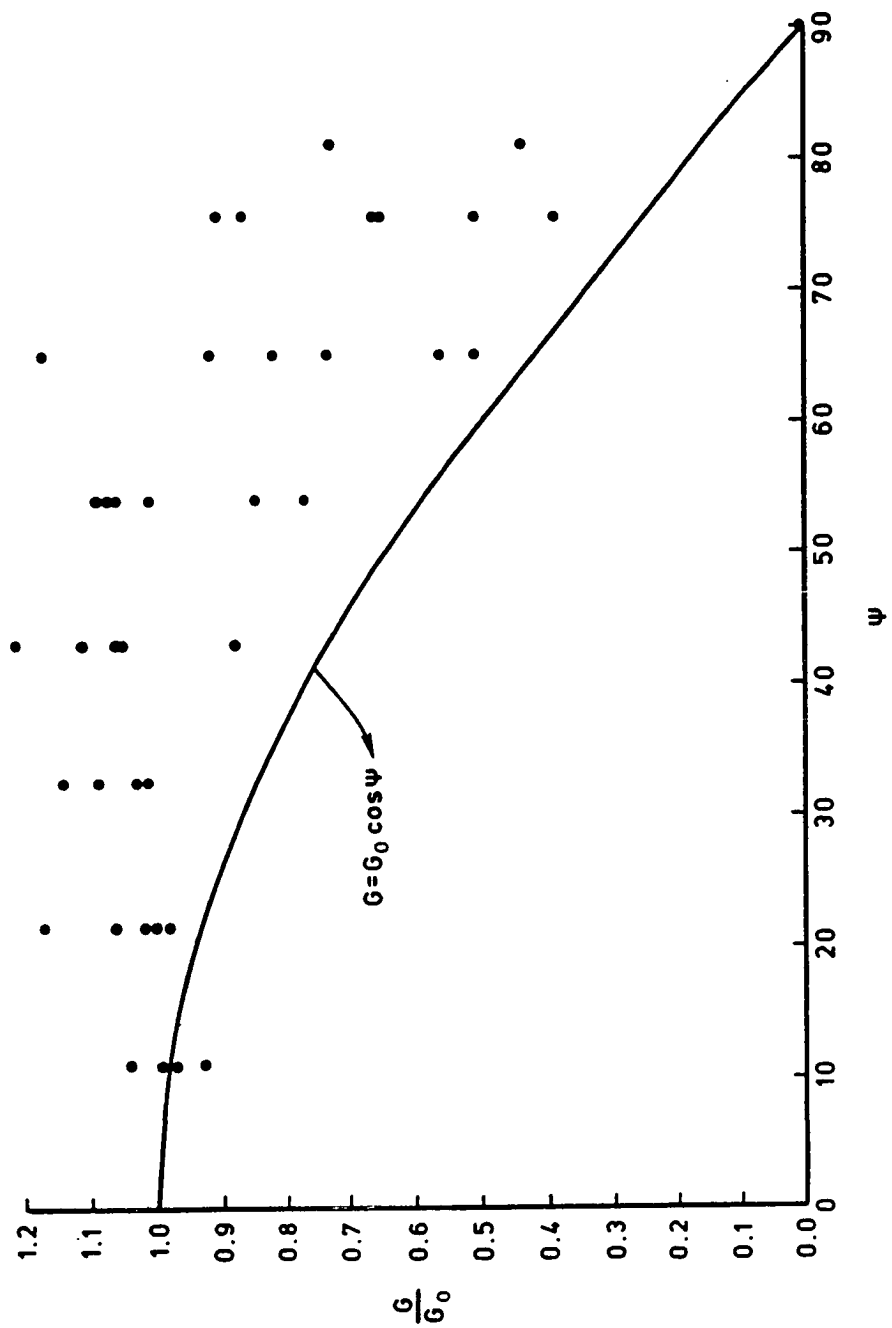
Figure 13. Pooled time lag data for all current meters and all runs.



were selected to test the cosine response. The tests were done by placing the meters at various angles to the plane of the pendulum motion and calculating the gain. Figure 14 shows the ideal cosine response and the measured response. Clearly, the cosine response of the meters does not appear to follow the ideal curve, although it does fall off to zero for $\phi = 90$ degrees. Meadows, 1981 (pers comm) showed a very good cosine response for his meters.

There is some indication that the reason for the difference between the ideal and measured cosine response may lie in the calibration facility. When a current meter is placed at an angle to the pendulum motion, there is a component of the resisting force that is perpendicular to the motion of the pendulum. This gives a sideways motion to the pendulum (as well as the to and fro swinging motion). The result is a figure eight motion, which leaves uncertainty as to the actual angle or how the true flow through the meter is affected.

Figure 14. Cosine response of the current meters plotted against the ideal cosine response (solid line).



CHAPTER 5

SUMMARY AND CONCLUSIONS

The calibration of the current meters also served as a test of the data acquisition system in addition to determining the necessary calibration constants for the meters. The calibration procedure provided the first opportunity to test the entire system as a unit in the water. Previous tests had been conducted in the lab. The performance of the electronics was an unequivocal success, particularly, the portion that was common to the field system. Figure 9 clearly indicates that the output of the meter follows the motion of the damped oscillation quite well. At the end of the run, one can see the problems associated with the small pendulum motion.

The calibration also brought out the versatility of the data acquisition system. Not only was it recording the current meter data, but it also handled the potentiometer data via the ADC without difficulty. The ease of interfacing to at least two different desk top computers is another example of the flexibility of the system.

The water tight integrity of the current meters was another area tested in the calibration. With only one exception, all of the meters passed this important test the first time. The exception was current meter 5 which shorted to ground immediately after it was initially immersed. The LEDs and associated circuitry in the housing were replaced and the meter resealed. No further problems of this type were encountered either during the calibration or in the field. The method of seal-

ing the current meters is quite adequate for the applications in this study but, there is room for improvement, particularly if deployed in deep water.

The portion of the LEDs that extend into the barrel of the meter should also have more protection from the elements in future versions. At present, the surfaces of the emitter bulb and the detector are exposed. There are indications from the field experiments that the failure of some of the meters to trigger an event may have been related to this problem. If these surfaces were protected, it would significantly improve the overall reliability of the current meters.

The calibration has clearly shown that these meters can measure wave orbital velocities at a period of approximately 3.5 seconds, the oscillation period of the pendulum. The time response of the meters indicate that shorter periods can also be measured.

The incorporation of the microprocessor in the design concept has resulted in a very flexible and versatile data acquisition system. It clearly has demonstrated the ability to record data from different sources. The calibration system has shown that it can accept data from the more common analog devices and from the current meters. The field system has shown that several devices can be controlled by the data acquisition system simultaneously. This was made possible by the ability to reprogram the microprocessor to meet the different sampling schemes and to interface with other computers.

The inherent low power consumption and high noise tolerance of the CMOS logic family used in the design of the data acquisition system is a distinct

advantage for systems that are to be deployed in the marine environment. This allows the present system to be battery operated. The addition of a portable "lap top" computer would then allow deployment of the system in remote locations without the expense and logistical problems of more sophisticated power supplies.

The total cost of the data acquisition system and the six current meters was approximately \$2500. The low cost allows an investigator the great possibility of deploying a large number of current meters without a major investment in equipment. This allows the opportunity to investigate a number of problems, for example, field studies of three dimensional fluid flow in the nearshore area.

The design and implimentation of the data acquisition system and current meters was very successful. All of the design requirements were met. The use of a microprocessor in the data acquisition system to control the current meters made for a versatile system. It also allowed for preprocessing of the data in the field which greatly reduced the required amount of onboard memory. The low cost of the system will permit one to deploy a large number of devices which will allow field studies of phenomena that are at the forefront of coastal research with a minimum expenditure of funds.

REFERENCES

- Bradshaw, M. P.; J. Chappell; R. S. Hales; L. D. Wright, 1979, Field monitoring and analysis of beach and nearshore hydrodynamics, 4th Australian Conf. on Coastal and Ocean Engin., pp 171-175.
- Hewlett-Packard, 1981a, HP82940 Interface installation and theory of operation, Hewlett-packard Co. Corvallis, OR.
- _____, 1981b, HP-85 I/O programming Guide, Hewlett- Packard Co, Corvallis, OR, 310pp.
- Horowitz, P. and W. Hill, 1983, The art of electronics, Cambridge University Press, NY, 716pp
- Hunter, W. L., 1978, CMOS databook, Tab Books, Blue Ridge Summit, PA, 280pp.
- KAYPRO, 1982, KAYPRO II Dealer reference manual, Non-Linear Systems, Inc, Solana Beach CA, 29pp.
- Lancaster, D., 1977, CMOS cookbook, Howard W. Sams & Co, Inc, Indianapolis, IN, 414pp.
- Meadows, G. A. 1977, Time dependent fluctuations in longshore currents, 15th Conf. Coastal Engin., pp 660-680 .
- _____, 1981 Personal Communication.
- National Semiconductor Corp., 1984, CMOS databook, National Semiconductor, Santa Clara, CA.
- Nielsen, P. and P. J. Cowell, 1981, Calibration and data correction procedures for flow meters and pressure transducers commonly used at the Coastal Studies Unit, Coastal Studies Unit Tech. Rep. 81/1, Dept. of Geography, Univ. of Sydney, Sydney, N.S.W. 2006, 27pp.
- Priestley, M. B., 1984, Spectral analysis and time series, Academic Press Inc., London, 890pp.
- RCA, 1981a, Microprocessor/Memory applications briefs, RCA Solid State Div., Somerville, NJ, 225pp.
- _____, 1981b, COSMAC microboard computer CDP18S604B, RCA Solid State Div., Somerville, NJ, 19pp.

- _____, 1982c, Memory/microprocessor products CDP1802A CDP1802AC types, File No. 1305, RCA Solid State, Somerville, NJ, 23pp.
- _____, 1979 COS/MOS memories, microprocessors, and support systems, RCA Solid State, Somerville, NJ, 440pp.
- _____, 1977, User manual for the CDP1802 COSMAC microprocessor, RCA Solid State, Somerville, NJ, 118pp.
- Smith, J. D., 1978, Measurement of turbulence in ocean boundary layers, Working Conf. on Current Measurements, pp 95- 128.
- Sonu, C. J.; S. P. Murrey; S. A. Hsu; J. N. Suhayda; and E. Waddell, 1973, Sea breeze and coastal processes, EOS, 54: 820- 833.
- Swan, T., 1981, Programming guide to the 1802, Hayden Book Co. Inc., Rochelle Park, NJ, 156pp.
- Zilog, 1983, Components data book, Zilog Inc., Campbell, CA, 849pp.

CHAPTER 1

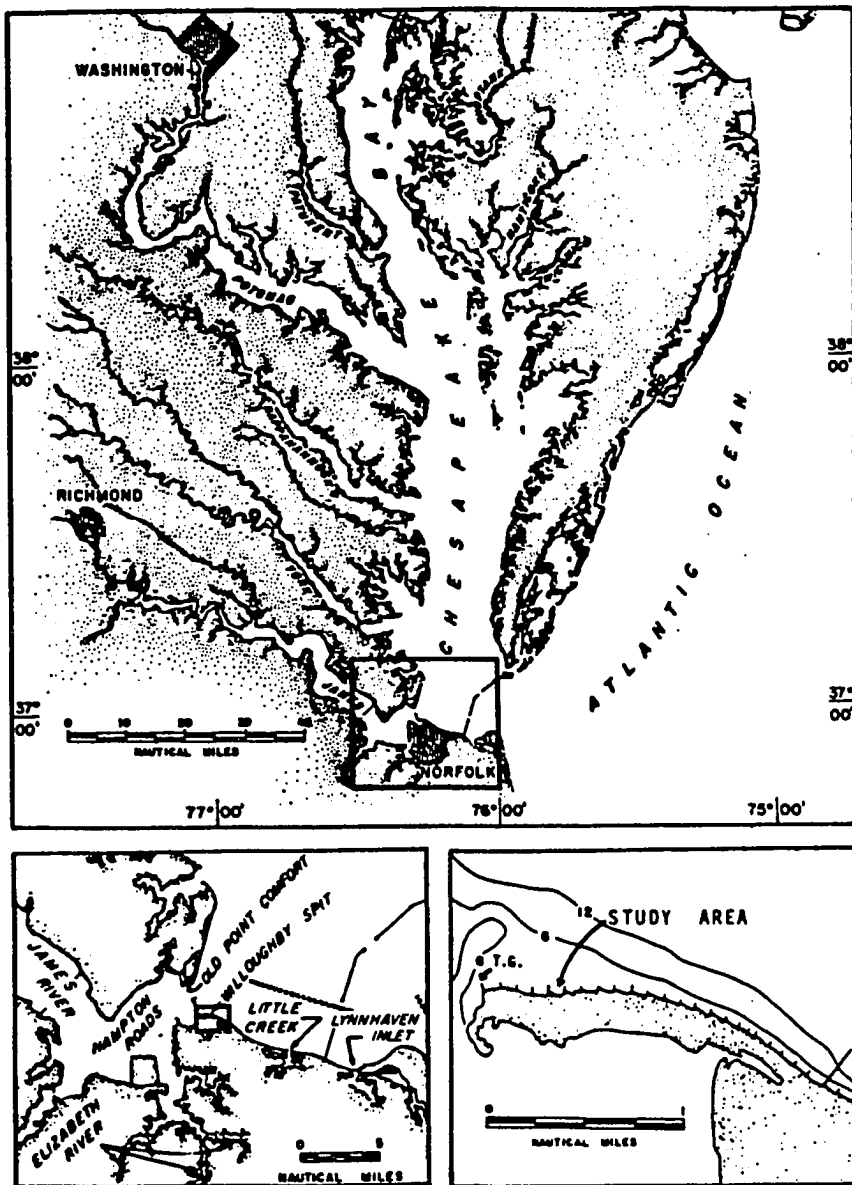
INTRODUCTION

Part I of this dissertation dealt exclusively with the development of a new microprocessor-controlled data acquisition system for an array of ducted impeller flow meters. The emphasis of Part II of the dissertation is on a field application of the new system to the study of rip currents that are thought to be associated with groin structures on beaches.

1.1. RECENT WORK AT WILLOUGHBY SPIT

The present study was carried out at Willoughby Spit in Norfolk, VA (Figure 1). It is one of a series of related projects by researchers from the Old Dominion University. Ludwick (1987) conducted bathymetric surveys over a period of three years in a test groin compartment at Willoughby Spit. Near bottom current measurements were taken to estimate the sediment transport rate and direction. Additionally, a mathematical model was developed to forecast the post-fill shoreline and fill life that included empirical coefficients for longshore and cross-shore transport rates (Ludwick 1987, Ludwick et. al. 1987). Kang (in preparation) used the detailed bathymetric surveys and the wave orbital velocity asymmetries to estimate the cross-shore sediment transport within the groin compartment. Reynolds (in preparation), has studied the longshore variation in wave height between the groins to estimate the longshore transport rate after fill had been placed in the groin sys-

Figure 1. Geographic location of the study area. (From Ludwick et al., 1987)



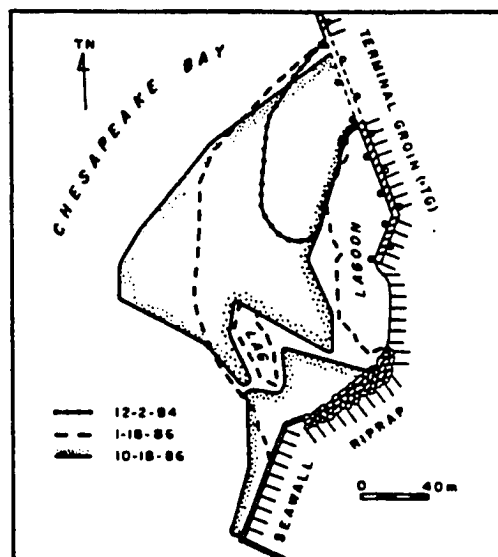
tem. He used detailed surveys of a terminal spit (figure 2) that formed after the fill placement to estimate the actual transport rate. The general thrust of these studies was to determine the current and sediment transport dynamics in a groin system. The focus of this study is on the flow near the groin wall.

1.2. PREVIOUS GROIN STUDIES

Groins are probably the most widely used structure in shoreline protection (SPM, 1984). Bruun (1977) traces their origin to the early 16th century Holland and cites evidence that groin-like structures may have been used much earlier. The function of a groin is to trap a portion of the longshore transport of sand in order to stabilize an eroding beach or to accumulate sediment between the groins. This is accomplished at the expense of the downstream beach (SPM, 1984). One of the underlying assumptions is an adequate supply of sand being input to the groin system. Often this is not the case and artificial beach nourishment must be used to fill the area between the groins (Tomlinson, 1980). Implicit to the use of groins is that loss of sediment to the beach is due to longshore transport and not cross-shore transport. Numerous studies have clearly shown that the cross-shore transport cannot be ignored and, in fact, can be an important factor.

Groins have excited much research interest over the years (e.g., Balsillie and Bruno, 1972; Bruun, 1972; Tomlinson, 1980). Most previous work has been concerned with the engineering aspects of groins such as design, materials, and construction; height, spacing and length; permeability; and shape. To a lesser extent, groin effectiveness has been studied in both the laboratory and field settings where

Figure 2. Geographic location of the terminal spit. (From Ludwick et al., 1987)



effectiveness has usually been measured in terms of sediment trapped by the groin or in changes to the shoreline. The performance of groins in the field has been quite variable. A particular design may perform up to its specifications in one location and fail in another (SPM, 1984). The main reason for this lies in an incomplete knowledge of the physical factors in the area that is to be protected. These factors include the longshore transport rate and direction; wind and wave climate; and tidal range and currents (SPM, 1984; Tomlinson, 1980).

Two critical factors are rarely, if ever, considered in evaluating groin effectiveness. The cross-shore transport rate for sediment is not normally considered. It is, however, important and should always be considered. An important mechanism for the cross-shore transport of sediment is a rip current along the groin. The effect of a groin system on the wave and current dynamics which are the basic driving forces of sediment transport is also rarely considered but should be. This study is intended to verify these conclusions.

Mathematical models used in the study of groins have generally considered two equations that are solved simultaneously to obtain the shoreline position. The first equation is for the longshore transport of sediment and its response to the wave energy and the second is the sediment transport continuity equation (Tomlinson, 1980). The longshore transport is:

$$I_l = K(EN)_b \sin \alpha_b \cos \alpha_b \quad (1)$$

where I_l is the immersed weight transport, $(EN)_b$ is wave energy flux at the breaker line, K is a dimensionless constant, and α_b is the breaker angle (Komar,

1976). The continuity equation is:

$$\frac{dy}{dt} = -\frac{1}{d} \frac{dS}{dx} \quad (2)$$

where d is the reference depth such that $d(\Delta y)$ is the cross section in which sediment erosion or deposition occurs, S is the longshore transport rate, y is the distance offshore, and x is the longshore distance (Komar, 1976).

Among the earlier numerical studies, was the work of Bakker (1968) and Bakker et al. (1970) which built upon the earlier work of Pelnard-Considere and summarized in Bakker (1968). Bakker (1968) considered only the shoreline changes due the presence of groins as a function of the breaker angle (α_b). Bakker et al. (1970) expanded this to include the effects of wave diffraction on the lee side of the groins. Currents and tidal effects were not considered and cross-shore transport was assumed to be zero. Hulsbergen et al. (1976) tested the Bakker's theoretical developments in a large wave basin at the Delft Hydraulics Laboratory. They found that the model performed reasonably well when the longshore current system was well defined and stable. When more complex circulation patterns developed, the theory was inadequate as a forecasting tool.

Kemp (1962) and Nagai and Kubo (1958) have also used physical models to study groin performance. Kemp (1962) focused on the effect of the alignment and type of groin on the longshore transport and longshore currents and their effect on the shore morphology. With regard to the present study, Kemp (1962) found that there was a return of sediment seaward along the downstream groin wall which intensified under storm conditions. When the tidal current alone was considered,

his data indicate that a weak gyre may form in the groin compartment when the top of the groin was above the water surface.

The model study of Nagai and Kubo (1958) varied the groin inclination and spacing to determine the optimum configuration when waves alone acted on the system. Pertinent to this study, they found an offshore flow along the downstream groin wall due to wave action.

The Waterways and Experimental Station of the Coastal Engineering Research Center designed a physical model to aid in the planning of shore protection measures at Imperial Beach, CA (Muslin, 1978). Five groins had been authorized in 1958 to stabilize erosion in the study area. Two were installed and met with little success. The model was first used to estimate the effectiveness of installing the other three groins. Results showed that relatively strong rip currents were generated along the groins and could transport sediment out of the compartment thereby reducing the effectiveness of the groins. This was in general agreement with aerial surveys of the site which indicated rip currents along the two existing groins.

Field studies of groins have primarily been concerned with the engineering aspects such as construction materials and techniques. Measures of effectiveness have been relatively rare and are concerned with the amount of sediment impounded or in the advance or retreat of the shoreline (Tomlinson, 1980). Little is known of the wave and current dynamics for installed groin systems.

1.3. PHYSICAL SETTING

The study site is a single groin compartment located on Willoughby Spit in Norfolk, Virginia (Figure 1). The spit is 3.2 km long, its width varies from 135 m to 535 m, and has an average elevation of 2 m relative to mean low water (MLW). The present rate of shoreline retreat is 7.6 cm per year (Byrne and Anderson, 1977). In 1939, 37 groins were constructed along a 5.5 km length of the spit and adjacent shoreline which replaced 62 groins previously installed by local property owners. The groins were constructed of timber, were shore normal, and straight. The inner section is 183 cm above MLW with a 23 m long inclined section connecting the outer section which was 61 cm above MLW (Ludwick et al, 1987).

In September, 1984, the 27 westernmost groins were filled with 410,590 m³ of fill. The fill sediment had a mean diameter of 0.9 mm and was poorly sorted (1.32). Broken shell made up 50% of the coarser size classes by weight and 10% to 15% of the finer size classes. The slope was graded to 1:20 sloping seaward. An artificial dune was constructed in the backshore with an average elevation of 3.7 m above MLW. After the space between the groins was filled, a new spit began to form to the west of the terminal groin (Fig. 2). Sediment in the new spit was fill material (Ludwick et al, 1987).

The tide at the study site is semidiurnal with a mean range of 0.76 m. The tidal currents are essentially shore-parallel beyond the ends of the groins and are flood dominant. Flood duration is 7 hours and ebb is 5.4 hours. (Fleischer, 1977; Ludwick, 1987). The mean tidal velocities are 27 cm/sec and 18 cm/sec for the

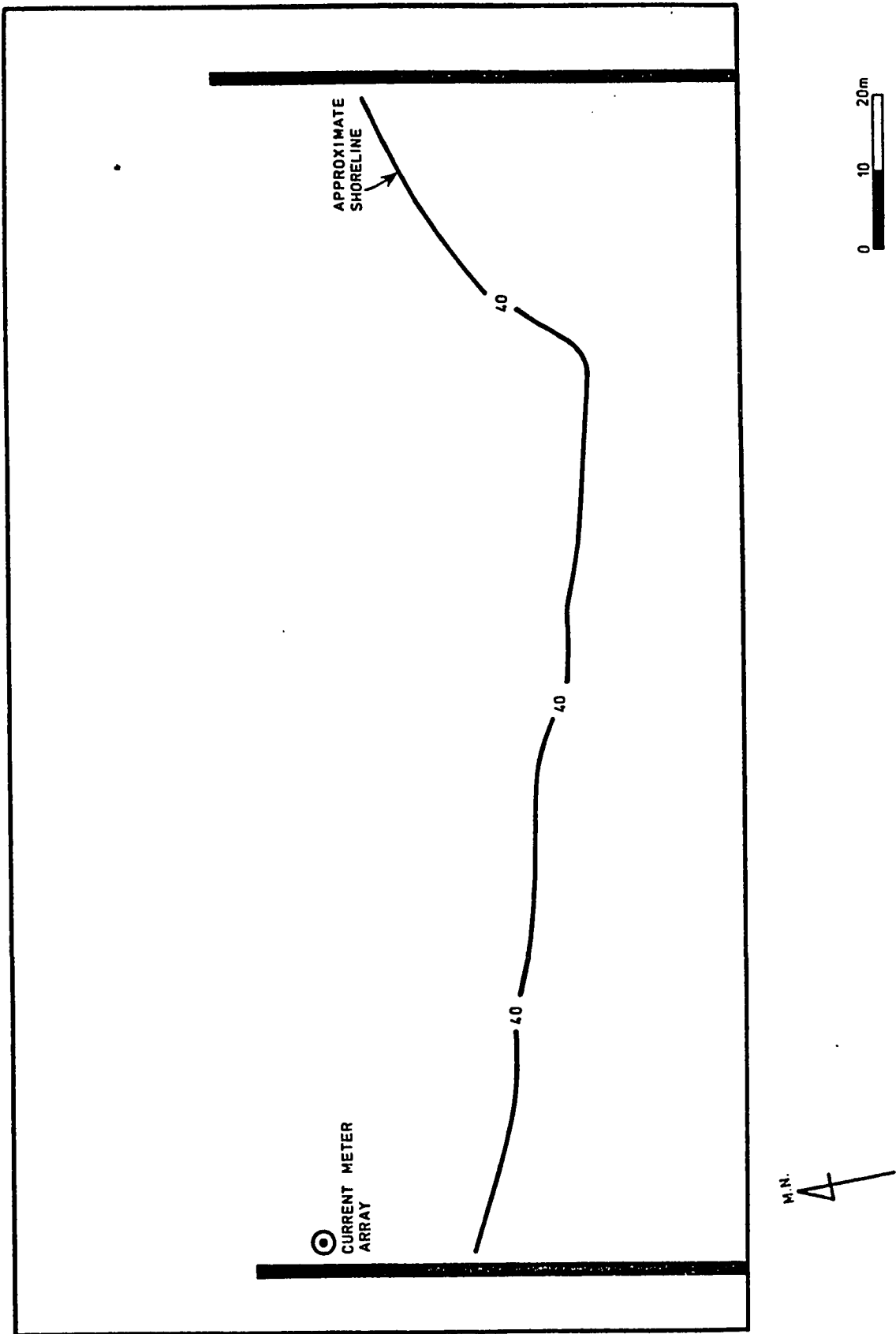
flood and ebb respectively. The outer portion of the groins are submerged for approximately 22% of the tidal cycle (Ludwick, 1987).

Ludwick (1987) proposed that sediment transport at Willoughby Spit occurs in two zones. Belt 1 is longshore transport in the swash zone. Transport in this zone is wave dominated and episodic. When the water level is at or above the top of the groin, sediment is washed into the adjacent compartment. The net transport in Belt 1 is to the west as evidenced by the growth of the new spit. Belt 2 is beyond the end of the groins and is influenced by the asymmetric tidal flow in the area which is flood dominant and to the west. Sediment from Belt 1 that becomes entrained in Belt 2 is lost to the groin system. One mechanism that removes sediment from the test compartment is the proposed seaward flowing action of rip currents along the upcurrent walls of the groins.

1.4. PURPOSE OF STUDY

The purpose of this study is to determine if there is a groin-associated rip current in the test compartment. Implications of seaward flow in this area are important in determination of sediment loss to Belt 2 in a groin compartment. Losses of sediment in the shore-normal direction are seldom considered in the design of groin systems. If sediment is lost in this manner, it would be a significant factor in the overall performance of the groin system. A current meter array was deployed on the updrift side near the downstream groin end in the test compartment (Fig. 3). Vertical velocity profiles were measured to determine if the rip current current existed and to determine its vertical structure.

Figure 3. Diagram of the test compartment showing the approximate location of the current meter array.



Once the data analysis began, it became apparent that the measured vertical velocity profiles could be used to better understand the actual wave-current interactions in the area between groins. These data could also be used to test the validity of using depth averaged velocities in the study of nearshore and coastal zone circulation patterns and sediment transport.

CHAPTER 2

EXPERIMENTAL PROCEDURES

2.1. FIELD PROCEDURES

The test compartment was occupied on five occasions during the months of May and June 1986. The first experiment was a "shake-down" of the equipment and procedures. A total of 51, fifteen minute data sets were obtained from the other four field days and of these, 3 were not usable because seaweed had fouled the current meters.

A vertical array of the six flow meters, mounted as orthogonal pairs at intervals of 20 cm, 60 cm, and 100 cm above the base of the mounting stand, was deployed in the test compartment. The array was positioned near the end of the westernmost groin in the compartment (Fig. 3). For each pair, one meter was parallel to the groin and the other perpendicular to it. The westernmost groin of the test compartment is the downstream groin for normal wave conditions and is where groin-associated rip currents are most likely to be found.

The mounting stand consists of a circular base approximately 1 m in diameter with a vertical rod attached at its hub. Lead weights were attached to the base to help anchor the stand. The flow meters were mounted on the vertical rod. The mounting stand was stable for wave conditions encountered during the field experiments. The maximum waves had a height of 1 m.

The cable from each flow meter terminated ashore at the data acquisition system. The data acquisition system, a KAYPRO portable computer, hand held anemometer, tools, etc. were housed in a tent ashore. Electrical power (120 VAC) was supplied from a nearby apartment via 550 ft. of heavy duty extension cord.

Each field experiment was 12 hours duration or approximately one tidal cycle. Fifteen minutes of data were collected every hour. The flow meter data were averaged every second and stored in the solid state memory of the data acquisition system. The data were then transferred to the KAYPRO at the end of each data run for storage on floppy disk. During each run, the wind speed and direction were measured using a hand held anemometer. The breaker height and breaker angle relative to the shore line were also estimated as was the water level in relation to the top of the groin. After each data run, a swimmer would measure the water level from the top of the vertical rod of the array. The water depth was then calculated knowing the overall height of the mounting stand. The swimmer would also visually inspect the flow meters for proper operation and fouling.

Backup data disks were made on a Zenith desk-top-computer and then uploaded to the VAX computer in the Computer Science Department where the data were analyzed.

2.2. ANALYTICAL PROCEDURES

The first step in the analytical procedure was to convert the raw data into velocity using the calibration curves developed in Part I of the dissertation. The

steady component of the velocity was extracted by computing the time mean of each current meter for each data run. Power spectra were computed using standard library subroutines on the VAX computer in the Computer Science Department.

Initial inspection of the velocity data revealed numerous spikes that occurred when the sign of the flow was changing. The data are one second averages (Part I). The data that the acquisition system is handling are counts of a clock pulse. The larger the count, the slower the rotation of the impeller, positive or negative. If the averaging window spans the cross over between positive and negative flow and these are algebraically added, then the difference between two relatively large numbers is a small number or count. When using the calibration curves to convert a count to a current velocity, the result is a large velocity when, in fact, the velocity is near zero. These spikes were removed by scanning the data in groups of three to determine if the first and third points were opposite in sign. If so, the second point was replaced by the linear interpolation of the first and third points. Appendix B contains the programming details.

The time constant of the flow meters was approximately 0.11 to 0.12 sec and the sampling interval is one second (Part I). In order to prevent aliasing of the data, one needs to sample at a rate of four to five times faster than the time constant of the instrument (i.e., approximately .02 sec in this case). Since that is not possible with this system, the data was initially passed through a low pass filter to remove the aliasing (Grosch, 1981). The cutoff frequency of the filter was 0.45 hz or a period of 2.2 sec.

International Mathematical & Statistical Libraries, Inc (IMSL) subroutines were used to compute the power spectra of each data set for each flow meter. However, a main objective of this research was to determine if a rip current was present along the groin, therefore, the time mean velocity for each flow meter was calculated to determine the steady component of the total measured velocity. The result of this analysis revealed that a weak rip current existed. The vertical structure of the mean flow showed some significant features heretofore not reported in the literature.

Current measuring devices placed in the nearshore/coastal zones measure the total velocity of the fluid flowing past or through the meter. This is expressed by:

$$u_T = \bar{u} + u' \quad (3)$$

where u_T is the total velocity measured by the device, \bar{u} is the steady component or the mean velocity, and u' is the non-steady or fluctuating component of the total velocity. If one considers u' to be the oscillatory velocity associated with the waves, then, by averaging over sufficient time interval, u' goes toward zero. Time averaging of the total velocity has been suggested by Grant and Madsen (1978) to extract the steady current component in the study of wave-current interactions in the field. Kemp and Simons (1982, 1983) used time means to determine the steady current in laboratory studies of wave-current interactions.

CHAPTER 3

RESULTS

3.1. SHAKE DOWN EXPERIMENT 11 MAY 1986

Five of the six current meters were deployed. Of these five, only the bottom, shore-normal meter (CM 1) indicated impeller rotation. Data from the remaining meters indicated no rotation of the impellers. Observations by swimmers verified that they were indeed rotating. Field checks of the electronics showed that the meters were sending signals to the data acquisition system and, in part, the system was responding. It did not, however, appear to recognize when both LED beams were simultaneously blocked (Part I), hence, it could not detect when an event had occurred. This was a problem that had not appeared in any of the laboratory tests of the electronics or during the calibration. Since the system did not recognize when an event had occurred, no impeller rotation was recorded. The problem was resolved by making the shades wider in arc length, thus ensuring the LEDs were blocked long enough for an event to be sensed by the data acquisition system. Once the modifications were made and bench tests completed, the system was ready for the field experiments. The problems encountered during the shake down did not recur in the subsequent experiments.

3.2. EXPERIMENT I, 23 MAY 86

The first full field experiment was conducted under generally calm conditions (Table I). The array was located approximately 9.5 m landward from the end of the groin and 1.5 m from the groin wall within the test compartment (fig. 3). After the flow meter array was deployed, a short test run indicated that all current meters except number 4 were functioning properly.

The average breaker wave height (H_b), based on visual estimates, was approximately 15 to 20 cm. The greatest H_b of 30 cm, occurred during runs 7 and 8 (Table I). The dominant wave direction was from the northeast which gave a breaker angle (α_b) that opened to the west throughout the day.

The top of the groin was underwater when the experiment began. The time mean shore normal currents were directed onshore and were weak, less than 1 cm/sec for runs 6 and 7. Runs 7 and 8 were taken near the time of high water. During run 8, the flow near the surface reversed and the time mean velocity increased to approximately 5 cm/sec while the flow near the bottom remained onshore and increased to 2 cm/sec.

There were a total of thirteen data runs conducted during this experiment. The bottom and mid depth meters functioned throughout the day while the top meter provided data for only the first five data runs. For the bottom meter, eleven of the thirteen runs had time mean flows directed onshore. The top and mid depth meters combined to give eight of thirteen runs with offshore directed flow.

Table I. Data summary of Experiment I, 23 May, 1986.

TABLE I Experiment I 23 May, 1986

Run/Time	Time Mean Velocity cm/sec (dimensionless depth)			Tide	H_b (cm)	α_b	Wind ° Mag. m/sec	groin
	bottom	mid	top					
6/0730	0.24 (0.85)	0.8 (0.69)	0.59 (0.33)	flood	15-18	0-5 W	318 6	covered
7/0830	0.81 (0.86)	0.23 (0.61)	0.83 (0.36)	high water	20-30	5-10 W	320-340 4-6	covered
8/0930	2.28 (0.86)	-0.7 (0.61)	-5.21 (0.36)	high water	20-30	0-5 W	315-329 4-6	covered
9/1030	1.21 (0.84)	-0.32 (0.56)	-2.65 (0.28)	ebb	15-20	0-4 W	330-350 3-4	covered
10/1130	1.66 (0.79)	0.56 (0.41)	-0.80 (0.03)	ebb	15-20	5 W	045 2	exposed
11/1230	0.18 (0.76)	1.04 (0.31)		ebb	≤15	5-10 W	230-250 3-5	exposed
12/1330	0.46 (0.70)	-0.59 (0.17)		ebb	≤15	10-15 W	280-300 5-7	exposed
13/1430	-1.09 (0.69)	-3.07 (0.14)		low water	13-20	5-10 W	290-295 5	exposed
14/1530	-1.09 (0.73)	-1.40 (0.23)		flood	10-18	0-5 W	295-310 5	exposed
15/1630	0.56 (0.78)	-2.79 (0.40)		flood	20-25	5-8 W	285-295 3-4	exposed
16/1730	1.74 (0.83)	-1.34 (0.52)		flood	15-25	5-8 W	330-340 1-2	exposed
17/1830	2.31 (0.82)	2.0 (0.50)		flood	15	0	255-275 3-4	exposed
18/1930	12.39 (0.84)	3.22 (0.55)		flood	13-18	0-3 W	070-080 2-3	awash

Note: (1) Negative velocities are offshore flow.

(2) Data are given only for those meters
whose axis is parallel to the groin
wall (i.e., shore-normal).

The near bed flow also demonstrated some dependence on the tidal current. Run 14 was early in the flood phase and the near bottom velocity was directed offshore. During run 15, the velocity diminished and reversed so that it was directed onshore. The flow steadily increased in strength through run 18. The mid meter also showed the same general pattern but began at run 15.

The opposed flow at the top and bottom meters was a common occurrence during this experiment and was noted on both flood and ebb tidal phases. Since α_b was to the west throughout the day, it was not possible to determine its influence on the structure of the flow. The existence of a seaward flowing current along the groin is verified.

3.3. EXPERIMENT II 17 JUNE, 1986

The environmental conditions during this experiment were quite variable and caused an early termination of the experiment (Table II). Initially the winds were from the WSW to W 5 m/sec. The wave approach was from the NW with α_b opening to the east approximately 10° . H_b was estimated to be 10 to 18 cm. The current meter array was in the wind and wave shadow for runs 19 through 22. The flow was offshore at all depths and weak during this time period. The top of the groin was initially exposed.

Between runs 22 and 23 at approximately 1045, the tide began to flood and the winds shifted to the NE and strengthened. In response, the wave approach shifted to the NE and α_b opened to the west. H_b began a steady increase from 10

Table II. Data summary for Experiment II, 17 June, 1986.

TABLE II Experiment II 17 June, 1986

Run/Time	Time Mean Velocity cm/sec (dimensionless depth)			Tide	H_b (cm)	α_b	Wind ° Mag. m/sec	groin
	bottom	mid	top					
19/0709	-0.81 (0.82)		-1.49 (0.18)	ebb	10-18	10-15 E	240-255 4-5G7	exposed
20/0800	0.15 (0.80)		-0.78 (0.11)	ebb	10-18	5-10 E	240-260 5-6	exposed
21/0900	-1.07 (0.79)		-2.49 (0.02)	ebb	10-15	7-9 E	275-290 5-6	exposed
22/1000	-1.34 (0.78)			low water	8-13	1-5 E	290-300 3	exposed
23/1100	0.68 (0.78)	-1.25 (0.39)		flood	10-15	3-5 E/W	035-045 4-5	exposed
24/1221	3.55 (0.81)	-5.63 (0.48)		flood	25-30	5-10 W	040-045 6-7	exposed
25/1300	4.78 (0.82)	-12.61 (0.52)		flood	38-51	3-7 W	040-045 8	exposed
26/1400	1.98 (0.86)	-10.49 (0.62)		flood	46-61	5-10 W	045 8-9	over- topped

Note: Negative velocities are offshore flow.

to 15 cm in run 22 to approximately 1 m by late afternoon. As H_b increased, the waves began to break further offshore. Late in the afternoon, the waves were breaking beyond the end of the groin, reforming and then breaking near the beach. The test compartment was essentially within the surf zone at this time. Unfortunately, the flow meters were fouled with seaweed and no data were available for the period of peak wind and wave intensities.

The vertical structure of the flow changed after the wind and wave direction shifted and H_b increased. A net shoreward movement of water was along the bottom while continued offshore flow was measured at mid-depth. The magnitude of onshore and offshore velocities increased as H_b increased. As waves began to overtop the groin in run 26, velocity magnitudes for the mid-depth meter diminished. At this point, the bottom meter became fouled and its data are unuseable. It is not clear if the time mean flow continued to diminish as the water level continued to rise above the top of the groin.

It was noted that the offshore flow was against a brisk wind. Drift wood placed near the groin also tended to move offshore against the wind and the waves. Additionally, swimmers reported an offshore drift when checking the current meters. These observations, during relatively high waves, support the continued existence of the seaward flowing current along the groin.

The data also indicate that the strength of both the onshore flow near the bed and the offshore flow in the upper levels was directly proportional to H_b . From run 23 through run 26, H_b increased from 10-15 cm to 46-61 cm. The offshore

flow increased in magnitude from -1.25 cm/sec in run 23 to a peak of -12.61 cm/sec in run 25. The offshore velocity diminished somewhat in run 26 when the waves began to overtop the groin. The near bed velocity increased 0.68 cm/sec in run 23 to 4.78 cm/sec in run 25. In run 26 the meter was fouled with seaweed and the data were not useable.

Between the hours of 1600 to 1800, water level rose above the groin top. Unfortunately, data are not available to determine how the rip current velocity changed. During this period, the longshore current became quite noticable. It was manifested by the strong pull on the cables from the flow meters to the data acquisition system ashore.

3.4. EXPERIMENT III, 19 JUNE, 1987

Winds for the third experiment were quite calm from the SSW to SW, 4-5 m/sec (Table III). H_b was on the order of 5-13 cm on average with only one period, run 41, where the waves exceeded 15 cm. The breaker angle was small and opened to the west. Only the mid-depth current meter functioned reliably during this experiment.

The flow at mid-depth was offshore at most hours throughout the day and was stronger during the flood tide than during the ebb. The current velocity decreased between runs 41 and 42 when the water level rose above the top of the groin.

Shortly after low water and early in the flood stage of the tidal cycle, an interesting phenomena was visually observed. About five minutes before the

Table III. Data summary for Experiment III, 19 June, 1986.

TABLE III Experiment III 19 June, 1986

Run/Time	Time Mean Velocity cm/sec (dimensionless depth)			Tide	H_b (cm)	α_b	Wind ° Mag. m/sec	groin
	bottom	mid	top					
31/0700		0.57 (0.64)		ebb	8-10	0-3 W	180-220 2-4	covered
32/0800		0.02 (0.60)		ebb	8-10	0-3 W	185-210 3-4	exposed
33/0900		-0.95 (0.52)		ebb	5-10	0	195-220 4-5	exposed
34/1000		-0.97 (0.50)		ebb	5-10	0	205-225 2-5	exposed
35/1100		-0.69 (0.41)		ebb	5-10	2-3 E	305-310 3	exposed
36/1200		-0.52 (0.36)		low water	5-13	0-2 E	220-260 3	exposed
37/1300		-0.95 (0.38)		low water	3-10	0	195-230 4-5	exposed
38/1359		-4.21 (0.45)		flood	5-10	0-3 W	100-130 1-2	exposed
39/1500		-6.34 (0.54)		flood	8-13	0-3 W	195-235 4-6	exposed
40/1600		-5.42 (0.58)		flood	8-13	2 E/W	205-235 3-5	exposed
41/1700		-4.33 (0.61)		flood	15-20	2-5 W	210-240 4-6	awash
42/1800		-2.61 (0.65)		flood	8-13	0-2 W	205-240 3-4	covered
43/1900		-2.79 (0.67)		flood	8-13	0-2 W	190-220 5-6	covered

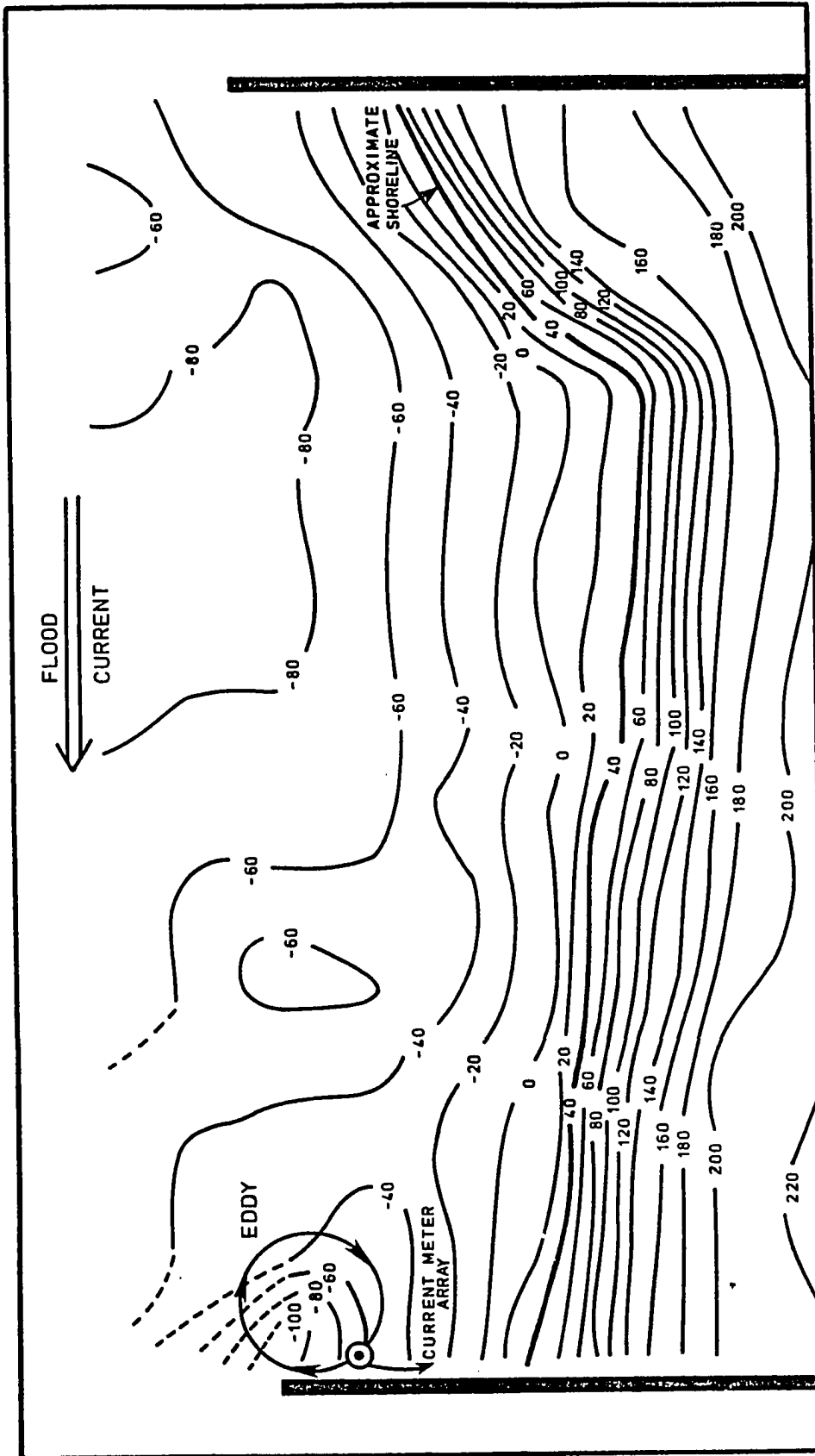
Note: Negative velocities are offshore flow.

scheduled data run, a small eddy formed on the upstream (relative to the tidal current) wall of the groin and near the end. This eddy moved seaward and was advected to the west by the tidal current. A second eddy formed in the same location as the first and was also advected downstream. At approximately 1359 hours, a third, much larger and stronger eddy formed. This eddy also moved seaward and was advected by the tidal current. The third eddy had a turbulent, swirling appearance where it formed and this appearance continued as the eddy moved with the currents. The rotational direction could not accurately be determined.

Figure 4 depicts the relative location where the eddies formed. The current meter array was positioned near the edge of the largest eddy. The data run 38 was started earlier than planned to measure the currents associated with the eddy (Figure 5). The first portion of the record, up to approximately 400 seconds, shows the strong influence of the eddy near the end of the groin. The most notable feature is the strong offshore velocities associated with the eddy, about 15 cm/sec. The wave orbital velocities were 7-10 cm/sec. The period of eddy formation and shedding from the current record is approximately 100 seconds. After the episode of eddy formation and the shedding of those eddies, net flow remained in the offshore direction with some indication of a long period oscillation that may not have been associated with eddy activity.

The data from run 39 appears to have eddy-like activity although no eddies were visually observed (Figure 6). The period of formation and shedding is 60-70 seconds. Note that the seaward flowing current was strong apparently enough to

Figure 4. Diagram showing the general location of the eddies and the bathymetry of the comartment.



M.N. 4

5-23-86

ELEVATION IN CENTIMETERS



Figure 5. Velocity data from run 38 showing the velocities associated with the eddy.

Run 38

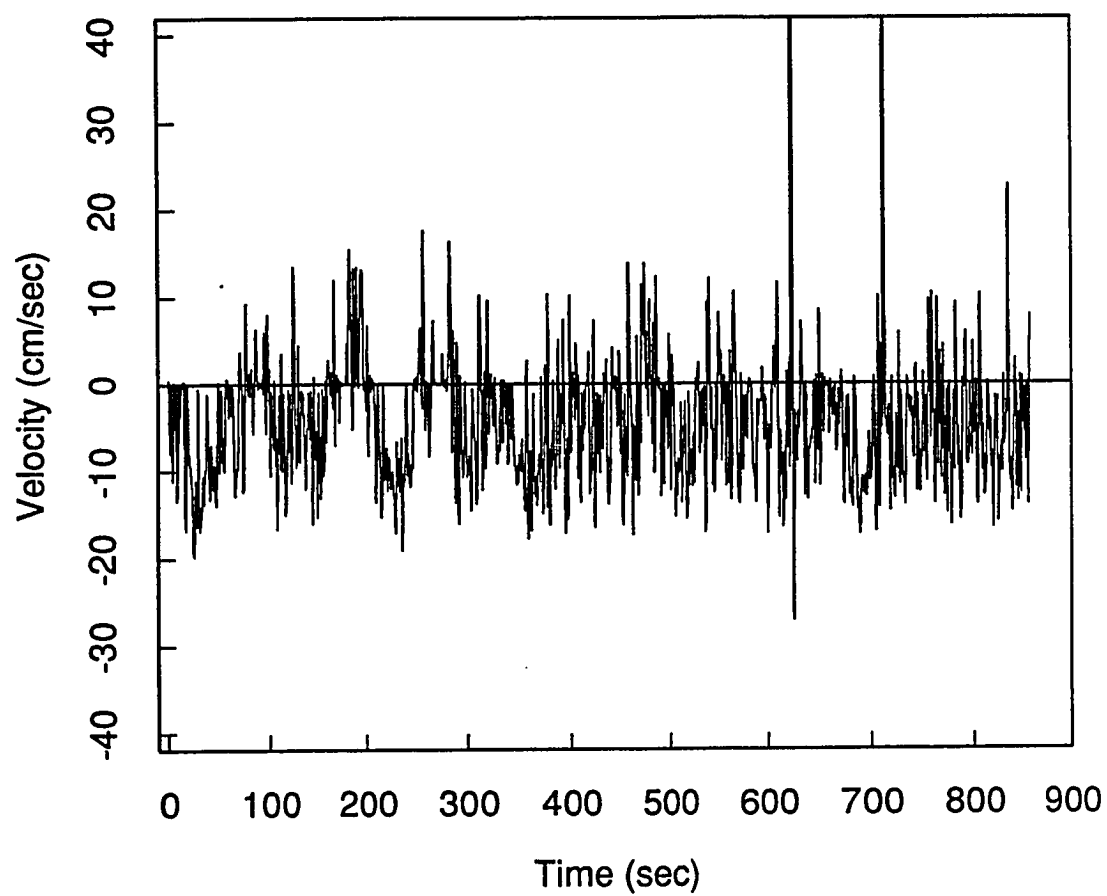
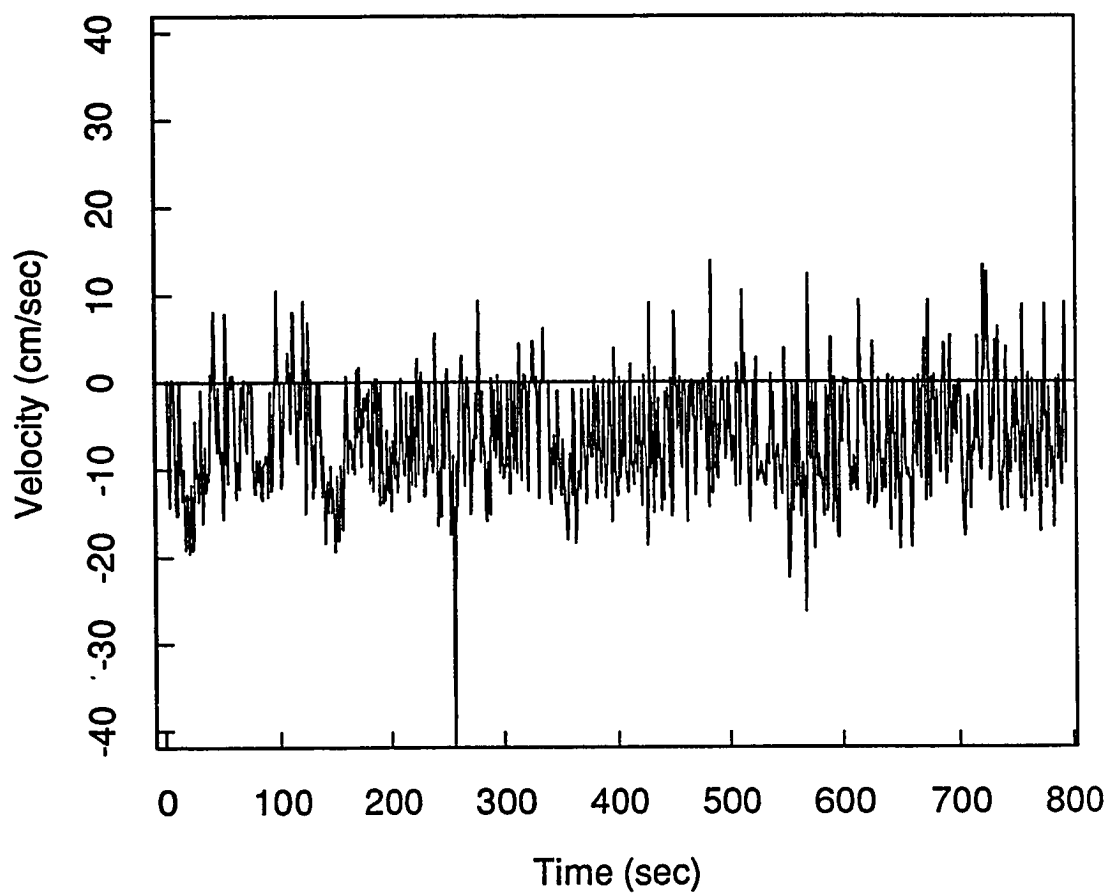


Figure 6. Velocity data from run 39.

Run 39



offset the wave orbital velocities such that only the strongest wave velocities produced a net onshore motion.

3.5. EXPERIMENT IV, 27 JUNE, 1986

Experiment IV was conducted on 27 June, 1986 (Table IV). The current meters for this experiment were all aligned parallel to the groin (i.e., shore normal). The array was positioned 4 m landward from the end and 2 m from the wall of the groin. Of the five meters deployed, only the bottom three functioned. The center meter, CM 2, was inconsistent with the meters above and below it. During this experiment, CM 2 showed smaller time mean velocities than the meter above or below it and on one occasion (run 52) it had a greater velocity than the other two meters. Since this meter did not calibrate as well as the others (Part I), it is not clear if this is a reflection of the actual conditions or if it is due to the performance of the meter. The data from this meter, therefore, is used only in a qualitative sense in the following analysis.

Winds were from the SSW to WSW, 3-5 m/sec. H_b was generally less than 15 cm with α_b opening to the west during flood and to the east during ebb. The time mean flow was offshore at all depths throughout the day. The flow was generally stronger during flood than ebb.

Between run 49 and run 50, there was a significant reduction in the current velocity at all depths. During run 49, the water level was below the top of the groin with occasional wave overtopping. The water level in run 50 was at or

Table IV. Data summary for Experiment IV, 27 June, 1986.

TABLE IV Experiment IV 27 June, 1986

Run/Time	Time Mean Velocity cm/sec (dimensionless depth)			Tide	H_b (cm)	α_b	Wind	groin
	bottom	mid	top				° Mag. m/sec	
44/0700	-0.55 (0.77)	-0.21 (0.56)	-0.54 (0.30)	ebb	8-10	5-10 E	215-240 4-5	exposed
45/0800	-1.25 (0.76)	-0.47 (0.53)	-0.65 (0.26)	low water	8-15	2-5 E	205-220 4-5G7	exposed
46/0900	-2.08 (0.78)	-0.92 (0.58)	-2.74 (0.33)	flood	5-10	5-7 E	205-220 3-4G7	exposed
47/1000	-5.12 (0.81)	-1.62 (0.64)	-7.13 (0.42)	flood	5-8	0-10 E	230-255 4-5	exposed
48/1100	-7.34 (0.84)	-1.98 (0.69)	-9.58 (0.50)	flood	8-13	2-5 W	210-255 4-5G7	exposed
49/1200	-7.40 (0.86)	-4.48 (0.73)	-8.69 (0.57)	flood	8-13	0-5 W	195-235 3-5G7	exposed
50/1300	-2.98 (0.87)	-2.0 (0.74)	-3.09 (0.59)	flood	5-13	3 E/W	220-250 3-5	awash
51/1400	-2.80 (0.87)	-2.1 (0.75)	-3.07 (0.61)	high water	8-15	2 E/W	220-250 3-5G7	covered
52/1500	-0.68 (0.87)	-1.16 (0.75)	-0.80 (0.60)	ebb	10-15	0	210-250 4-5	covered
53/1600	-0.58 (0.86)	-0.96 (0.73)	-1.35 (0.56)	ebb	10-15	3-5 E	210-235 5G8	exposed
54/1700	-1.86 (0.83)	-0.84 (0.68)	-1.46 (0.49)	ebb	10-18	0-5 E	200-230 4-6	exposed
55/1800	-2.28 (0.81)	-1.50 (0.63)	-2.58 (0.41)	ebb	10-15	0-3 E	190-220 4-5G7	exposed
56/1900	-5.47 (0.77)	-3.99 (0.56)	-5.67 (0.30)	ebb	8-10	0-3 E	215-230 4-7	exposed

Note: Negative velocities are offshore flow.

slightly higher than the top of the groin and waves were freely washing over the groin.

Eddies were observed visually on three separate occasions when the water level was below the top of the groin. Two of the episodes occurred during regular data runs (46 and 56) and the third was between runs 48 and 49 at about 1130 hours.

The first episode was during run 46 when a small eddy was observed to form on the upstream (east) wall of the groin shortly after the tide began to flood. Figures 7-9 show the velocity measurements from this run. The velocity for the weak eddy that formed shortly after the run began shows the same general character as the eddy measured during the previous experiment (figure 5). Five to six minutes into the run, a weak eddy was again observed and detected in the velocity records at all three levels, where it is manifested as pulses of strong offshore flow (Figure 9).

The second episode of eddy activity was between runs 48 and 49. A swimmer (the author) determined that the eddy rotated in a clockwise fashion. This confirmed the tentative visual observations of previous eddies reported in this study and by Kang (1986). This eddy was strong enough to require an extra effort by the swimmer to avoid being carried into the groin wall. The eddy moved seaward and into the tidal current which advected it to the west.

The third episode occurred during run 56. Figures 10-12 are plots of the velocity data for current meters 1-3 respectively. The tide was ebbing during this

Figure 7. Velocity data from run 46, current meter 1 (bottom meter).

Run 46 CM 1

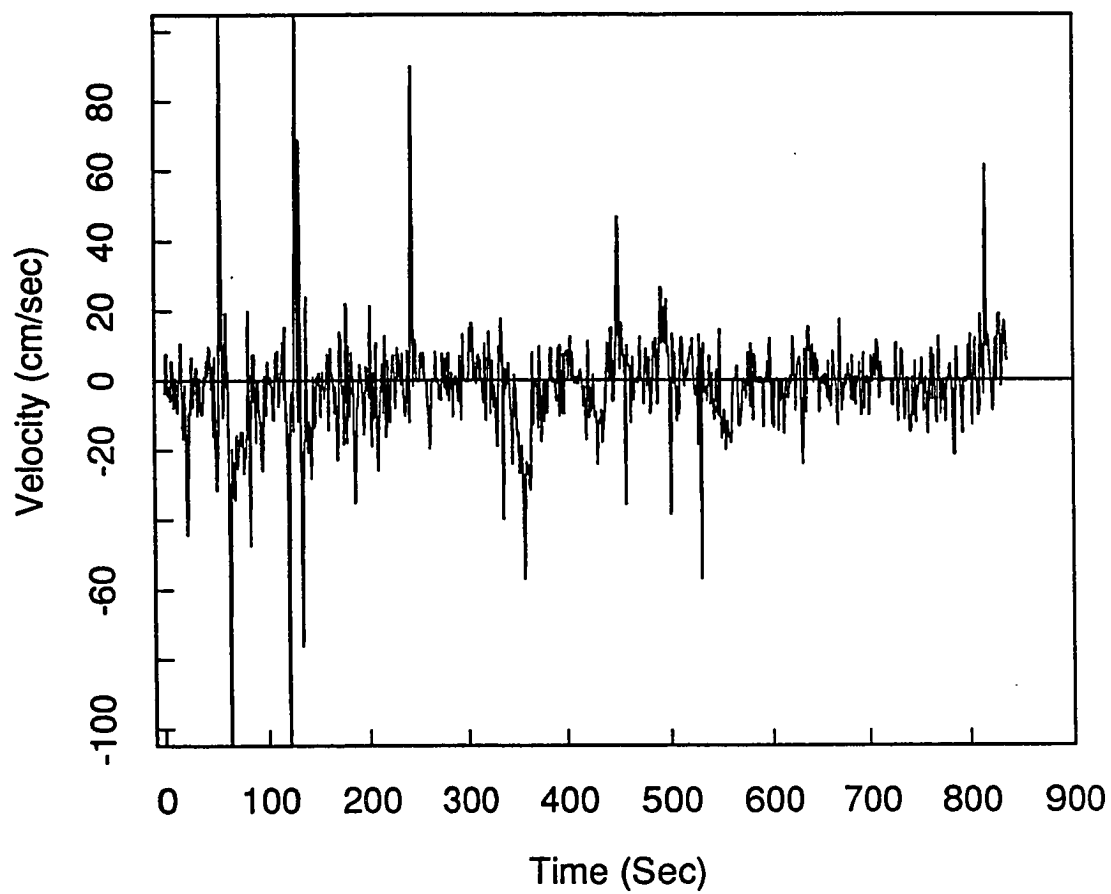


Figure 8. Velocity data from run 46, current meter 2 (mid depth meter).

Run 46 CM 2

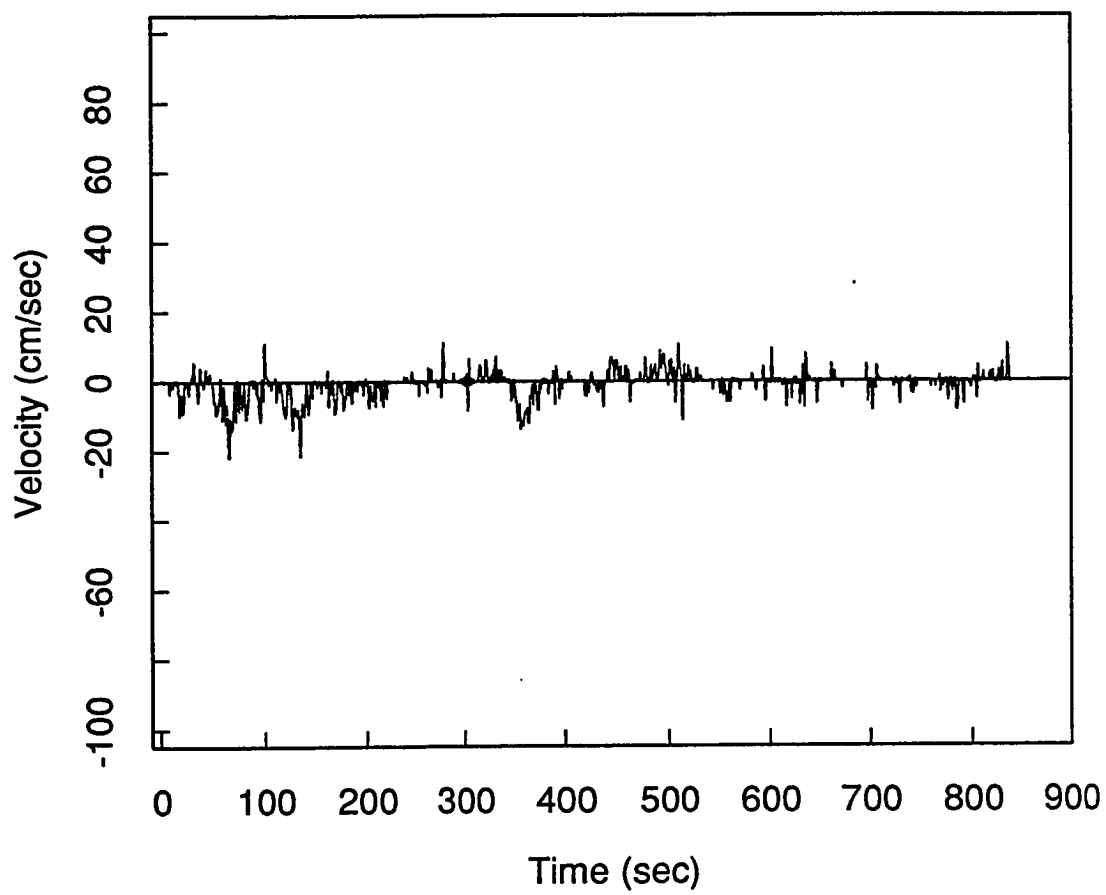


Figure 9. Velocity data from run 46, current meter 3 (top meter).

Run 46 CM 3

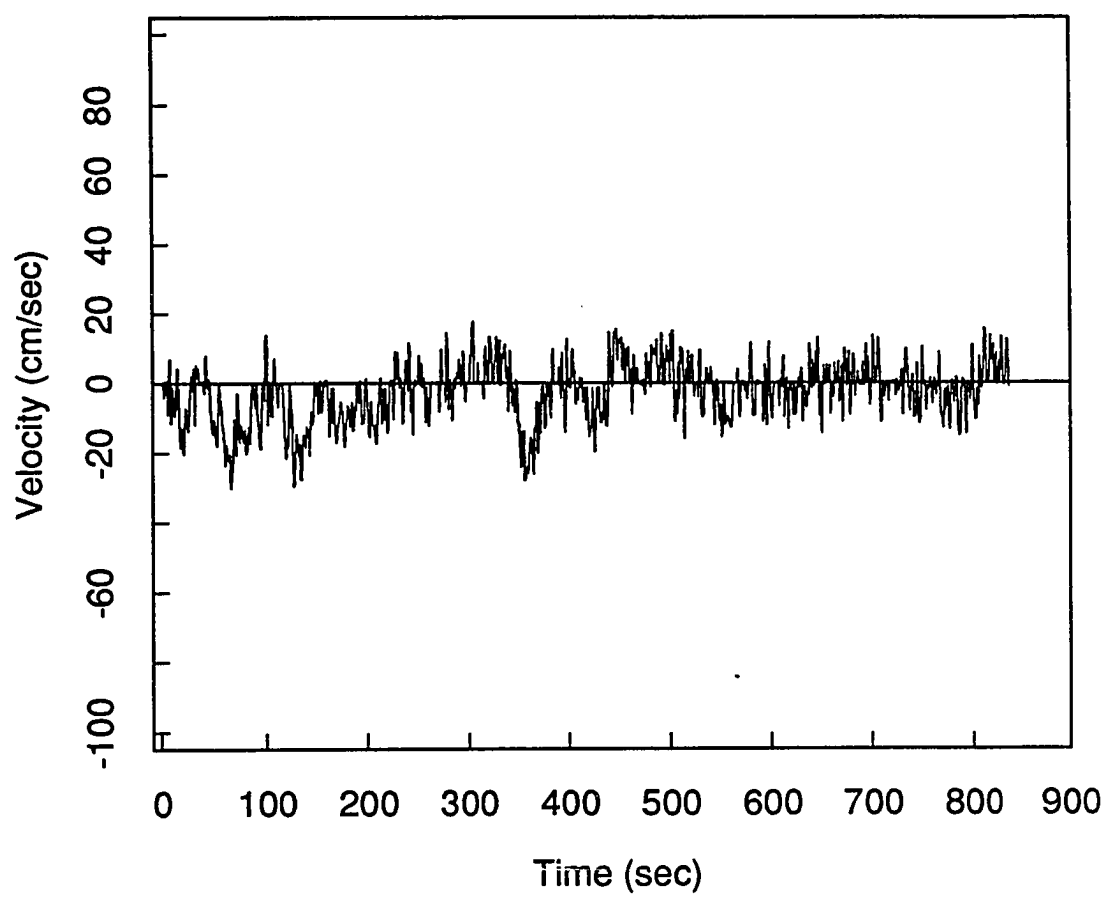


Figure 10. Velocity data from run 56 current meter 1 (bottom meter).

Run 56 CM 1

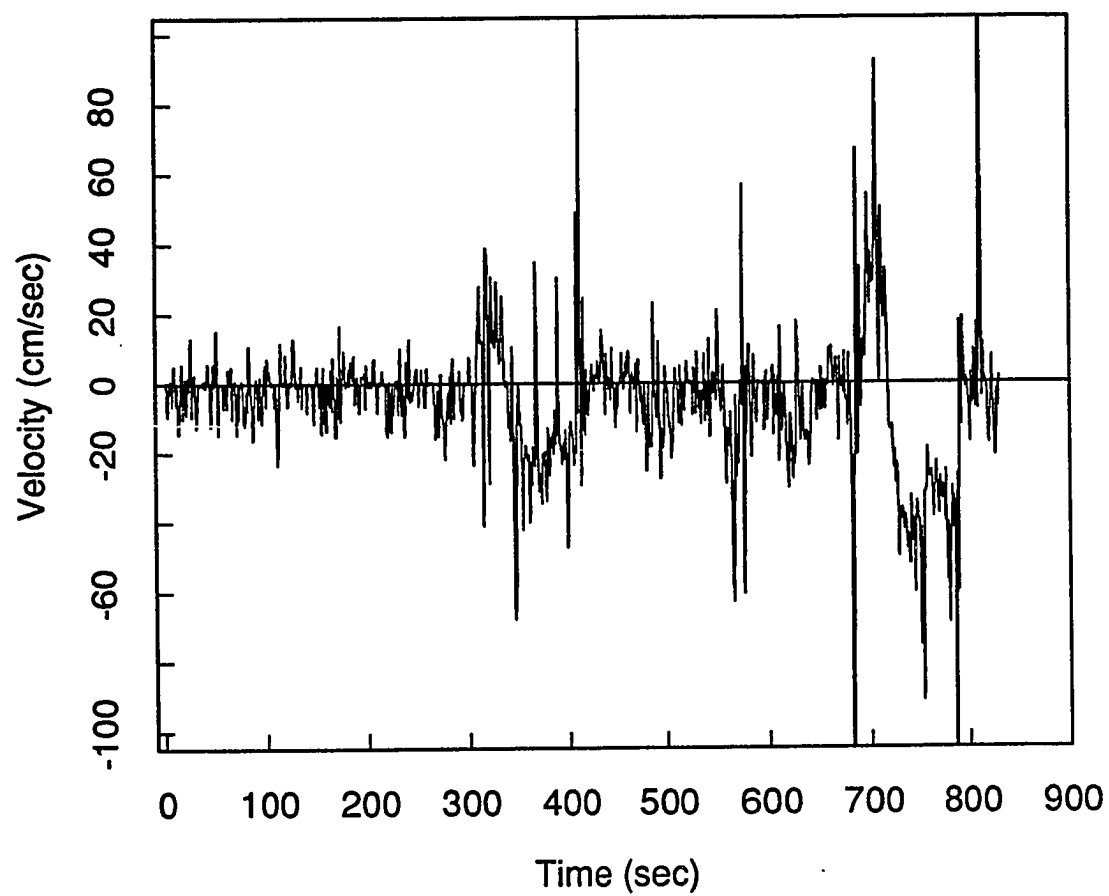


Figure 11. Velocity data from run 56 current meter 2 (mid depth).

Run 56 CM 2

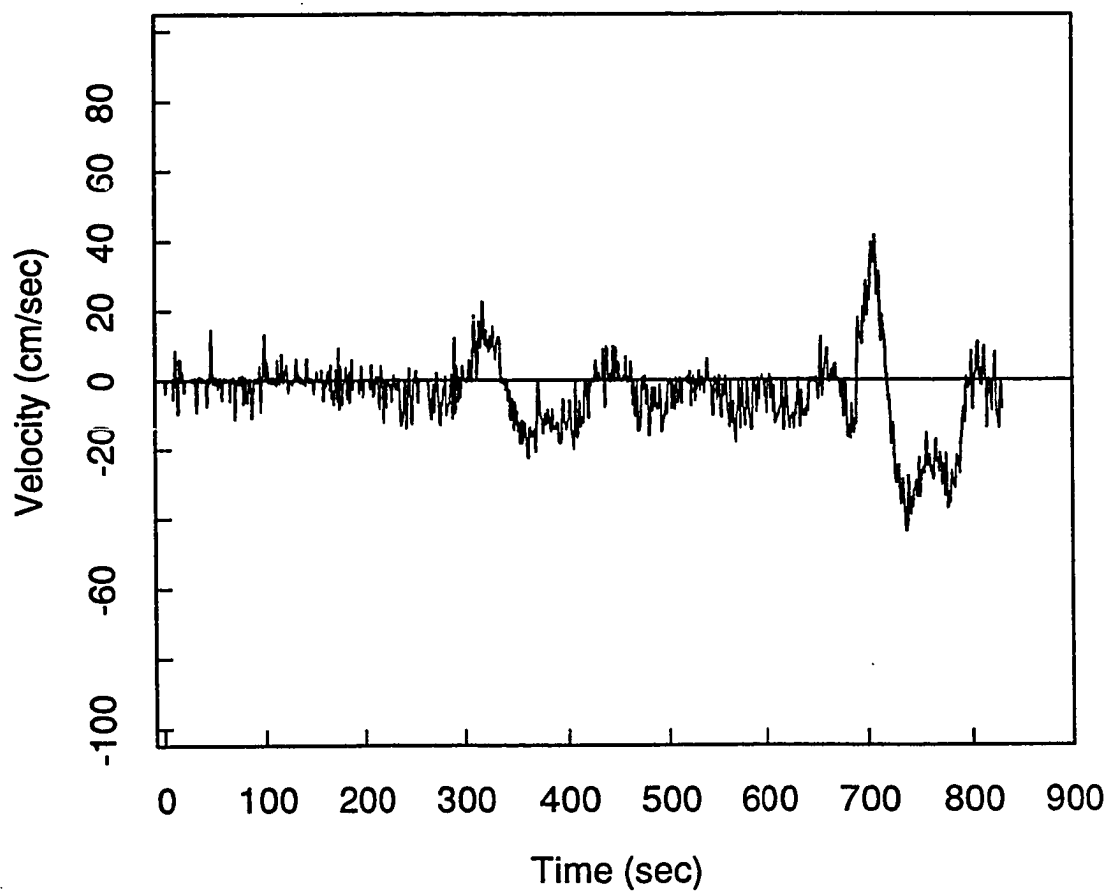
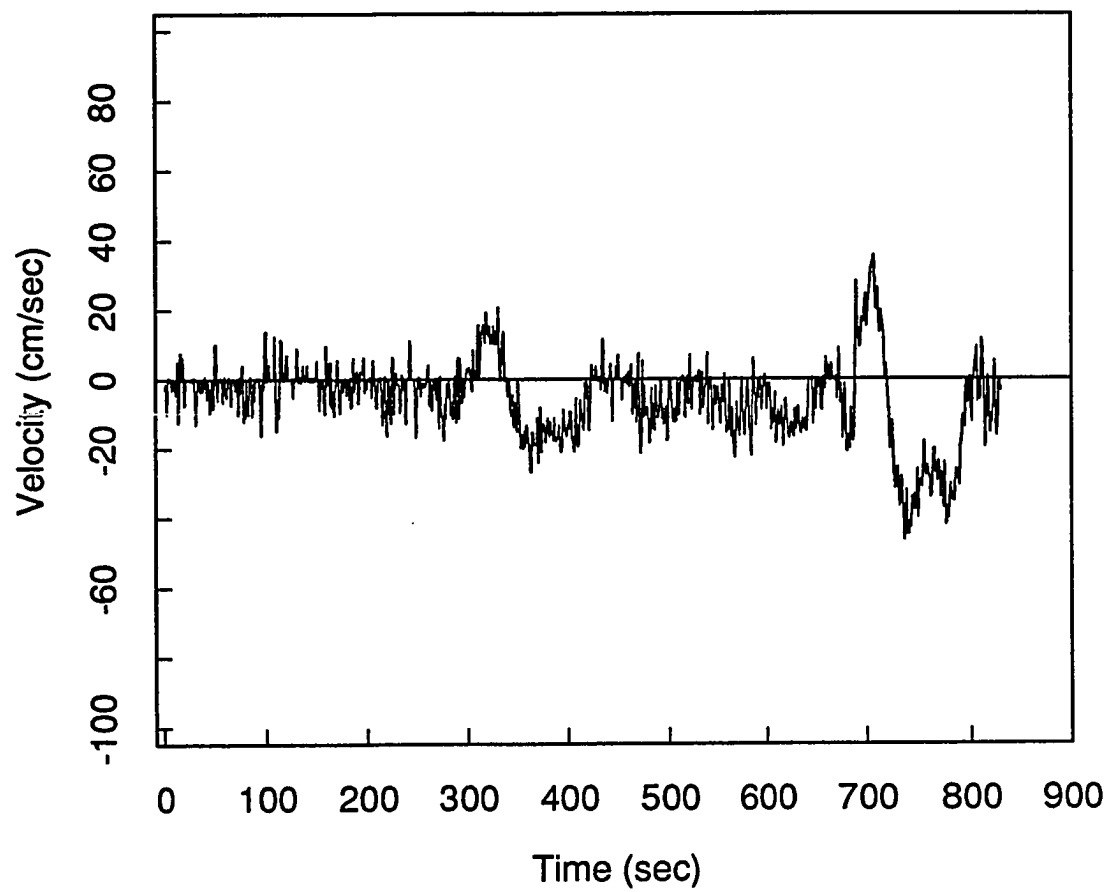


Figure 12. Velocity data from run 56 current meter 3 (top).

Run 56 CM 3



run and was the first time eddies had been observed during this tidal phase. Visual observations indicated that the rotation was clockwise and this finding is confirmed by the interpretation of the data records. The eddies formed on the upstream (relative to the ebb current) wall of the groin. In this case on the west wall of the groin in the adjacent compartment. Two eddies were formed and were shed into the tidal flow and then migrated to the northeast with the ebb current.

The velocity data shows that initially (at $t = 325$ sec) there is a strong onshore flow followed by a strong offshore flow. This is consistent with an eddy rotating in the clockwise direction. As the eddy moves from the west wall and around the groin, the initial current is onshore as the leading edge of the eddy passed the groin. As the eddy continues its motion to the east, the trailing edge of the eddy had an offshore motion roughly equal in magnitude to the onshore motion.

3.6. DATA SUMMARY

The data from the four experiments show a weak seaward flowing rip current along the groin wall. Two mechanisms are proposed for the generation of the seaward flow along the western groin in the test compartment. The first occurs when α_b opens to the west and is fundamentally related to the mass transport of water into the compartment by wave action. The second mechanism is associated with longshore variation in wave set-up as a result of wave diffraction around the groin end when α_b opens to the east. The vertical structure of the rip current can be complex and often has a flow reversal near the bottom. The intensity of the

offshore flow near the surface and the onshore flow near the bed appears to be directly proportional to H_b . The tidal flow around the ends of the groin can generate strong, clockwise rotating eddies on the upstream wall relative to the tidal current.

CHAPTER 4

DISCUSSION

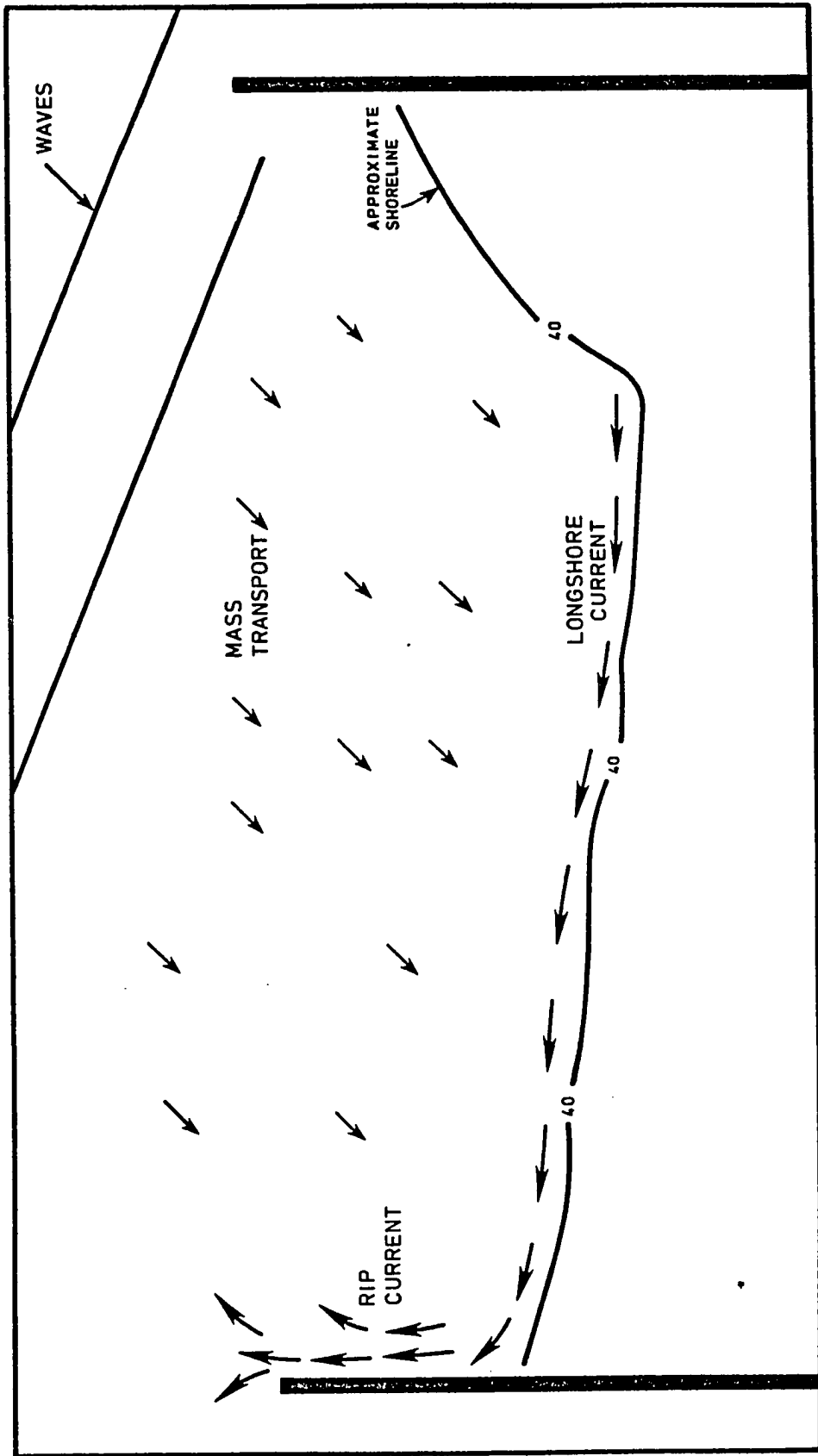
4.1. RIP CURRENT ALONG THE GROIN WALL

4.1.1. PREVIOUS DEVELOPMENT

Previous investigators have stated that a rip current may be expected along the groin wall that is downstream relative to the direction of longshore transport (e.g., SPM, 1984; Silvester, 1974; or Wiegel, 1964). Nevertheless, few, if any, field studies have been conducted to verify their existence. Most studies have either used physical models or mathematical models to study groin dynamics and often do not consider the details of flow within a groin compartment. In these studies, the shape and position of the shoreline is considered without reference to the driving forces that act to produce that shoreline.

Rip currents arise when the mass transport due to waves brings water into the groin compartment. Conservation of mass in the compartment dictates a return flow. This is in the form of a rip current that forms along the wall of the downstream groin (Figure 13); (SPM, 1984). This approach is fairly simple and straight forward. Wave diffraction at the groin ends is not considered nor are tidal currents, which are an important factor in the estuarine environment. There is evidence from the data gathered during the present study that wave diffraction may cause an along shore variation in wave set-up that can become great enough to

Figure 13. Diagram of the rip current generated as a result of mass transport into the compartment.



generate a weak rip current. The former case will be discussed first.

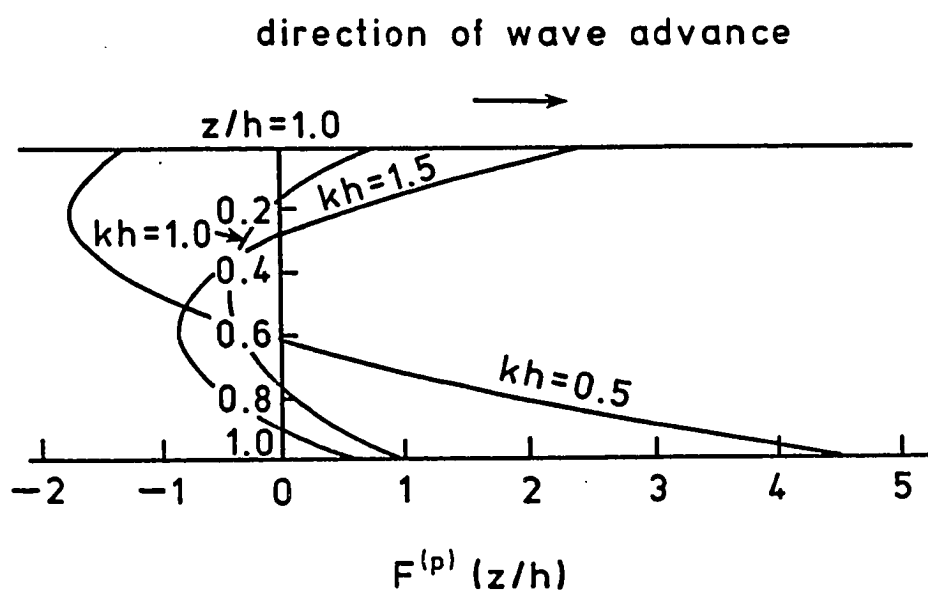
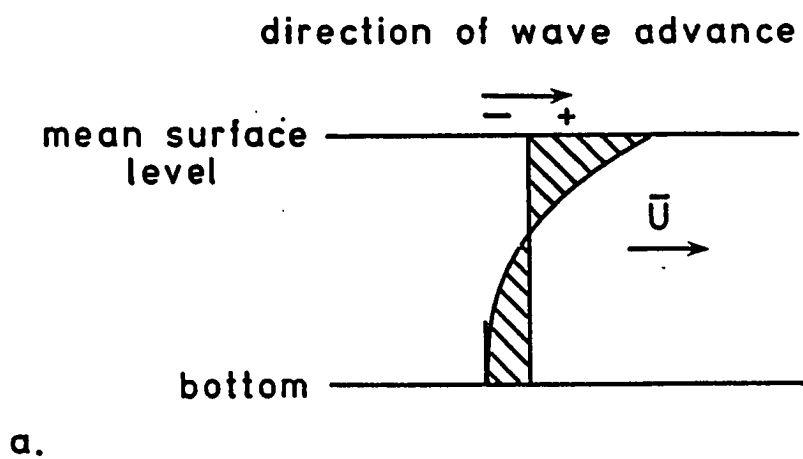
Mass transport by waves brings water into the groin compartment. If there is limited or no exchange of water with the adjacent compartments, this transport must be balanced by an offshore flow of water, generally in the form of a seaward flowing rip current along the downstream groin relative to the longshore current.

Stokes (1847) second order wave equation gives a small drift in the direction of wave propagation. His theory assumes small amplitude waves in an inviscid fluid in deep water (Figure 14a).

Longuet-Higgins, (1953) developed a theory for mass transport for laminar flows where viscosity is considered. Implicit to his development is that there is no horizontal motion perpendicular to the direction of wave advance (i.e., a narrow channel) and that there is no net transport in the vertical cross section. Figure 14b shows the various shapes of the velocity profile for Longuet-Higgins conduction solution. This figure has been widely referred to in the scientific literature and has given rise to the concept of the "mid-depth return" in coastal studies. In all cases, the drift velocity near the bottom is in the direction of wave propagation. In comparison, if the Stokes drift velocity is adjusted for the no net transport condition, flow near the bottom is counter to the direction of wave propagation.

Russell and Osorio (1958) conducted laboratory experiments in a closed channel and verified Longuet-Higgins theoretical development. They also found that the drift velocity near the bottom was always in the direction of wave propagation.

Figure 14. Velocity profiles of the mass transport due to waves for a Stokes second order wave (a) and from Longuet-Higgins (b). (From Longuet-Higgins, 1953).



One important deviation from the theory in their investigation occurred when the water depth was small compared to the channel width. This is a condition more likely to be encountered in the field studies of groins. In this case, Russell and Osorio found evidence for large scale horizontal circulation pattern with greater forward drift down one side of the channel than the other.

Other investigators have developed theories for wave drift velocities based on various wave theories. Gonsalves and Swart (1982) developed a theory based on vocoidal wave theory. A vocoidal wave becomes an Airy wave in deep water and approximates a solitary wave in shallow water. They used the data of Russell and Osorio (1958) to compare with their theory and found that when viscosity is included, their development gave greater near-bed drift velocities than Longuet-Higgins (1953) in deep water and smaller velocities when in shallow water. In deep water, the velocity profile reduced to that predicted by Stokes for both the viscous and non-viscous solutions. Isaacson (1976) developed a theory for mass transport using cnoidal wave theory which is based on the shallow water approximation. Isaacson (1978) tested his theory and others for the transport near the bed using laboratory data. He concluded that the theoretical developments, both his and others, gave reasonable results for the near bottom mass transport but that when the boundary layer was turbulent, they were less reliable. Unfortunately, a turbulent boundary layer is most likely to be encountered under field conditions.

The above developments were for waves propagating in a narrow, closed channel and no net transport. These restrictions are seldom, if ever, encountered in

the coastal environment and are not encountered in the present study. The theoretical velocity profiles are therefore of questionable use for field applications where one encounters an open beach. The net mass transport in this case is probably in the direction of wave propagation or the shoreward direction. Mass balance is achieved by two-dimensional circulation patterns that often include a seaward flowing rip current. The rip current spacing for ungroined beaches is governed by the locations of edgewave nodes, along shore variations in wave set-up, or by topographic variations along the shore.

The groins of a groin system act as barriers to the longshore current whenever the water level is below the top of the groin. The longshore current turns seaward and flows offshore along the groin wall as a rip current whose intensity is, in part, a function of H_b , α_b , and wind velocity (Figure 13). The steady current near the groin was extracted by calculating the time mean velocity of the flow meters parallel to the groin. The meters perpendicular to the groin generally had zero or near zero velocities for most data runs and were not included in the analysis. The exception was when the water level was above the top of the groin.

One of the primary variables affecting mass transport is the wave amplitude. For example, Longuet-Higgins found the near bed drift velocity to be:

$$\bar{U} = \frac{5}{4} \frac{a^2 \sigma k}{\sinh^2 kh} \quad (4)$$

where \bar{U} is the mean velocity near the bottom, a is the wave amplitude, $k = \frac{2\pi}{L}$,

$\sigma = \frac{2\pi}{T}$, h is the depth, T is the wave period, and L is the wave length. From eqn

4, one can readily see that the drift velocity near the bed is directly proportional to the square of the amplitude. The implication for the rip current in the groin compartment is that as the wave height increases, the water transported into the compartment also increases which should be balanced by an increase in the rip current velocity.

4.1.2. DISCUSSION OF DATA

Data from experiment II shows that from runs 23 to 26, the estimated H_b steadily increased from approximately 10-15 cm to 56-61 cm. The measured offshore velocity for the upper flow meters increased from 1.25 cm/sec to 12.61 cm/sec in run 25. The offshore velocity decreased somewhat in run 26 and is attributed to the fact that the wave crests began to overtop the groin. During the same time period, the wind was from the NE and increased in speed from 4-5 m/sec to 8-9 m/sec. The swimmer reported an offshore current when checking the array after runs 25 and 26. Drift wood placed near the groin wall and the beach face moved steadily offshore against the wind and wave action. The bottom meter had a net current that flowed onshore and intensified from run 23 through run 25 (Table II). This is attributed to the mass transport by waves having a greater influence on the near bottom current.

The affect of α_b on the offshore flow appears data to be more dependent on direction than on magnitude. Stronger offshore flows generally occur when α_b opens to the west than when it opens to the east. In general, the data in Tables I-

IV show that the currents were stronger when α_b opened to the west than when it opened to the east. Also note that flow reversal near the bottom occurred only when α_b opened to the west.

The strength of the rip current as a function of the water level relative to the top of the groin is not as straight forward as expected. As a first approximation, one would expect that, if the water level were initially above the groin, the offshore flow would become stronger as the water level falls below the top of the groin during ebb tide. During the following flood tide, the rip current is expected to remain relatively strong until the water level again overtops the groin, at which time the velocity would decrease. The offshore current did indeed show such a pattern on flood tide as the water level overtopped the groin. This can be seen in Tables I-IV between runs 16 and 17, 25 and 26, 41 and 42, and 49 and 50. However, only once did the current increase as the ebb tide brought the water level below the top of the groin. This may be because the flood current has a small component directed into the compartment (Ludwick, 1987). This would increase the transport of water into the compartment over and above the transport due to waves. The rip current would then become stronger to achieve mass balance in the groin compartment. The result is that the offshore flow tends to be stronger during flood than ebb.

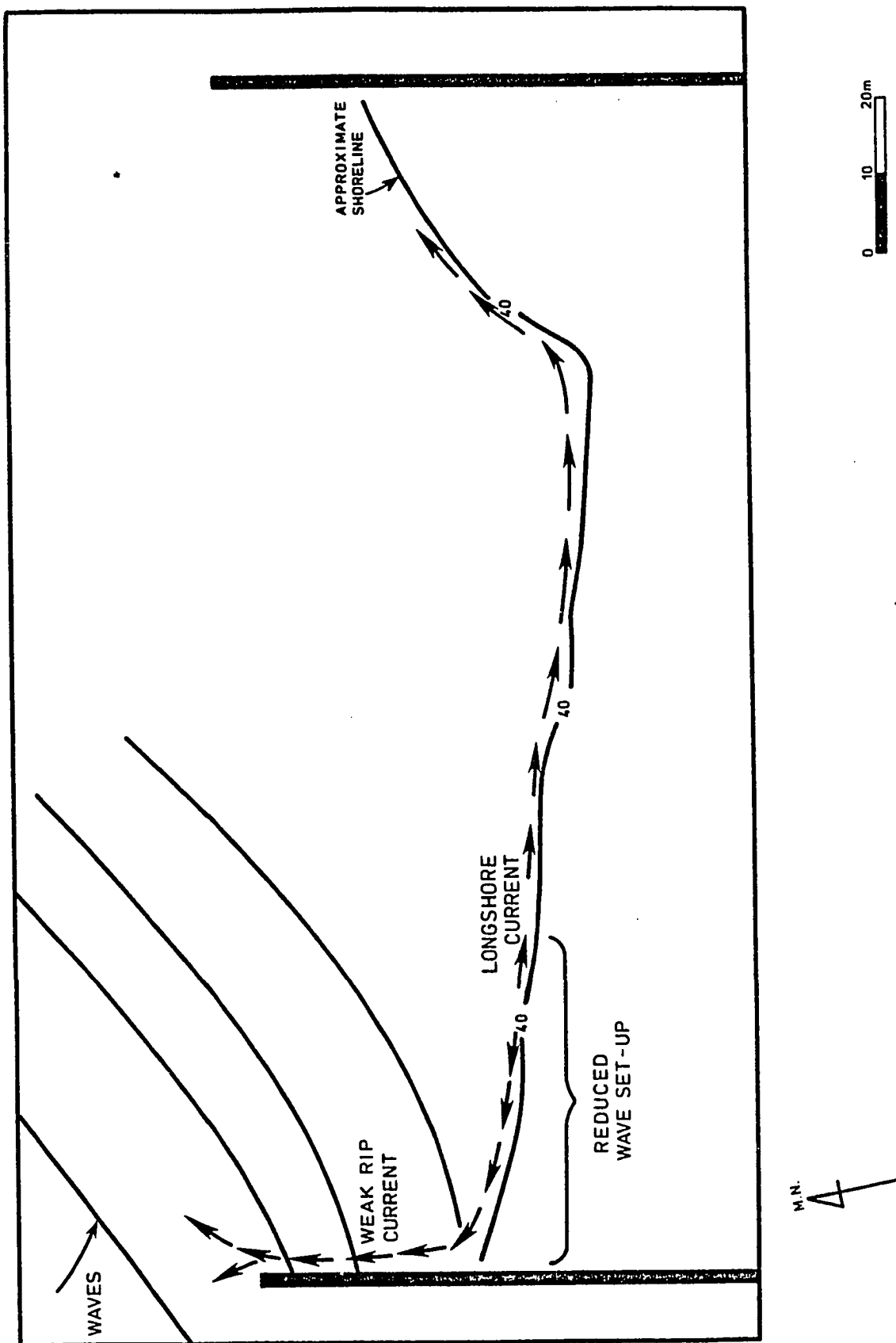
The circulation patterns in the groin compartment and the rip current were not only a function of mass transport by waves, but also a function of wave diffraction around the end of the groins. Along shore variations in wave set-up could be

produced by the reduction in wave height in the regions affected by diffraction. Reynolds (in preparation) showed that in the test compartment there can be an along-shore increase in wave height as one moves from the up-wave groin to the down-wave groin. If this variation is large enough, it could drive a longshore current in the opposite direction of α_b (Figure 15).

The general conditions for the morning of Experiment II and throughout Experiment IV were conducive for this type of flow near the west groin of the compartment where the flow meter array was located. In both cases, the waves were breaking with an α_b opening to the east. Waves entering the compartment would then be diffracted around the end of the groin where measurements were being taken. This condition is similar to the second possible mechanism for rip current generation in a groin compartment given by Dean (1978) and quoted in SPM (1984). Dean's basic premise is that wave sheltering by the up-wave groin causes the wave set-up to be reduced in the lee. A circulation cell is induced within the compartment with offshore flow on the lee side of the up-wave groin.

During runs 19 through 22, α_b opens to the east (Table II). The time mean flow at all depths is offshore with the exception of the bottom meter in run 20, which is near zero. A flow reversal with depth from offshore at the surface to onshore near the bed does not occur until α_b opens to the west in run 21. On June 27, (Table IV), α_b opened to the east for most of the day except runs 48 and 49. The wind was blowing offshore throughout the day. The time mean flow was offshore at all depths the entire day. Although wave height measurements along

Figure 15. Diagram of the rip current generated as a result of wave diffraction around the groin end.



N

0 10 20m

the shore were not taken, one would expect wave diffraction to reduce the wave height in the region near the groin which would result in less wave set-up near the groin.

No flow reversal with onshore flow near the bed and offshore flow at higher elevations occurred when α_b opened to the east on either June 17 or June 27. The reduction in wave height by refraction may have reduced the near bed mass transport so that it was overwhelmed by the net offshore flow. However, more data are needed to better define the flow dynamics under these conditions.

The wind was blowing offshore during experiment IV and the morning of experiment II. This would tend to enhance the offshore flow. However, the strongest offshore flow occurred in the afternoon of the 17 June in the face of a strong opposing wind. It is not possible from the data to isolate the effects of wind on the offshore flow.

To summarize, return flow along the groin wall was measured under two distinct wave conditions. The first was when α_b opened to the west. Mass transport due to wave action brings water into the groin compartment which flows to the west as the longshore current. This current encounters the groin wall and flows seaward as a rip current. The rip current serves to balance the influx of water into the compartment. The strength of the rip current appears to be related to the H_b , to the water level in relation to the top of the groin, and the direction of the tidal current. For H_b greater than about 15 cm and α_b opening to the west, there is a flow reversal from offshore in the upper layers to a net flow shoreward at the

bottom meter. For greater wave heights, there is evidence that the onshore bottom flow also becomes stronger presumably as a result of the increased mass transport near the bottom. Concurrently, the offshore flow in the upper layers becomes stronger for greater H_b . The strength of the rip current is relatively weak when compared to rip currents on open, high energy beaches. The measured rip currents in the present study are indicative of the low energy estuarine environment at Willoughby Spit.

The second wave condition exists when α_b open to the east. Wave diffraction produces an along-shore gradient in wave set-up that results in a weak rip current along the up-wave groin wall within the test compartment (Fig. 15).

4.2. WAVE-CURRENT INTERACTIONS

Although it was not one of the original objectives of this study to do so, the data may be helpful to the understanding of the effect of wave-current interactions in the area near the groin.

Previous theoretical studies of wave current-interactions considered only isolated portions of the whole problem and had limited laboratory data to verify them. Grant and Madsen (1978, 1979) undertook one of the first studies to develop a more comprehensive approach to this problem. One of their significant findings was that the shear stress on the bottom increased by up to a factor of two over the simple algebraic addition of the individual wave and current contributions.

They also found that outside the wave boundary layer, a steady current would feel a greater flow resistance when waves are present. The greater resistance is a result of the increased apparent bottom roughness. The increased flow resistance is consistent with the previous work by van Hoften and Karaki (1972) and by the later work of Kemp and Simons (1982a, 1983) and Ismail (1984). Lundgren (1972) attributed the reduction in the near bed velocity to the increased eddy viscosity due the interaction of the steady current and waves. Van Hoften and Karaki (1972) concluded that the energy was extracted from the waves and diffused downward to be dissipated on the bed as increased bed shear. Kemp and Simons (1982a, 1983) report that the turbulence is increased near the bed as a result of the wave-current interaction and that it varied over the wave cycle with greater turbulence observed for waves propagating against a current than propagating with a current. The turbulence near the bed was dominated by the periodic formation of vortices (Kemp and Simons, 1982b). Ismail (1984) also found in laboratory studies that the mass transport by waves was increased near the bottom and that it tended to converge toward the current.

Information on high frequency turbulence can not be extracted directly from the present data set because energy at frequencies greater than 0.45 Hz was filtered from the data. However, since much of the turbulence associated with wave-current interactions may be associated with wave frequencies (Kemp and Simons, 1982a,b; 1983), one can assume that there may be greater energy near the bottom at wave frequencies due to turbulent input than in the interior of the flow.

Experiment IV most closely resembles the experimental conditions in the laboratory work of Kemp and Simons (1982a, 1983). The time mean flow on that day was offshore at all measured depths and the wave heights were between 5-13 cm. Figures 16 and 17 are examples of the velocity records for the bottom and top meters respectively and figures 18 and 19 show the velocity energy spectra for each record. Comparing figures 18 and 19, the total energy and the energy at individual frequencies is substantially greater at the bottom meter. This pattern was consistent throughout the day for this particular experiment. This does not provide overwhelming evidence to support the laboratory results of Kemp and Simons in the field setting. In fact, for experiment II when there was reversal from offshore at the upper levels to onshore near the bed and more intense wind and wave conditions, the opposite was true (Figs 20-23). This was probably caused by the increased energy input from breaking waves and wind at the surface. Accordingly, no firm conclusions can be drawn from these experiments to confirm the laboratory data of Kemp and Simons. By re-programming the data acquisition system to measure and store each event and the time it occurred, a field experiment could be designed to specifically address this problem. The data would then retain more of the higher frequency turbulent data that is presently removed by the one second averaging in the data acquisition system and the subsequent low pass filter. The re-programming would be quite similar to the calibration system program.

The previous laboratory and theoretical work have been devised to study a particular phenomena such as wave-current interactions or mass transport due to

Figure 16. Velocity data from run 50, current meter 1 (bottom).

Run 50 CM 1

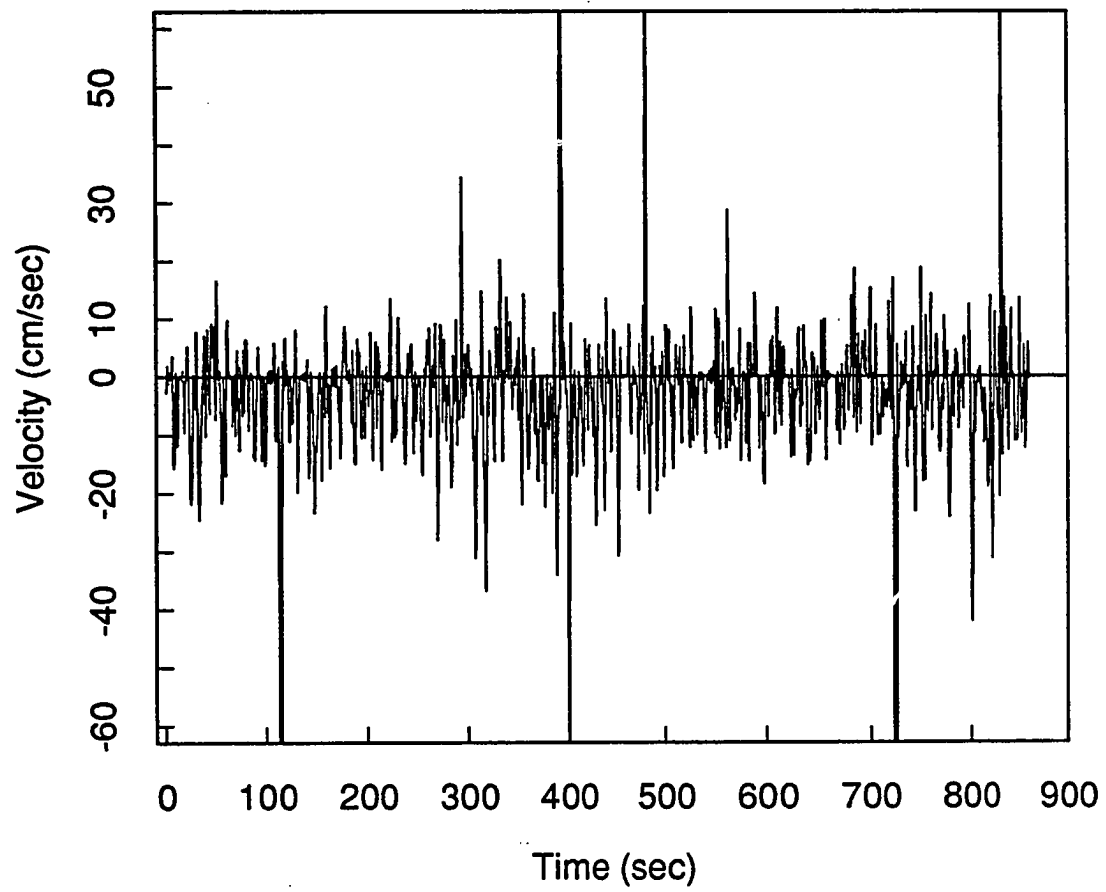


Figure 17. Velocity data from run 50 current meter 3 (top).

Run 50 CM 3

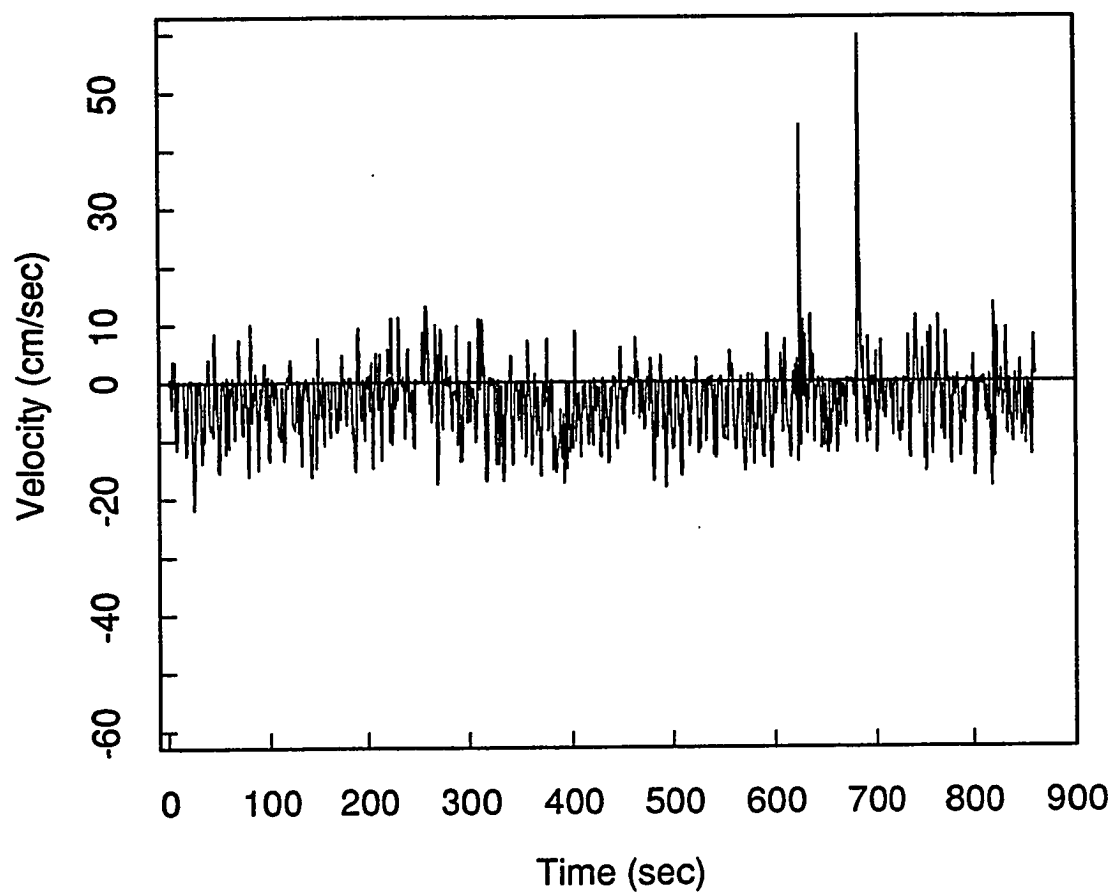


Figure 18. Energy spectrum from run 50 current meter 1 (bottom).

Energy Spectrum Run 50 CM 1

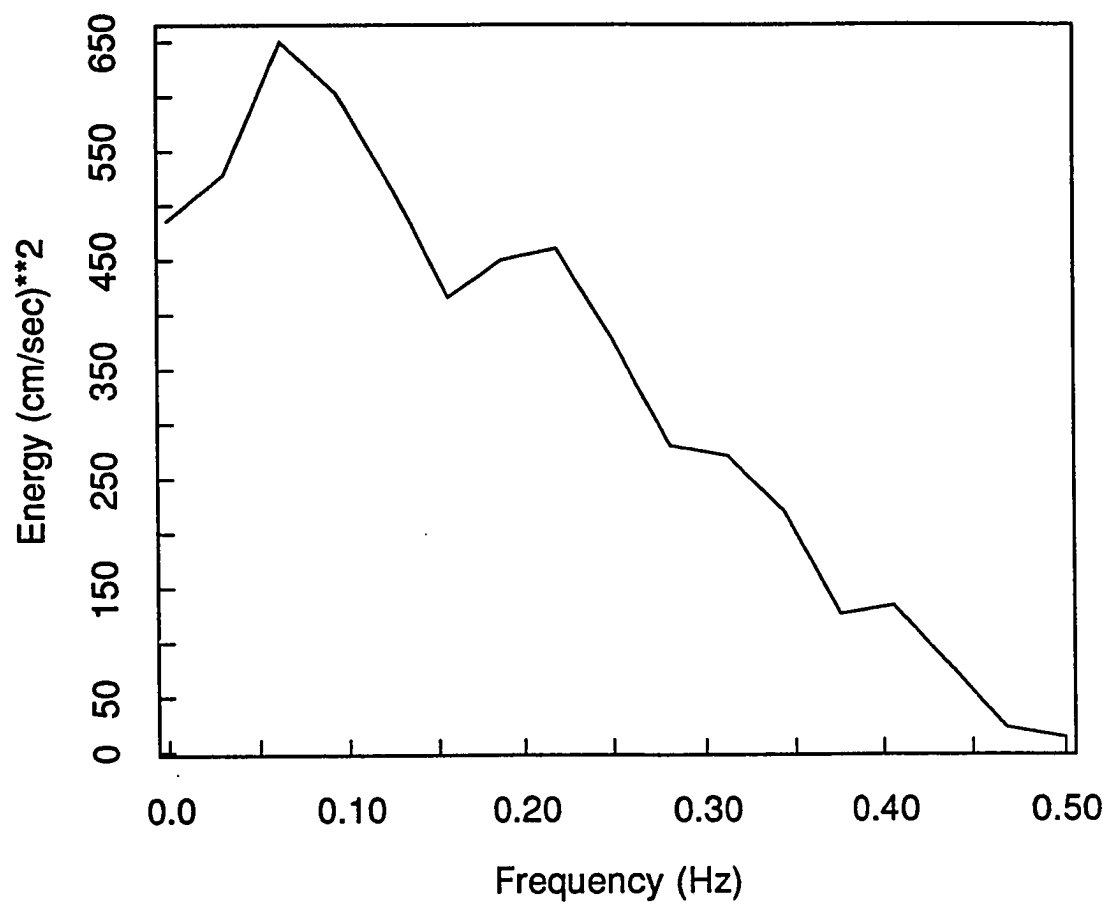


Figure 19. Energy spectrum from run 50, current meter 3 (top).

Energy Spectrum Run 50 CM 3

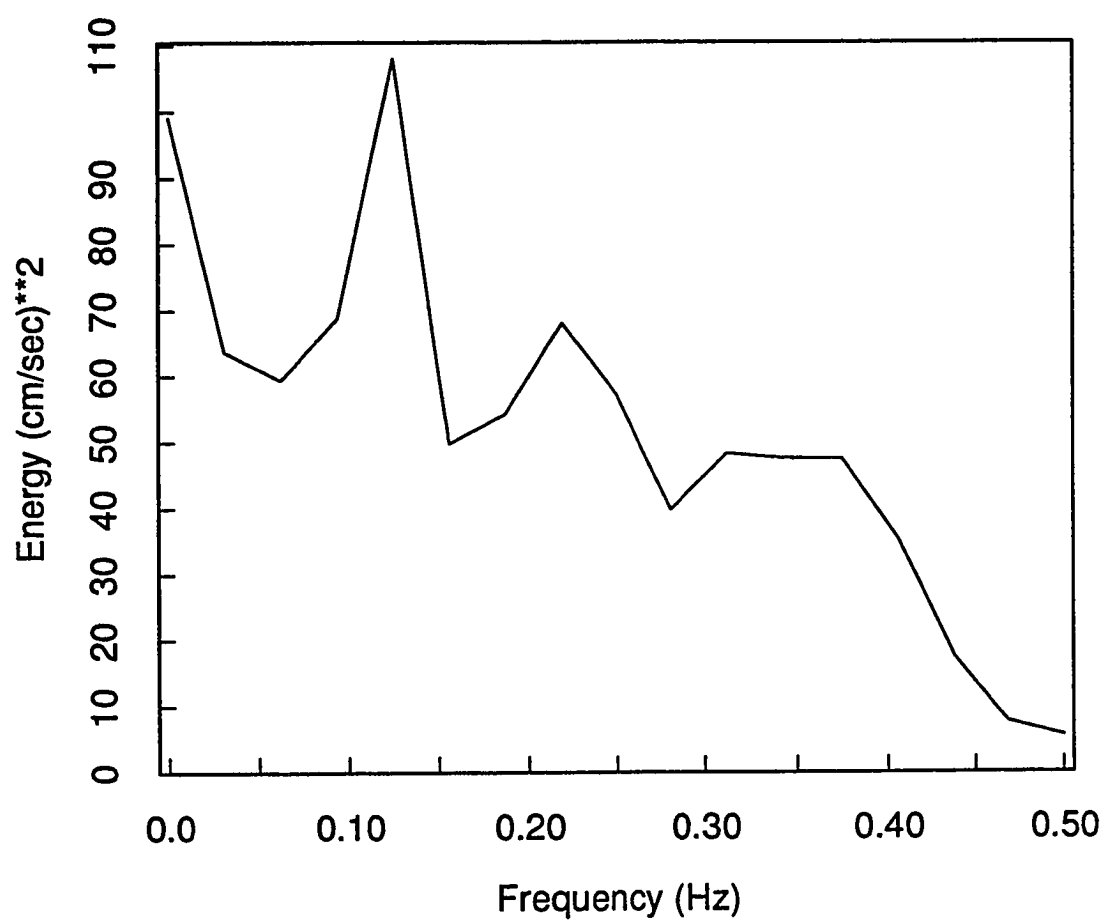


Figure 20. Velocity data from run 25, current meter 1 (bottom).

Run 25 CM 1

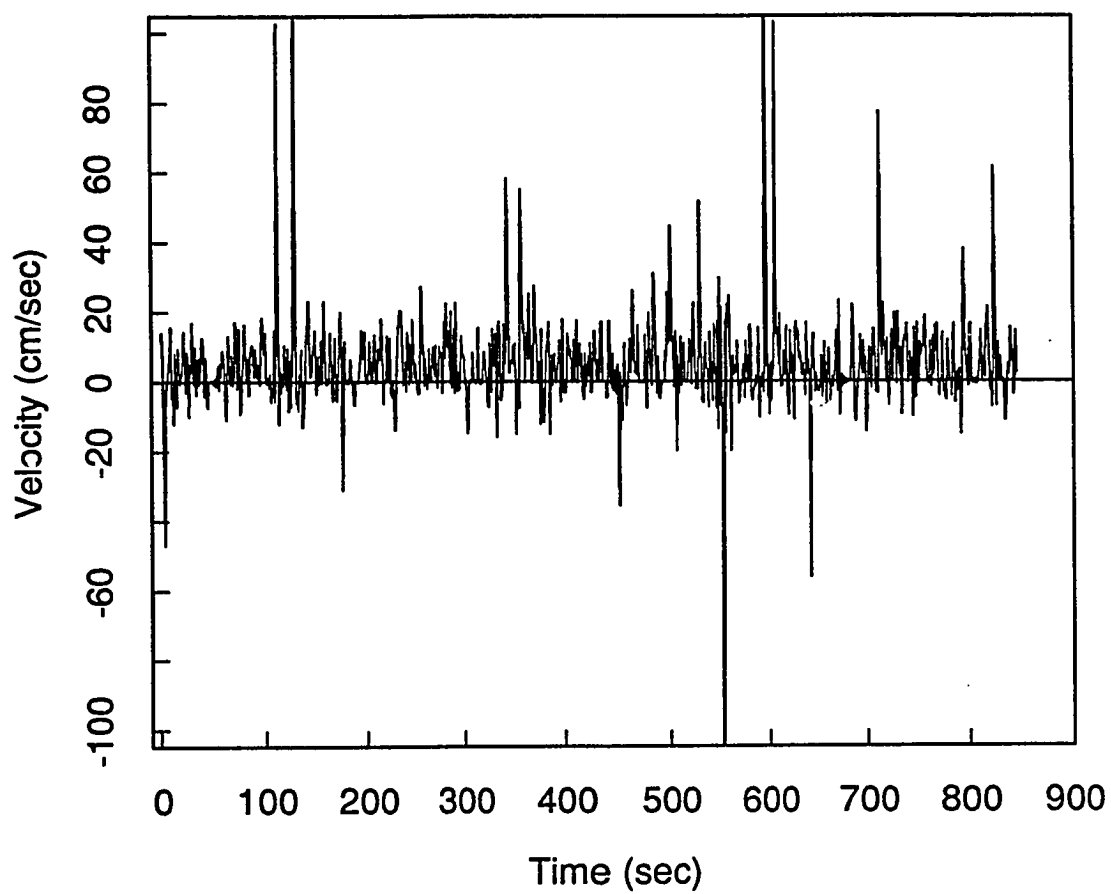


Figure 21. Velocity data from run 25, current meter 3 (mid-depth).

Run 25 CM 3

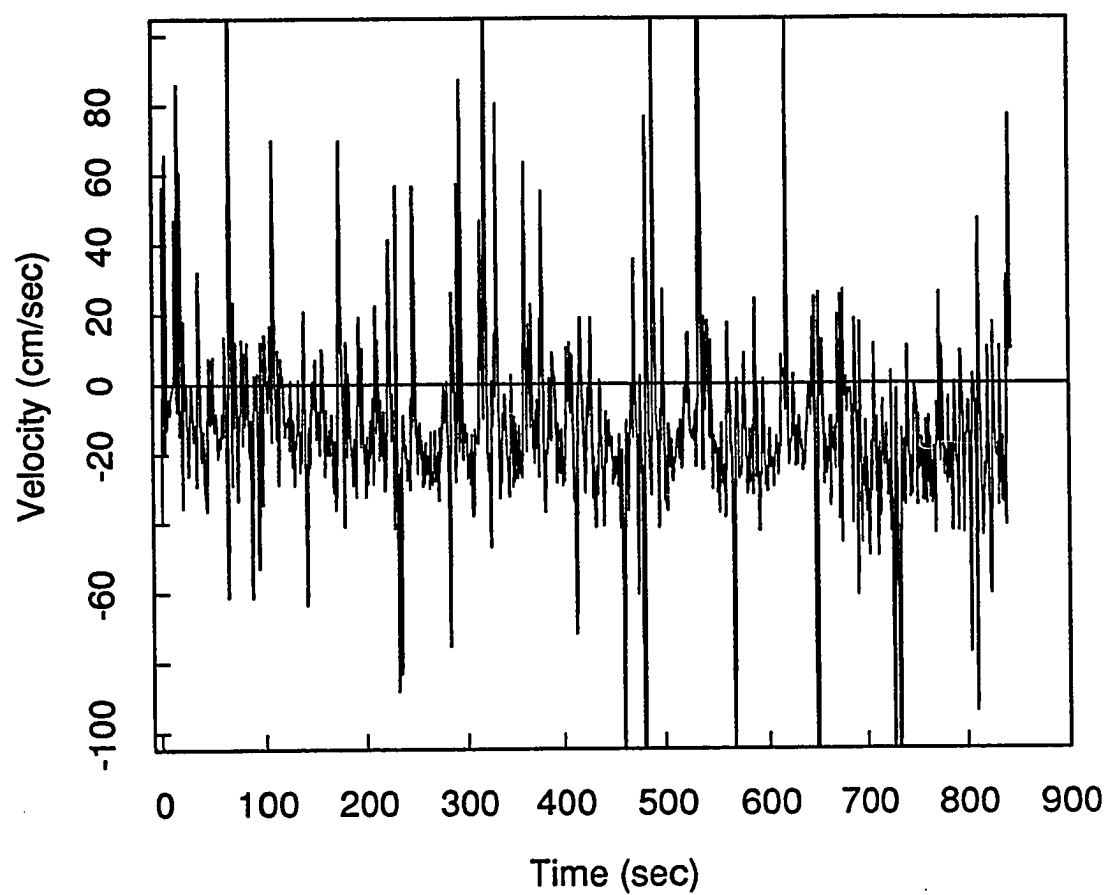


Figure 22. Energy spectrum from run 25, current meter 1 (bottom).

Energy Spectrum Run 25 CM 1

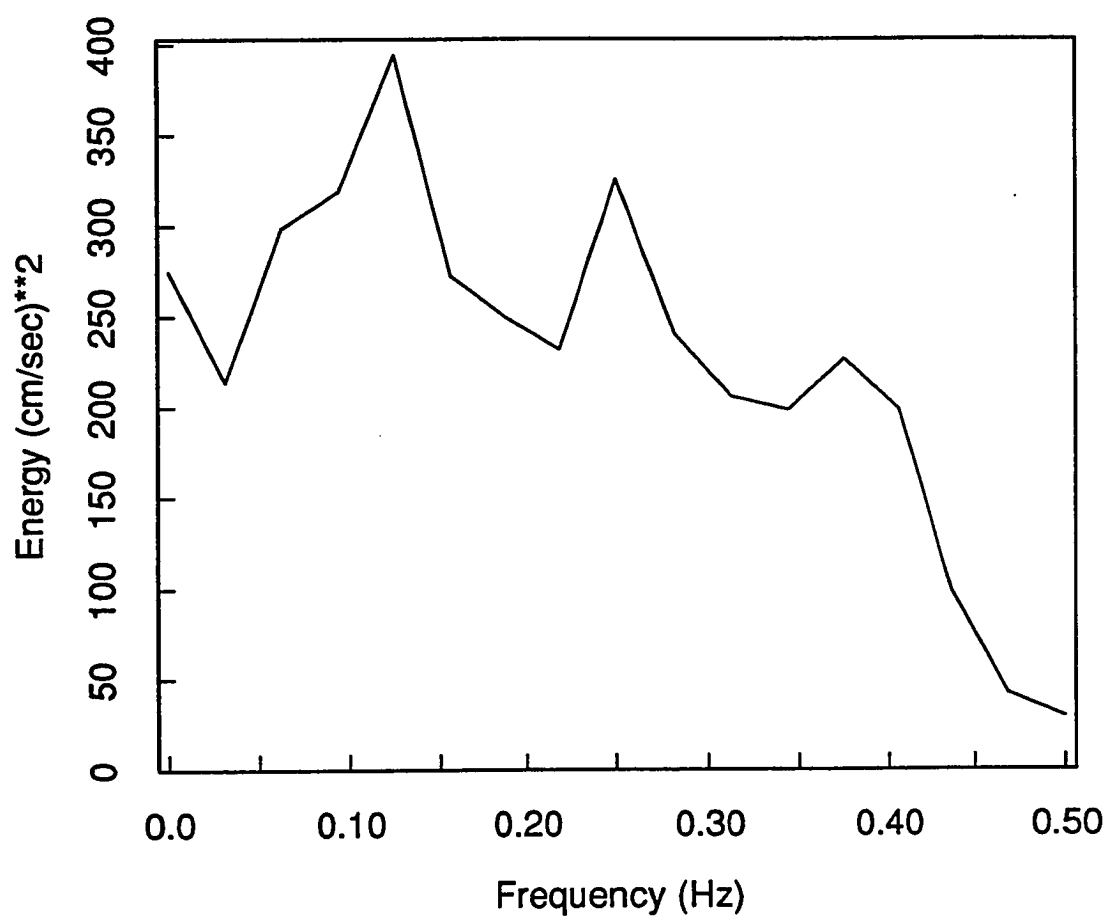
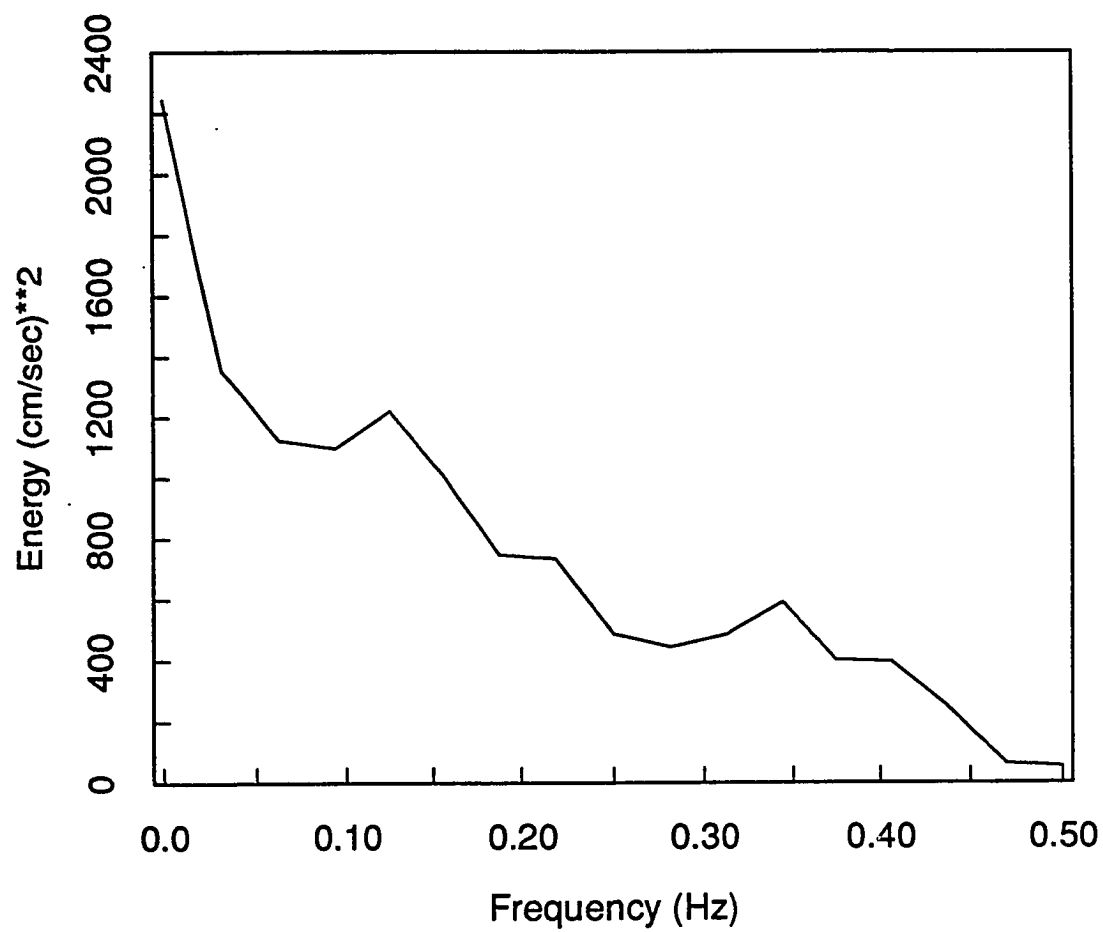


Figure 23. Energy spectrum from run 25, currnet meter 3 (mid-depth).

Energy Spectrum Run 25 CM 3



waves. In the natural setting, these processes are not isolated, but are concurrent, have complex interactions, and are of varying relative importance. In this study, the measured velocity profiles give some insight into the interactions between the rip-current near the groin and the near bed mass transport by wave action.

The measured velocity profiles summarized in Tables I-IV call into question one of the underlying assumptions in much of the theoretical work on wave-current interactions. Most investigators have assumed the steady current has a logarithmic profile. This clearly was not the case in the data from Willoughby Spit where flow reversals were common near the bottom. Haines (1984) also found that the logarithmic profile did not agree with his measured vertical profiles on two open beaches in Canada. He found that the vertical profiles developed by Longuet-Higgins (1953) did not agree with his data. Only on the simplest beaches did he find agreement with Longuet-Higgins' predictions for the near bottom flow. For a more complex beach Haines, found no agreement with theory at any level.

The increase in the bed shear stress due to the wave-current interaction will have a direct impact on the sediment transport along the groin. The work of Grant and Madsen (1979) showed that total bed shear for waves-current interactions is significantly greater than the linear superposition of the individual contributions. Kemp and Simons (1982b) report that from their flume studies, there is a dramatic increase in the amount of sediment put into suspension when a current interacts with waves. They found that the sediment moved in a thin layer near the bed when only waves were present. When a current was added, the sediment was

rapidly dispersed throughout the water column.

No models have been developed to predict sediment transport due to rip currents (Seymour and King, 1982). But, if the above results apply in the field, one would expect a greater loss of sediment along the groin due to the interaction of the rip current and the incoming waves. Additionally, the amount of sediment put into suspension would be significantly greater. No direct measurements of sediment transport were made during this study. Visual observations, however, often show a sediment plume along the groin under even calm wind and wave conditions.

Seymour and King (1982) compared the predictive skills of several cross-shore transport models using measured wind and wave conditions and the measured beach volume changes at Torrey Pines, CA during the National Sediment Transport Study (NSTS). They found that the models were able to forecast only about a third of the observed variations in the beach volume.

The current measurements used from the NSTS study were at a single elevation above the bed. The vertical velocity profiles taken during the present study show that the profiles can be complex, often with flow reversals. Models for suspended transport that use current measurements at one level would, therefore give incorrect estimates for the sediment transport and may even predict transport in the wrong direction. Models of bedload transport would under estimate the total transport rate if a significant amount of sediment is put into suspension by wave-current interactions.

Basco (1983) pointed out that most models of circulation in the nearshore and coastal zones use a depth averaged flow. This is clearly not valid in light of the present study and the work by Haines (1984). Haines (1984) found that the vertical profiles could be quite variable from one location to another. In view of the complex nature of the vertical velocity in the coastal zone one must use caution when applying sediment transport models to this area, particularly cross-shore transport models. The measured time mean shore normal velocities are small, on the order of a few cm/sec and often reverse direction with depth. By assuming a constant velocity with depth, one can not reliably predict the direction or magnitude of cross-shore sediment transport.

4.3. TIDAL EFFECTS

Superimposed on currents generated as a result of wave action, are effects of the tidal currents in the groin compartment. Ludwick (1987) and Ludwick et al (1987) show strong evidence for a current gyre within the test compartment that is induced by the tidal current flowing beyond the ends of the groin. Kang, (1987) used the numerical model developed by Gatski and Grosch, (1985) to further study this phenomenon. The effect is for the current near the beach to flow in the opposite direction of the tidal current outside the compartment. Figure 24(a,b) depicts the current gyre for both the flood and ebb currents. The shoreward leg of the gyre will either help or hinder the longshore current depending on α_b . A gyre of this type is to be expected and can be seen in numerical studies of flow past a cavity (Gatski et al., 1982, Gatski and Grosch 1985).

Figure 24a. Diagram of the current gyre within the test compartment during the flood current.

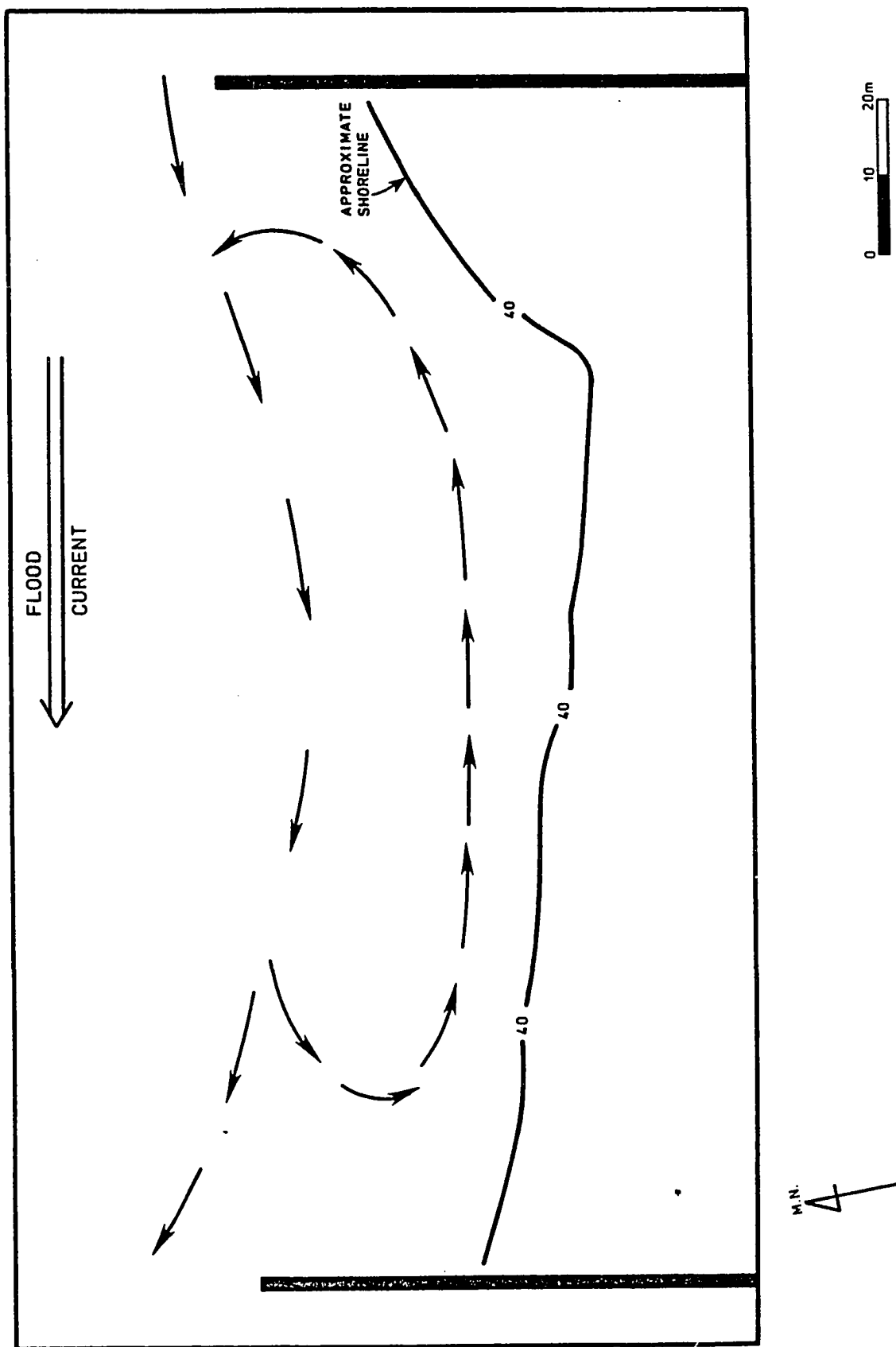
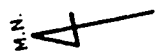
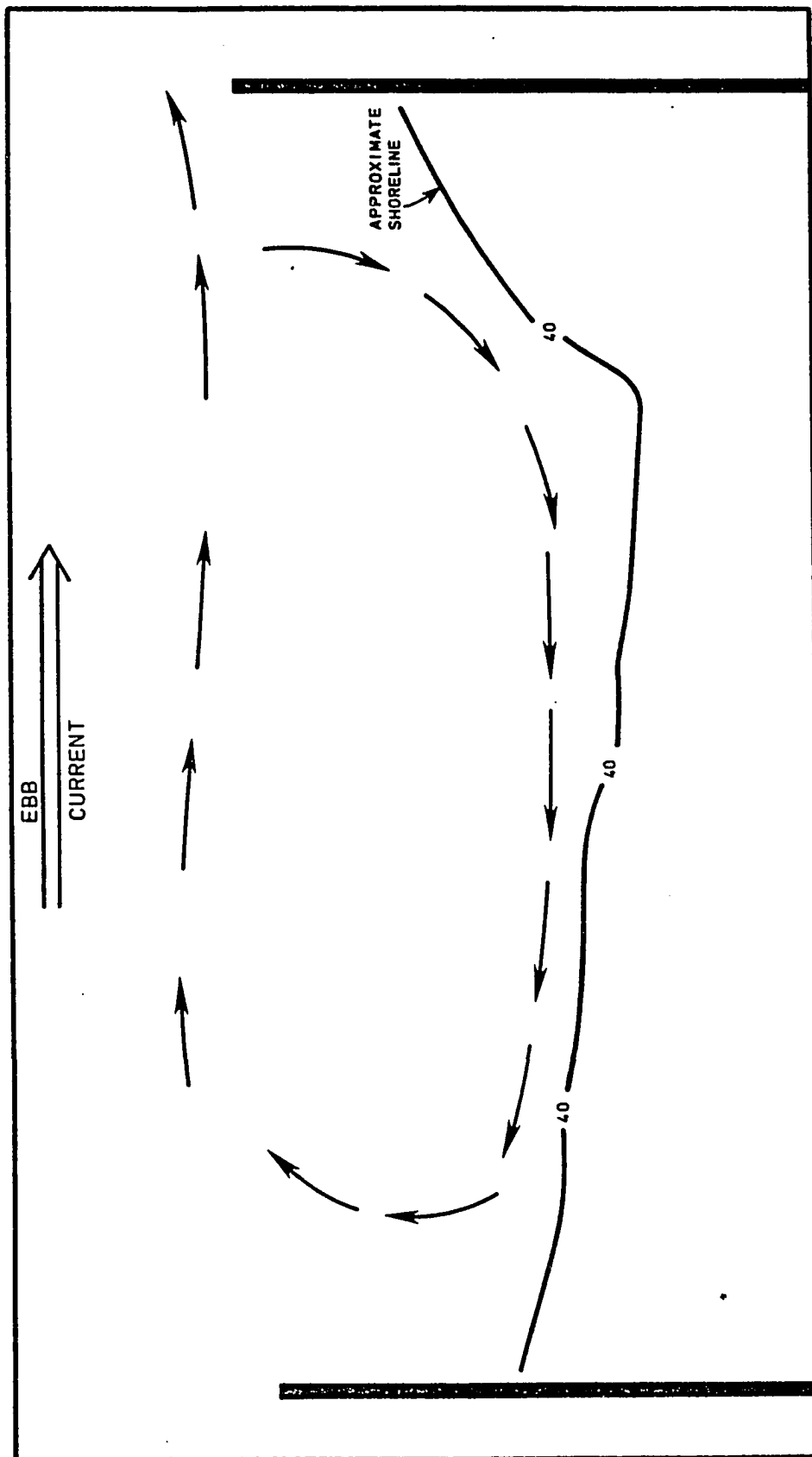


Figure 24b. Diagram of the current gyre within the test compartment during the ebb current.



During this study, the formation of clockwise rotating eddies was observed on the upstream wall of the downstream groin relative to the tidal current. These eddies were observed several times during the field experiments. All but one occurred on the flood current. They formed when the water level was below the top of the groin and on days when the wind and wave conditions were calm. Once developed, the currents associated with them were strong. Speeds ranged from 15 cm/sec to 40 cm/sec and were measured at all depths. Visual observation of the eddies indicated a great deal of turbulence as they interacted with the surrounding waters.

One possible explanation for the formation of the eddies may be related to the current gyre in the compartment and the flow divergence as part of the tidal current turns into the compartment and the main current continues on its course around the groin. This flow divergence produces negative vorticity and a clockwise rotation (Pedlosky, 1982 or Pond and Pickard, 1983).

The implication of these eddies to sediment transport in the immediate area of the groin ends may be a significant factor in the scour near the end of the groins (Fig. 4). In a broader sense, eddies of this type may be important to the flow and sediment transport around jetties and breakwaters that extend into a strong tidal flow and may have an important bearing on the construction of coastal structures. More work is needed to better define and understand this phenomena.

CHAPTER 5

SUMMARY AND CONCLUSIONS

The time mean data at the different elevations clearly show a net offshore flow in the upper half of the water column in the majority of the observations. The flow in the lower half often demonstrated flow opposite to the upper flow or onshore.

There appears to be two distinct mechanisms for generating a rip current, both related to the breaker angle relative to the shoreline. The first occurs when α_b opens to the west. A longshore current is generated that flows to the west until it encounters the groin. The groin acting as a barrier, diverts the flow seaward in the form of a weak rip current along the groin wall. The second mechanism occurs when α_b opens to the east. Diffraction around the groin ends reduces the wave which causes the longshore wave set-up to be reduced near the groin. If the variation in set-up is great enough, a relatively weak longshore current can flow opposite to the breaker angle and flow seaward along the groin wall. The two processes probably occur simultaneously but at opposite groins within the compartment.

The theoretical work by Grant and Madsen (1979) showed that the shear stress on the bed is significantly increased by a current interacting with waves. The increased bed shear would increase the sediment transport rate in the direction of net flow. The laboratory studies of Kemp and Simons show that more sediment

is placed in suspension by the interaction of waves and a current. It is expected, therefore, that the interaction of the rip current and waves near the groin would tend to increase the offshore loss of sediment in that area, thereby reducing the effectiveness of the groin.

The time mean vertical velocity profiles show that the vertical structure can be quite complex. The notion of a logarithmic velocity profile may have little meaning for a groined beach. The interactions of the mass transport of water by waves and rip current near the bed often produced a net onshore flow while the upper flow is offshore. The present study and that of Haines (1984) show that the velocity profile from the various theories of mass transport by waves are not applicable to most open and groined beaches.

The flow of the tidal currents around the ends of the groin can generate relatively strong, clockwise rotating eddies. These eddies may contribute significantly to scour near the ends of the groin, particularly when the waves and the rip current are weak.

Finally, the new current meter system functioned well. The LEDs of the current meters were directly exposed to the marine environment which caused the reliability of the meters to be reduced. The replacement of the LEDs by fiber optic cables would greatly improve the reliability by removing all electrical circuits from the sensors. The data collected was of high quality and was entirely adequate for the measurement of wave dominated velocities as well as the small, time mean velocities. The low cost of the meters will allow the deployment in the future of a

relatively large number of current meters to study three dimensional flow in the nearshore and coastal zones.

REFERENCES

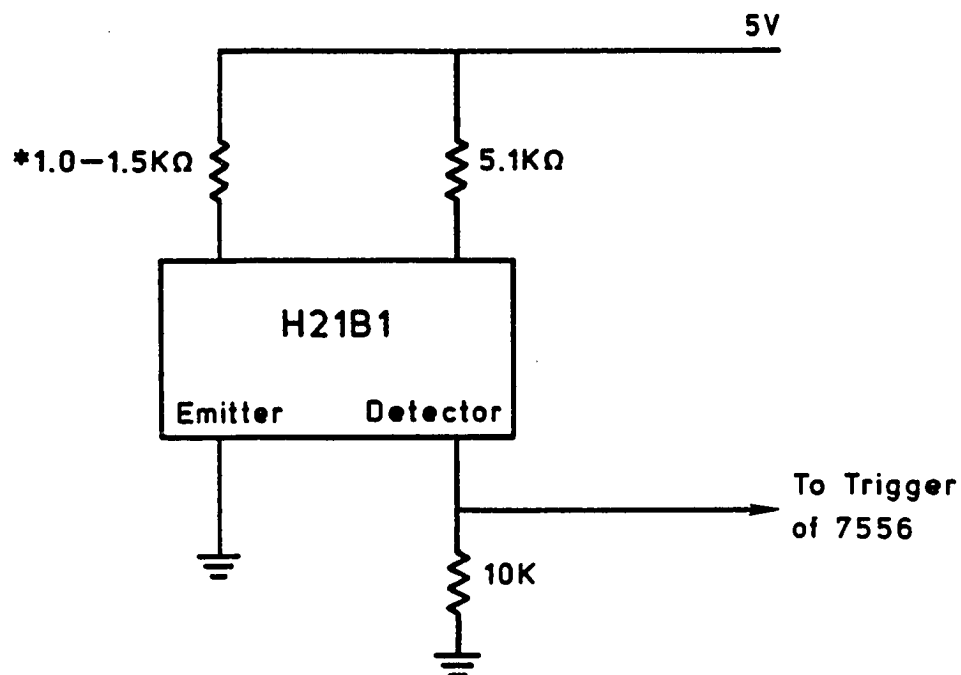
- Bakker, W. T., 1968, The dynamics of a coast with a groin system, Proc. 11th Coastal Engng. Conf., pp. 492-517.
- _____.; E. H. J. Klein-Breteler; and A. Roos, 1979, The dynamics of a coast with a groin system, Proc. 12th Coastal Engng. Conf., pp 1001-1020.
- Balsillie, J. H. and R. O. Bruno, 1972a, Groins: An annotated bibliography, CERC Misc. Paper No. 1-72, Wash. D. C. 249 pp.
- _____. , 1972b, State of groin design and effectiveness, Proc. 13th Coastal Engng Conf., pp1367-1383.
- Basco, D. R., 1983, Surfzone currents, Coastal Engng, Vol. 7, pp 331-355.
- Bruun, P., 1972, The history and philosophy of coastal protection, Proc. 13th Coastal Engng Conf., pp33-74.
- Byrne, R. J. and G. L. Anderson, 1977, Shoreline erosion in Tidewater, Virginia, Special Rep. Applied Marine Sci. and Ocean Engng, No. 111, VA Inst. Mar. Sci. Gloucester, VA, 102pp.
- Gatski, T. B.; C. E. Grosch; and M. E. Rose, 1982, A numerical study of the two-dimensional Navier-Stokes Equations in vorticity-velocity variable, J. Comp. Phys., Vol. 98, No. 1, pp 1-22.
- _____. , and C. E. Grosch, 1985, Embedded cavity drag in steady laminar flow, AIAA J., Vol. 23, No. 7, pp 1028-1037.
- Gonsalves, J. W. and D. H. Swart, 1982, Mass transport in vocoidal theory, Proc. 18th Coastal Engng. Conf., pp 328-341.
- Grant, W. D. and O. S. Madsen, 1978, Bottom friction under waves in the presence of a weak current, NOAA Tech. Mem. ERL. MESA-29 131 pp.
- _____. , 1979, Combined wave current interactions with a rough bottom, J. Geophys. Res., Vol. 84, pp 1707-1808.
- Grosch, C. E., 1981, Statistical wave theory class notes (unpublished).
- Haines, J. W., 1984, Steady flows in the nearshore zone, Proc. 19th Coastal Engng. Conf., pp 2280-2292.

- Hulsbergen, C. H.; W. T. Bakker; and G. van Bochove, 1976, Experimental verification of groyne theory, Proc. 15th Coastal Engng. Conf., pp 1439-1458.
- Kang, H. J., 1986, Personal Communication.
- _____, 1987, Cross-shore transport in relation to currents and waves between a groin field, Old Dominion Univ. Ph.D. Diss. (in preparation).
- Kemp, P. H., 1962, A model study of the behaviour of beaches and groynes, Jnl. ICE, London, Vol. 22, pp 191-210.
- _____. and R. R. Simons, 1982a, Interaction between waves and a turbulent current: Waves propagating with the current, J. Fluid Mech. Vol. 116, pp 227-250.
- _____. 1982b, Wave and current interaction in the near bed region, Proc. 18th Coastal Engng. Conf., pp 404-412.
- _____. 1983, Interaction of waves and a turbulent current: Waves propagating against the current, J. Fluid Mech. Vol. 130, pp 73-89.
- Komar, P. D., 1976, Beach processes and sedimentation, Prentice-Hall Inc. New Jersey, 429 pp.
- Longuet-Higgins, M. S., 1953, Mass transport by water waves, Phil. Trans. Roy. Soc. Ser A, Vol. 245, No. 903, pp 535-581.
- Ludwick, J. C., 1987, Currents and sediment transport in a groin field, Tech Rep. Dept. Ocean., Old Dominion Univ. (in preparation).
- _____.; H. J. Kang; and R. N. Reynolds, 1987, Loss of filled sand from an estuarine groin system, Coastal Seds. 87, ASCE (in press).
- Lundgren, H., 1972, Turbulent currents in the presence of waves, Proc. 13th Coastal Engng. Conf., pp 623-634.
- Muslin, D., 1978, Environmental solutions to beach stabilization, Coastal Zone '78, ASCE, pp 745-761.
- Nagai, S. and H. Kubo, 1958, Motion of sand particles between groins, Jnl. Waterways and Harbors Div. ASCE, Vol. 84 No. WW5, paper 1876.
- Pedlosky, J., 1982, Geophysical fluid dynamics, Springer-Verlag, New York, NY, 624 pp.

APPENDICES

Figure A1. Optical sensor assembly circuit for one emitter-detector pair.

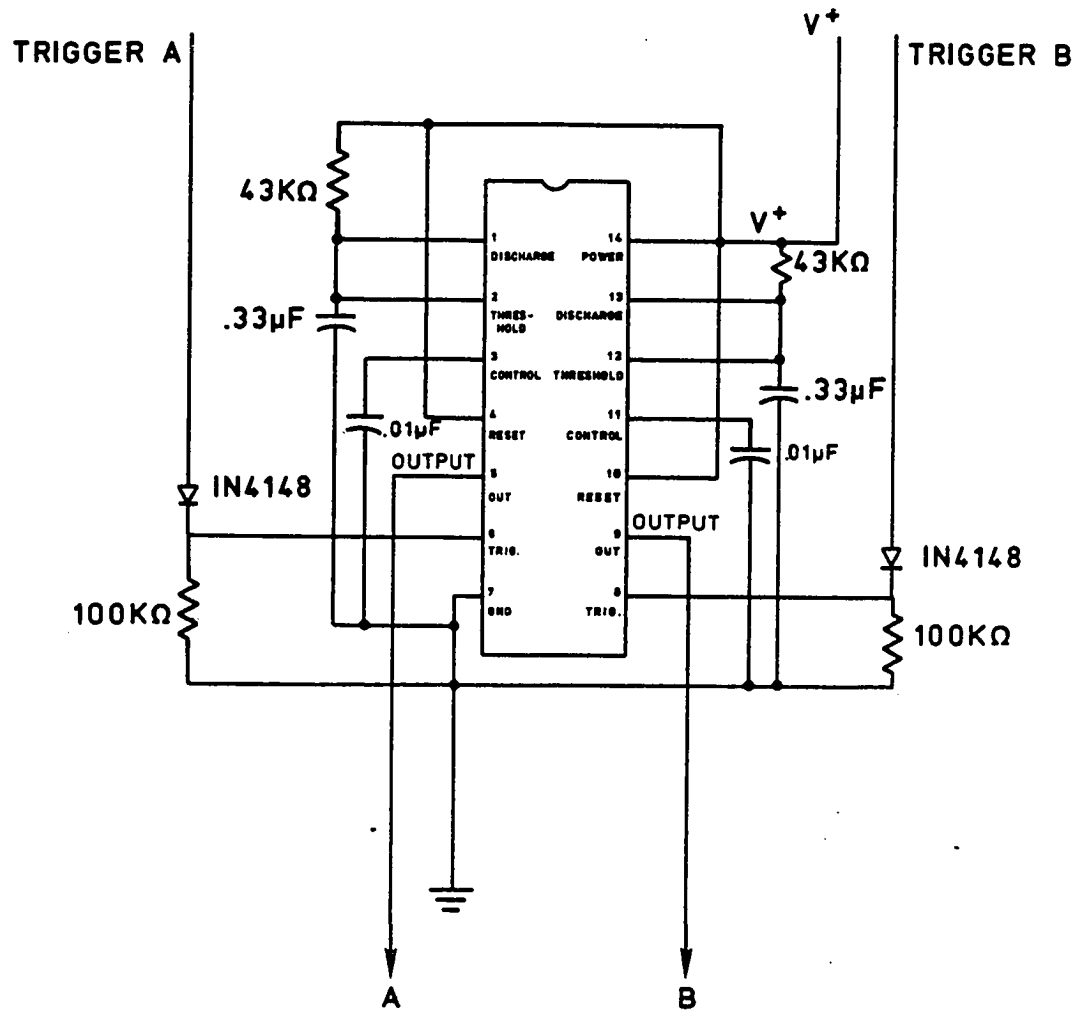
SENSOR ASSEMBLY



***SELECT RESISTANCE FOR PROPER
OPERATION. NORMALLY $\sim 1K\Omega$**

Figure A2. Wiring diagram for a 7556 duel timing device. The 7556 is wired as a one-shot trigger.

7556 WIRING DIAGRAM



WIRED AS A 'ONE SHOT' TRIGGER

Figure A3. Bottom view of a current meter circuit board that contains the circuits to shape the pulses from the current meters, the timing devices, timer control circuits, and data bus registers for two current meters. (Note: All circuit diagrams show the bottom view or the wiring side of the circuit boards).

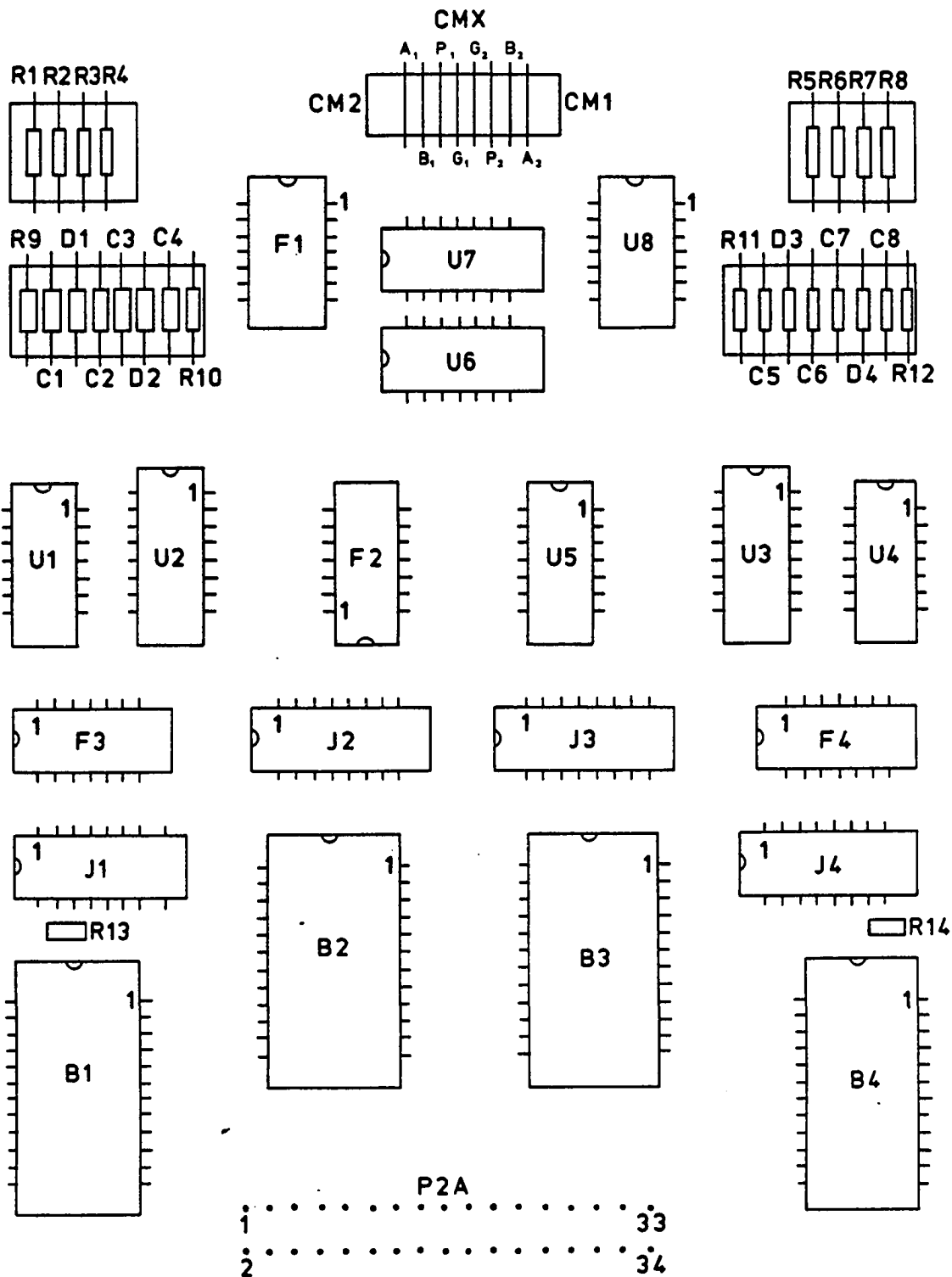


Table A-I. Electronic components for the current meter boards.

Table A-I Table of Electronic Components

Board Locator	Component	Description
B1, B2, B3, B4	4034	8 Bit bidirectional parallel/serial input/output bus register
F1,F2,F3,F4	4013	Dual 'D' type flip-flop
J1,J2,J3,J4	4520	Dual 4 bit up counter
U1,U4	7556	CMOS timer wired as monostable multivibrator
U2,U3	4555	Dual binary 1 to 4 decoder/demultiplexer
U5,U8	4071	Quad 2-input OR gate
U6	4081	Quad 2-input AND gate
U7	4069	Hex inverter
C1,C4,C5,C8	.33 microfarad capacitor	
C2,C3,C6,C7	.01 microfarad capacitor	
D1,D2,D3,D4	1N4148 diode	
R1,R2,R7,R8 R13,R14	100 kohm resistor	
R9,R10,R11,R12	43 kohm resistor	
R3,R4,R5,R6	10 kohm resistor	

Figure A4. Power and ground connections for the current meter board.

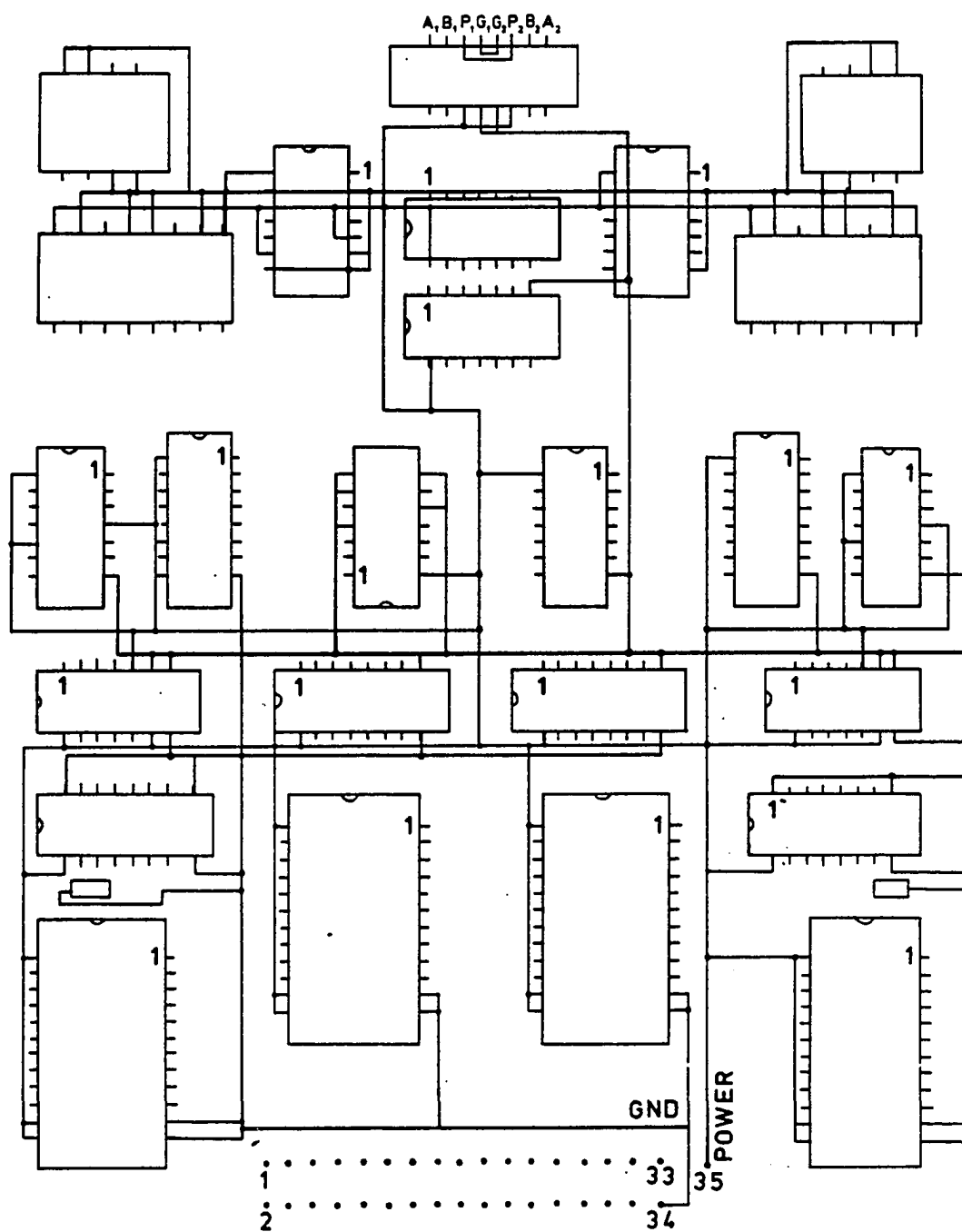


Figure A5. Logic circuits that controll the timing devices and genertate the ready signals. (See Figure A6 for details of the logic circuitry).

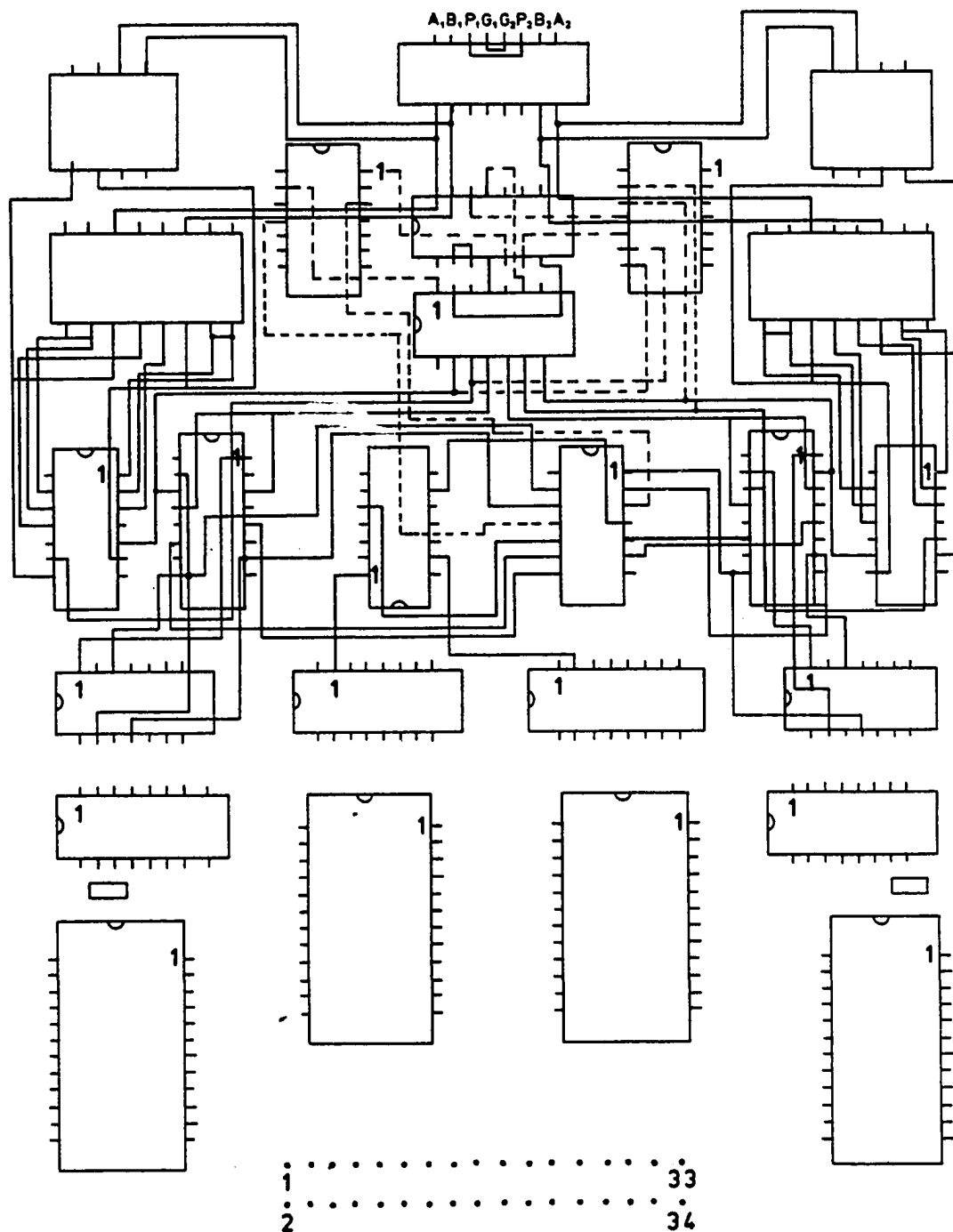


Figure A6. Timer controll logic circuitry.

Figure A7. Timer output, data lines, and data bus circuitry.

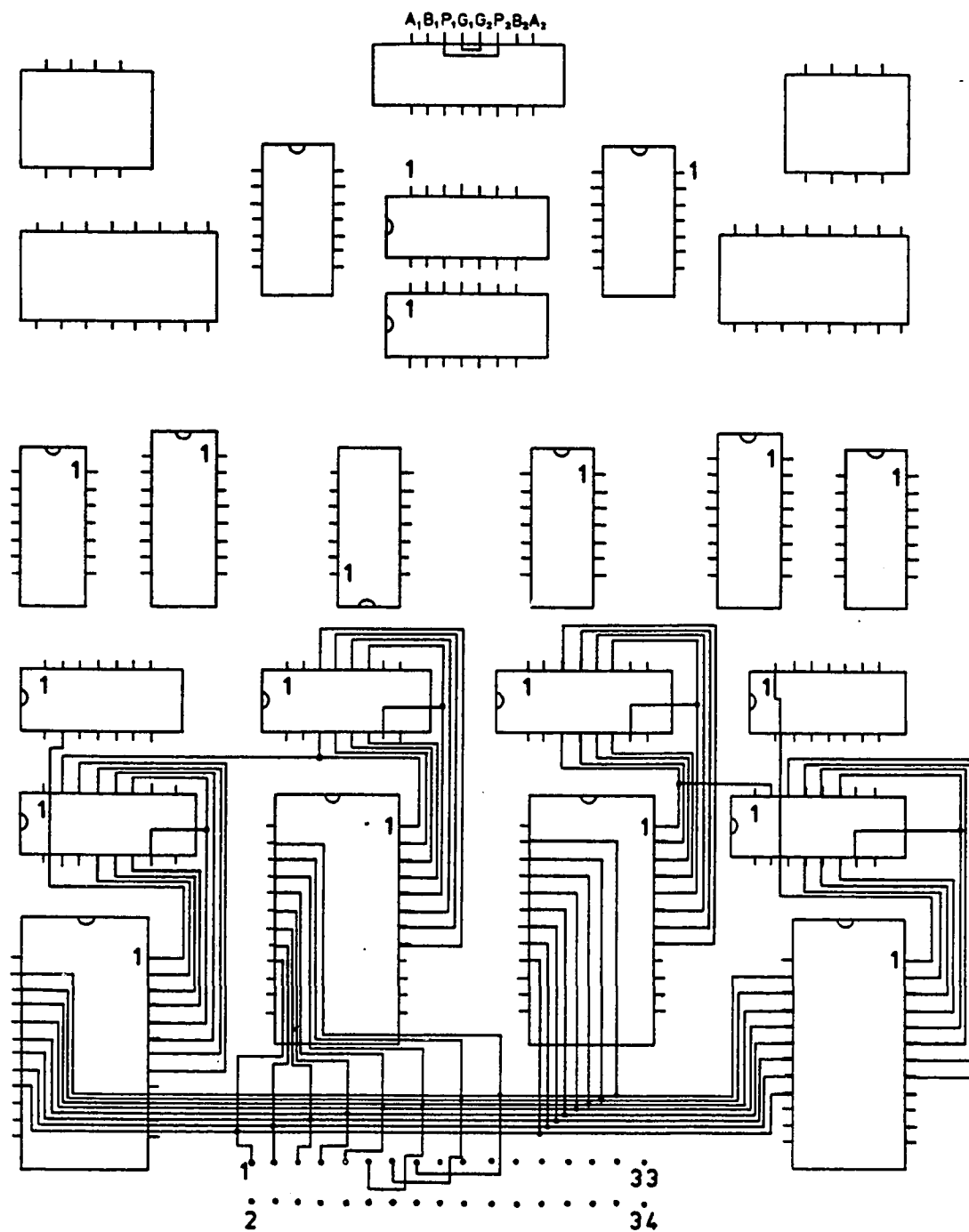


Figure A8. Control signals to and from the microprocessor board via the interface.

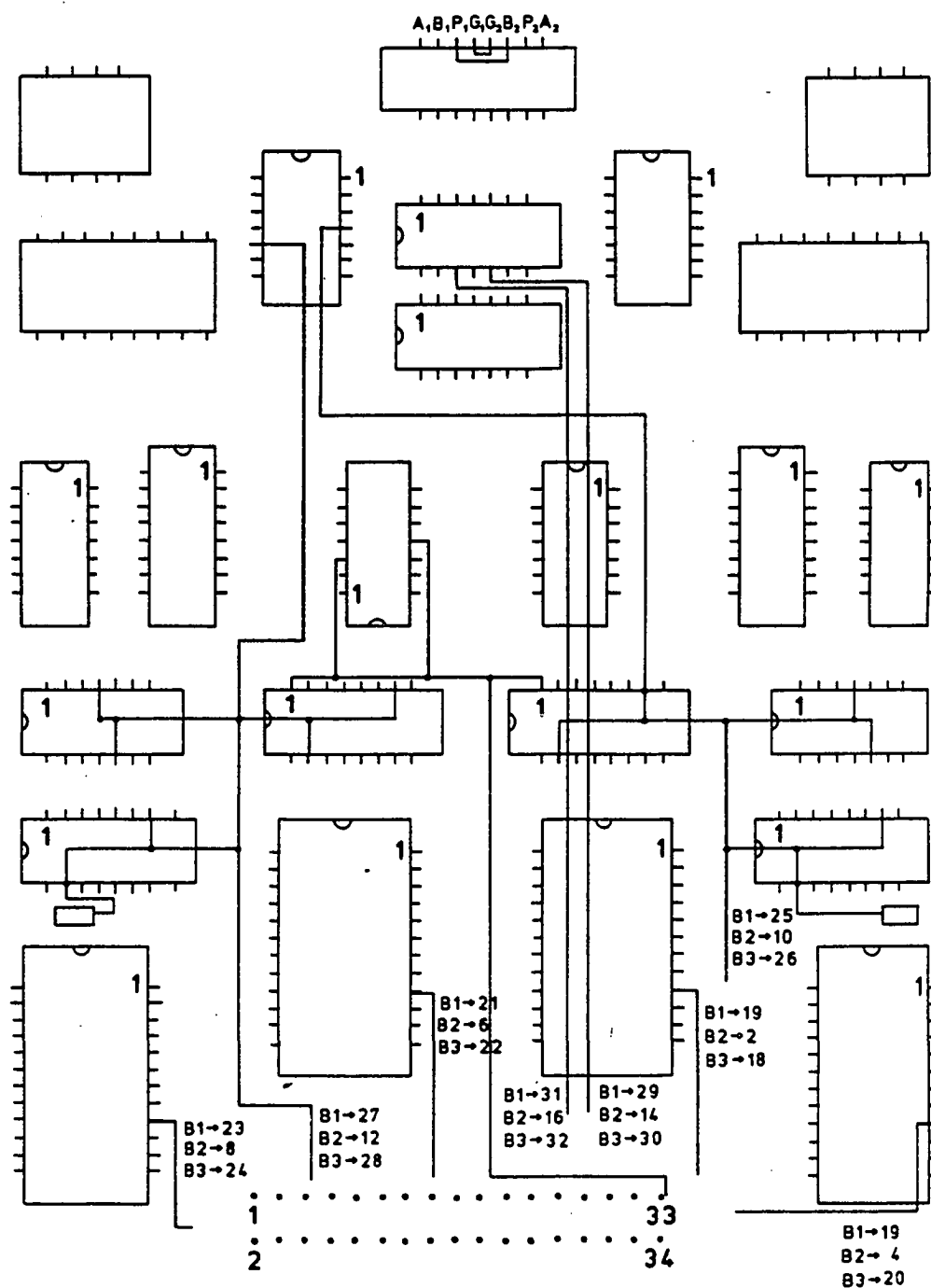


Figure A9. Bottom view of the interface board component layout.

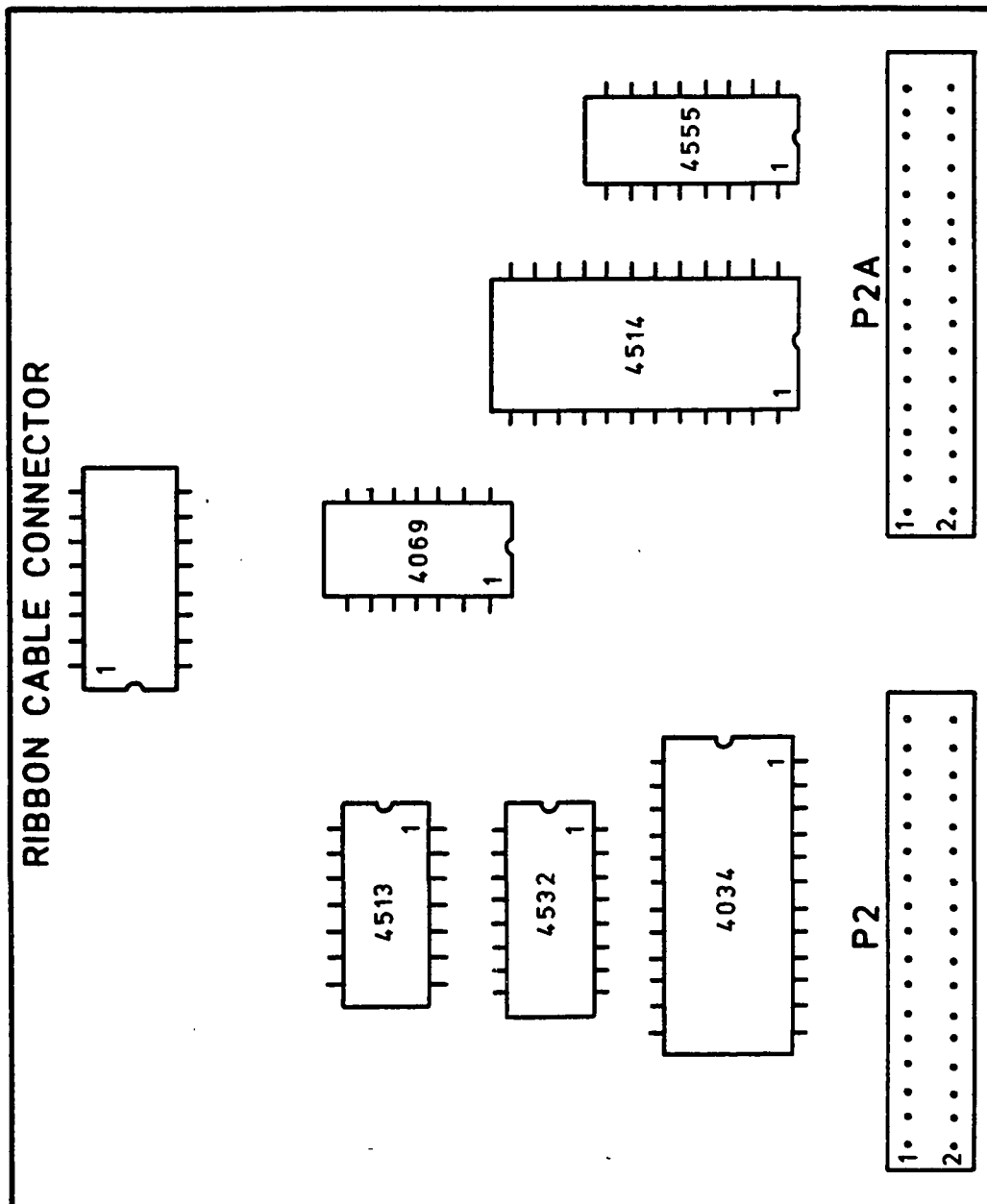


Table A-II. Ribbon cable pin connections from the microprocessor board to the interface board.

Table A-II Ribbon Cable Connections

Pin	Signal	Function
1	SC0	State Code 0
2	SC1	State Code 1
3	DO0	Data out, bit 0
4	DO1	Data out, bit 1
5	DO2	Data out, bit 2
6	MRD	Memory Read
7	MWR	Memory Write
8	TPA	Timing Pulse A
9	TPB	Timing Pulse B
10	DMAI	Direct Memory Access In
11	8 Hz	Start signal for ADC (calibration system)
12	64 Hz	Run Time Clock Signal (calibration system)
13	4 KHz	Event Time Clock Signal
14	N1	An I/O Signal
15	1 Hz	1 sec average signal
16	524 KHz	ADC clock (calibration system)

Note: Signals on pins 1-10 were not used by either system. They were made available to the interface board for potential system expansion or modification.

Table A-III. P2A pin connections.

Table A-III P2A Pin Connections

Pin	Function	Pin	Function
1	Data Bit 0	2	CM3 Low Byte Enable
3	Data Bit 1	4	CM3 High Byte Enable
5	Data Bit 2	6	CM4 Low Byte Enable
7	Data Bit 3	8	CM4 High Byte Enable
9	Data Bit 4	10	CM3 Reset Signal
11	Data Bit 5	12	CM4 Reset Signal
13	Data Bit 6	14	CM3 Ready Signal
15	Data Bit 7	16	CM4 Ready Signal
17	CM1 Low Byte Enable	18	CM5 Low Byte Enable
19	CM1 High Byte Enable	20	CM5 High Byte Enable
21	CM2 Low Byte Enable	22	CM6 Low Byte Enable
23	CM2 High Byte Enable	24	CM6 High Byte Enable
25	CM1 Reset Signal	26	CM5 Reset Signal
27	CM2 Reset Signal	28	CM6 Reset Signal
29	CM1 Ready Signal	30	CM5 Ready Signal
31	CM2 Ready Signal	32	CM6 Ready Signal
33	4 KHz Clock	34	Ground

Note: (1) A 5 volt power line is jumped from the interface board to the current meter boards.
(2) The data lines are cross-connected from P2A to the P2 data input lines to the 1802.

Figure A10. Interface board power and ground connections.

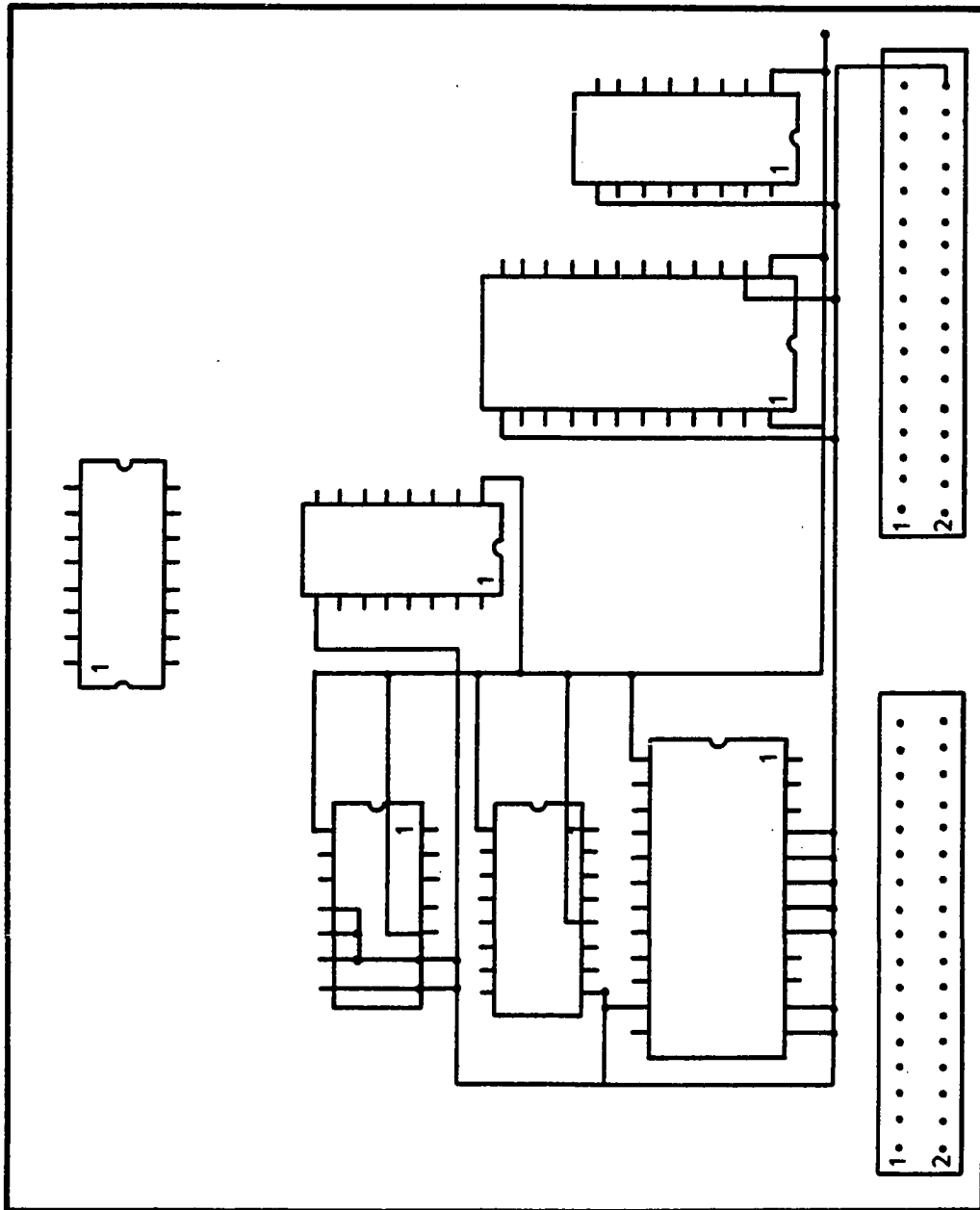


Figure A11. Current meter data bus enable signals, vectored interrupt circuitry, and current meter address signals.

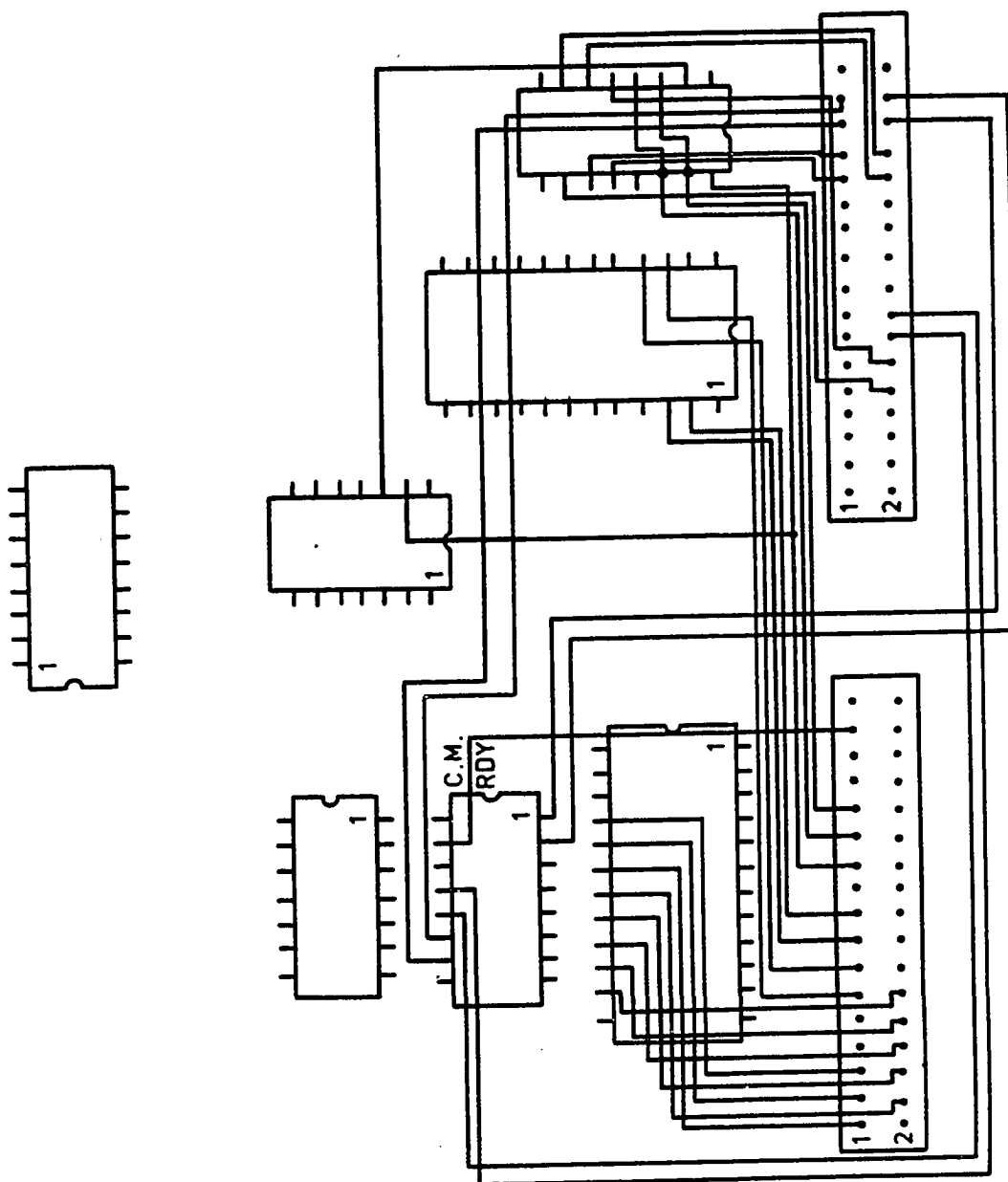


Figure A12. Priority encoder input and output, reset code input from the microprocessor to the decoder and the decoder output to the individual meters.

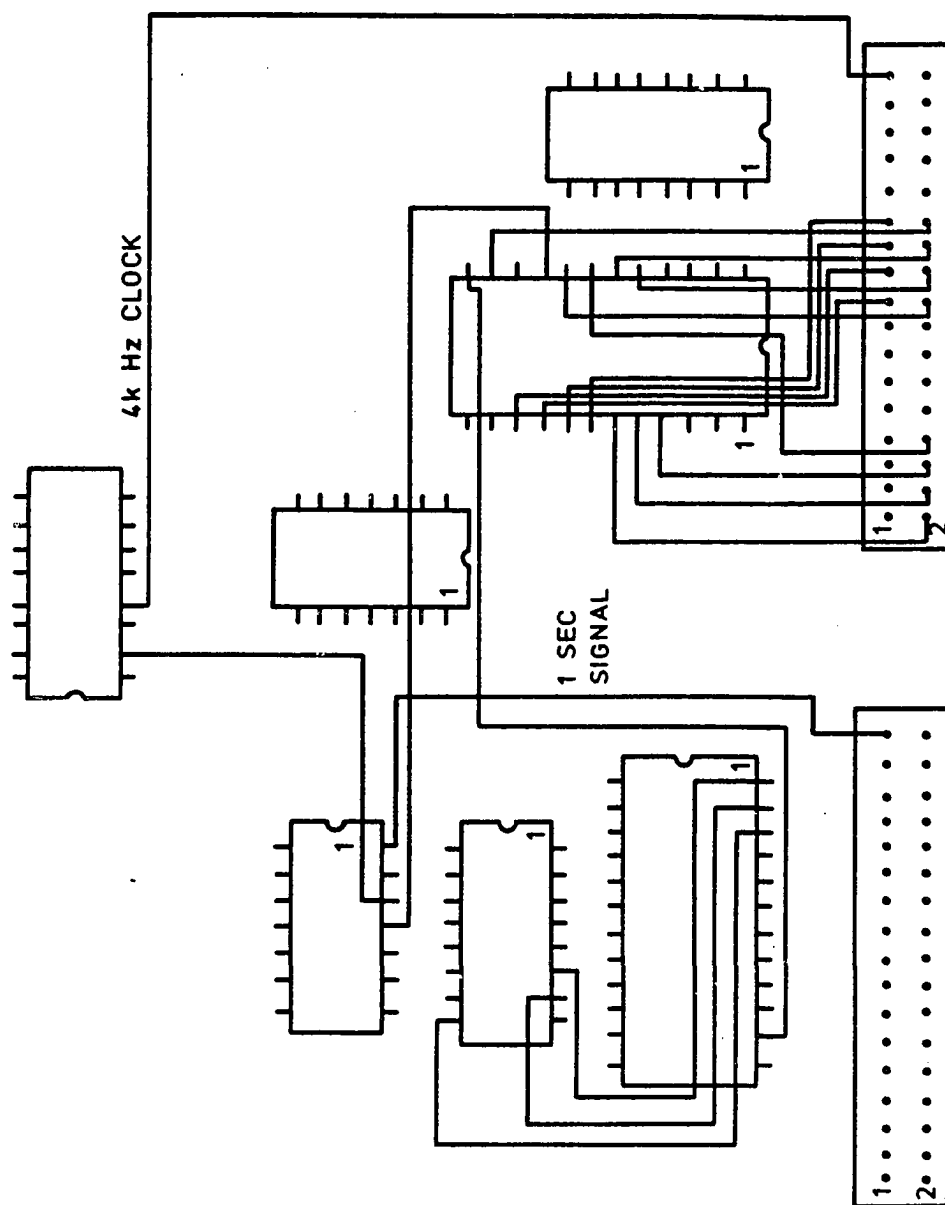


Table B-I. RCA CDP-1802 register allocation for the field system.

Table B-I 1802 Register Allocation

Register	Use
R(0)	Main Program Pointer
R(1)	Primary Memory Ponter
R(2)	Memory Stack Pointer
R(3)	Addition Subroutine Address
R(4)	Subtraction Subroutine Address
R(5)	Division Subroutine Address
R(6)	Memory Pointer (Dummy variable)
R(7)	Data Read Subroutine Address
R(8)	Work Space Memory Pointer
R(9)	Loop Counter (In division subroutine)
R(A)	Not Assigned
R(B)	Not Assigned
R(C)	Memory Pointer (Data transfer)
R(D)	Registers D, E, & F used for temporary data storage by arithmetic subroutines to pass initial/final data.
R(E)	
R(F)	

MACHINE LANGUAGE PROGRAM FOR THE FIELD SYSTEM

ADDRESS	OPCODE		COMMENTS
0000	F8	FF --> D	LINES 00-11 INITIALIZE RAM TO
0001	FF		0.
0002	B8	D -> R(8).1	
0003	A8	D -> R(8).0	
0004	E8	X -> R(8)	MAKE R(8) THE MEMORY POINTER
0005	F8	00 -> D	
0006	00		
0007	73	D --> M(R(8)); R(8)-1	
0008	98	R(8).1 -> D	
0009	FB	D XOR 08 -> D	
000A	08		
000B	3A	IF D .NE. 0 THEN GOTO 05	
000C	05		
000D	88	R(8).0 -> D	
000E	FB	D XOR 01 -> D	
000F	01		
0010	3A	IF D .NE. 0 THEN GOTO 05	
0011	05		
0012	7B	1 -> Q	
0013	E0	X -> R(0)	
0014	61	OUTPUT 08 TO SELECT THE I/O PORTS	
0015	08	ON THE MICROPROCESSOR BOARD	
0016	F8	0B -> D	
0017	0B		LINES 16-1B LOAD HEX NO.
0018	B2	D -> R(2).1	0B9B INTO R(2), THE
0019	F8	9B -> D	STACK POINTER
001A	9B		
001B	A2	D -> R(2).0	
001C	F8	00 -> D	
001D	00		LINES 1C-21 LOAD ADDRESS
001E	B3	D -> R(3).1	OF ADD. SUBROUTINE INTO
001F	F8	D1 -> D	R(3)
0020	D1		
0021	A3	D -> R(3).0	
0022	F8	00 -> D	
0023	00		LINES 22-27 LOAD ADDRESS
0024	B4	D -> R(4).1	OF SUBTR. SUBROUTINE
0025	F8	EA -> D	INTO R(4)
0026	EA		
0027	A4	D -> R(4).0	
0028	F8	02 -> D	
0029	02		LINES 28-2D LOAD ADDRESS
002A	B5	D -> R(5).1	OF DIVISION ROUTINE
002B	F8	01 -> D	INTO R(5)
002C	01		
002D	A5	D -> R(5).0	
002E	F8	0C -> D	
002F	0C		LINES 2E-33 LOAD START

```

0030    B1      D -> R(1).1      ADDRESS OF RAM INTO R(1)
0031    F8
0032    01      01 -> D
0033    A1      D -> R(1).0
0034    F8      0A -> D
0035    0A      LINES 34-39 LOAD A
0036    B6      D -> R(6).1      MEMORY POINTER INTO R(6)
0037    F8      00 -> D
0038    00
0039    A6      D -> R(6).0
003A    62      OUTPUT 01
003B    01
003C    62      OUTPUT 02
003D    02
003E    62      OUTPUT 03      LINES 3A-45 RESET THE CM
003F    03      COUNTERS AND FLIP-FLOPS
0040    62      OUTPUT 04
0041    04
0042    62      OUTPUT 05
0043    05
0044    62      OUTPUT 06
0045    06
0046    F8      01 -> D      LINES 46-48 LOAD UPPER
0047    01      BYTE OF DATA READ
0048    B7      D -> R(7).1      SUBROUTINE INTO R(7).1
0049    C4
004A    C4
004B    62      OUTPUT E0      RESET D FLIP-FLOP FOR
004C    E0      1 SEC SIGNAL TO EF4
004D    62      OUTPUT 00      DESELECT ANY DECODERS
004E    00
*****END SYSTEM INITIALIZATION*****
*****BEGIN EF TESTING*****
004F    C4
0050    34      IF EF1=T THEN GOTO 6E      TEST FOR 1 SEC SIGNAL
0051    6E
0052    35      IF EF2=T THEN GOTO 5A      TEST FOR A READY CM
0053    5A
0054    37      IF EF4=T THEN GOTO A7      TEST FOR DATA TRANSFER
0055    A7      REQUEST
0056    30      GOTO 50      REPEAT TEST SEQUENCE
0057    50
0058    C4
*****END OF EF TESTING*****
*****BEGIN DATA READ SUBROUTINE*****
0059    C4
005A    E0      X -> R(0)      R(0) IS MEM POINTER
005B    62      OUTPUT D0      ENABLE CM ADDRESS
005C    D0      DATA REGISTER
005D    E6      X -> R(6)      R(6) IS MEM POINTER
005E    6A      INPUT THE CM ADDRESS
005F    C4
0060    C4
0061    C4

```

0062	E0	X -> R(0)	R(0) IS MEM POINTER
0063	62	OUTPUT 00	DISABLE THE DECODERS
0064	00		
0065	E6	X -> R(6)	R(6) IS MEM POINTER
0066	A7	D -> R(7).0	PUT CM ADDRESS INTO R(7)
0067	D7	P -> R(7)	R(7) IS PROG. POINTER

NOTE: LINE 67 IS CALLING A SUBROUTINE FOR CM WHOSE ADDRESS WAS READ IN LINE 5E. IT RETURNS TO LINE 68.

0068	22	R(2)-1	PUT POINTER AT BOTTOM OF STACK
0069	E0	X -> R(0)	R(0) IS MEM POINTER
006A	62	OUTPUT 00	TURN OFF DECODERS
006B	00		
006C	30	GOTO LINE 54	RETURN TO EF TEST
006D	54		SEQUENCE
*****END THE DATA READ SUBROUTINE*****			
*****BEGIN THE 1 SEC AVERAGE SUBROUTINE*****			
006E	E0	X -> R(0)	R(0) IS MEM POINTER
006F	62	OUTPUT E0	RESET 1 SEC FLIP-FLOP
0070	E0		
0071	C4		
0072	F8	08 -> D	
0073	08		LINES 72-77 LOAD START
0074	B8	D -> R(8).1	ADDRESS OF MEM LOCATION
0075	F8	01 -> D	CM EVENT COUNTERS AND
0076	01		ACCUMULATORS
0077	A8	D -> R(8).0	
0078	C4		
0079	F8	00 -> D	
007A	00		
007B	A9	D -> R(9).0	
007C	89	R(9).0 -> D	
007D	FB	D XOR 06 -> D	
007E	06		
007F	32	IF D=0 THE GOTO 98	
0080	98		
0081	48	M(R(8)) -> D; R(8)+1	
0082	AF	D -> R(F).0	
0083	F8	00 -> D	
0084	00		
0085	BF	D -> R(F).1	
0086	48	M(R(8)) -> D; R(8)+1	
0087	AE	D -> R(E).0	
0088	48	M(R(8)) -> D	
0089	BE	D -> R(E).1	
008A	19	R(9)+1	INCREMENT LOOP COUNTER
008B	79	MARK	LINES 8B & 8C ARE A
008C	D5	P -> R(5)	SUBROUTINE CALL
008D	22	R(2)-1	DECREMENT STACK POINTER
008E	C4		
008F	C4		
0090	8D	R(D).0 -> D	
0091	51	D -> M(R(1))	LINES 90-95 PUT AVERAGE

```

0092      11      R(1)+1      FOR CM(I) INTO MEMORY
0093      9D      R(D).1 -> D
0094      51      D -> M(R(1))
0095      11      R(1)+1
0096      30      GOTO 7C
0097      7C
0098      E0      X -> R(0)      R(0) IS THE MEM POINTER
0099      62      OUTPUT 00      DISABLE DECODERS
009A      00
009B      E8      X -> R(8)      R(8) IS MEM POINTER
009C      F8      00 -> D
009D      00      LINES 98-A6 ZERO EVENT
009E      73      D -> M(R(8))      COUNTERS & ACCUMULATORS
009F      88      R(8).0 -> D
00A0      FB      D XOR 00
00A1      00
00A2      32      IF D=0 THEN 54
00A3      54
00A4      30      GOTO 9C
00A5      9C
00A6      C4
*****END OF 1 SEC AVERAGE SUBROUTINE*****
*****BEGIN DATA TRANSFER SUBROUTINE*****
00A7      E0      X -> R(0)      R(0) IS MEM POINTER
00A8      62      OUTPUT 00      DISABLE DECODERS
00A9      00
00AA      F8      FF -> D
00AB      FF
00AC      51      D -> M(R(1))
00AD      11      R(1)+1
00AE      51
00AF      11      LINES AC-B4 PUT 5 FFs
00B0      51      AT END OF THE DATA
00B1      11
00B2      51
00B3      11
00B4      51
00B5      F8      0C -> D
00B6      0C      LINES B5-BB PUT START
00B7      BC      D -> R(C).1      ADDRESS OF DATA INTO
00B8      F8      01 -> D      R(C) & MAKE R(C) THE
00B9      01      MEM POINTER
00BA      AC      D -> R(C).0
00BB      EC      X -> R(C)
00BC      37      IF EF4=FALSE THEN GOTO BC
00BD      BC
00BE      C4
00BF      C4
00C0      62      OUTPUT DATA TO THE DESK TOP COMPUTER
00C1      C4
00C2      C4
00C3      7A      0 -> Q      SIGNAL THAT A BYTE IS
00C4      C4      READY
00C5      7B      1 -> Q      SIGNAL READY TO SEND

```

```

                                ANOTHER BYTE
00C6      3F      IF EF4=TRUE THEN
00C7      C6      GOTO C6      LINES C6 & C7 WAIT FOR
00C8      C4      DATA RECEIPT SIGNAL
00C9      C4
00CA      C4
00CB      C4
00CC      C4
00CD      30      GOTO BC REPEAT PROCEDURE FOR NEXT BYTE
00CE      BC
00CF      30
*****END OF DATA TRANSFER SUBROUTINE*****
*****BEGIN ADDITION SUBROUTINE*****
00D0      70      RETURN TO CALL POINT
00D1      72      M(R(7)) -> D      LINES D1-D4 LOAD IN
00D2      BC      D -> R(C).1      DATA PARAMETERS THAT
00D3      72      M(R(7)) -> D      TELL WHERE IN MEMORY
00D4      AC      D -> R(C).0      EVENT COUNTER AND
                                ACCUMULATOR LOCATED
                                CM(I)
00D5      EC      X -> R(C)      R(C) IS MEM POINTER
00D6      F0      M(R(X)) -> D      LOAD EVENT COUNTER
00D7      FC      D+1      INCREMENT EVENT COUNTER
00D8      01      FOR CM(I)
00D9      5C      D -> M(R(X))      RESTORE EVENT COUNTER
00DA      60      R(C)+1
00DB      8F      R(F).0 -> D      LINES DA-E1 ADD NEW
00DC      F4      M(R(C))+D -> DF,D      DATA TO ACCUMULATOR
00DD      5C      D -> M(R(C))      FOR CM(I)
00DE      9F      R(F).1 -> D
00DF      60      R(C)+1
00E0      74      M(R(C))+D+DF -> DF,D
00E1      5C      D -> M(R(C))
00E2      E2      X -> R(2)      R(2) IS MEM POINTER
00E3      60      R(2)+1      PUT STACK POINTER AT
                                RETURN ADDRESS
00E4      30      GOTO D0      RETURN INSTRUCTION
00E5      D0
00E6      C4
*****END OF THE ADDITION SUBROUTINE*****
*****BEGIN SUBTRACTION SUBROUTINE*****
00E7      C4
00E8      C4
00E9      70      FOR LINES E9-F3 SEE COMMENTS ON LINES D0-DA
00EA      72      OF ADDITION SUBROUTINE
00EB      BC
00EC      72
00ED      AC
00EE      EC
00EF      F0
00F0      FC
00F1      01
00F2      5C
00F3      60

```

```

00F4    8F    R(F).0 -> D          LINES F3-FA SUBTRACT NEW
00F5    F5    M(R(C)-D -> D,DF    DATA FROM THE ACCUMULATER
00F6    5C    D -> M(R(C))        FOR CM(I)
00F7    60    R(C)+1
00F8    9F    R(F).1 ->D
00F9    75    M(R(C))-D-(NOT DF) -> D,DF
00FA    5C    D ->M(R(C))
00FB    E2
00FC    60    FOR LINES FB-FE SEE COMMENTS FOR LINES E2-E5
00FD    30
00FE    E9
00FF    C4

```

*****END OF THE SUBTRACTION SUBROUTINE*****

ADDRESS FROM 0100 TO 011F CONTAIN C4 - NO OPERATION

*****BEGIN SUBROUTINE TO READ DATA FROM CM(1)*****

```

0120    E7    X -> R(7)          R(7) IS MEM POINTER
0121    62    OUTPUT 01          ENABLE LOW BYTE DATA
0122    10    REGISTER
0123    E6    X -> R(6)          R(6) IS MEM POINTER
0124    6A    BUS -> D,M(R(6))   INPUT LOW BYTE
0125    AF    D -> R(F).0
0126    E7    X -> R(7)          R(7) IS MEM POINTER.
0127    62    OUTPUT 20          ENABLE HIGH BYTE DATA
0128    20    REGISTER
0129    E6    X -> R(6)          R(6) IS MEM POINTER
012A    6A    BUS -> D,M(R(6))   INPUT HIGH BYTE
012B    FE    MSB -> DF          SHIFT MSB TO DATA FLAG
012C    33    IF DF=1 THEN GOTO 36 GOTO SUBTR SUBROUTINE
012D    36
012E    F6    0 -> MSB          RESTORE ORIG. NO. LESS
                                THE SIGN

012F    BF    D -> R(F).1
0130    79    MARK              LINES 0130 & 0131 CALL
0131    D3    P -> R(3)          THE ADD SUBROUTINE
0132    08    LINES 0132 & 0133 ARE IN-LINE DATA PARAMETERS
0133    01    GIVING THE MEM LOCATION OF EVENT CTR/ACCUMULATOR
0134    30    GOTO 013C
0135    3C
0136    F6    0 -> MSB          SEE NOTE LINE 012E
0137    BF    D -> R(F).1
0138    79    MARK              LINES 0138 & 0139 CALL
0139    D4    P -> R(4)          SUBTR SUBROUTINE
013A    08    SEE NOTE FOR LINES 0132 & 0133
013B    01
013C    E7    X -> R(7)          R(7) IS MEM POINTER
013D    62    OUTPUT 01          RESET CM(1)
013E    01
013F    D0    P -> R(0)          RETURN TO MAIN PROGRAM

```

*****END DATA INPUT FOR CM(1)*****

*****BEGIN DATA INPUT FOR CM(2)*****

```

0140    E7
0141    62

```

```

0142    30
0143    E6      REFER TO CM(1) SUBROUTINE FOR COMMENTS
0144    6A
0145    AF
0146    E7
0147    62
0148    40
0149    E6
014A    6A
014B    FE
014C    33
014D    56
014E    F6
014F    BF
0150    79
0151    D3
0152    08
0153    04
0154    30
0155    5C
0156    F6
0157    BF
0158    79
0159    D4
015A    08
015B    04
015C    E7
015D    62
015E    02
015F    D0
*****END DATA INPUT FOR CM(2)*****
*****BEGIN DATA INPUT FOR CM(3)*****
0160    E7
0161    62
0163    E6
0164    6A
0165    AF      REFER TO CM(1) SUBROUTINE FOR COMMENTS
0166    E7
0167    62
0168    60
0169    E6
016A    6A
016B    FE
016C    33
016D    76
016E    F6
016F    BF
0170    79
0171    D3
0172    08
0173    07
0174    30
0175    7C
0176    F6

```



```

0177    BF
0178    79
0179    D4
017A    08
017B    07
017C    E7
017D    62
017E    03
017F    D0
*****END DATA INPUT FOR CM(3)*****
*****BEGIN DATA INPUT FOR CM(4)*****
0180    E7
0181    62
0182    70
0183    E6      REFER TO CM(1) SUBROUTINE FOR COMMENTS
0184    6A
0185    AF
0186    E7
0187    62
0188    80
0189    E6
018A    6A
018B    FE
018C    33
018D    96
018E    F6
018F    BF
0190    79
0191    D3
0192    08
0193    0A
0194    30
0195    9C
0196    F6
0197    BF
0198    79
0199    D4
019A    08
019B    0A
019C    E7
019D    62
019E    04
019F    D0
*****END DATA INPUT FOR CM(4)*****
*****BEGIN DATA INPUT FOR CM(5)*****
01A0    E7
01A1    62
01A2    90
01A3    E6      REFER TO CM(1) SUBROUTINE FOR COMMENTS
01A4    6A
01A5    AF
01A6    E7
01A7    62
01A8    A0

```

```

01A9      E6
01AA      6A
01AB      FE
01AC      33
01AD      B6
01AE      F6
01AF      BF
01B0      79
01B1      D3
01B2      08
01B3      0D
01B4      30
01B5      BC
01B6      F6
01B7      BF
01B8      79
01B9      D4
01BA      08
01BB      0D
01BC      E7
01BD      62
01BE      05
01BF      D0
*****END DATA INPUT FOR CM(5)*****
*****BEGIN DATA INPUT FOR CM(6)*****
01C0      E7
01C1      62
01C2      B0
01C3      E6
01C4      6A      REFER TO CM(1) SUBROUTINE FOR COMMENTS
01C5      AF
01C6      E7
01C7      62
01C8      C0
01C9      E6
01CA      6A
01CB      FE
01CC      33
01CD      D6
01CE      F6
01CF      BF
01D0      79
01D1      D3
01D2      08
01D3      10
01D4      30
01D5      DC
01D6      F6
01D7      BF
01D8      79
01D9      D4
01DA      08
01DB      10
01DC      E7

```

01DD 62
 01DE 06
 01DF D0

*****END DATA INPUT FOR CM(6)*****

NOTE: LINES 01E0- 01FF CONTAIN C4 (NO-OP) INSTRUCTION

*****BEGIN DIVISION SUBROUTINE*****

NOTE: THIS SUBROUTINE WILL DIVIDE POSITIVE AND NEGATIVE NUMBERS. POSITIVE NUMBERS ARE DIVIDED BY SUCCESSIVE SUBTRACTIONS AND NEGATIVE BY SUCCESSIVE ADDITIONS.

0200	70	RETURN	RETURN TO CALLING LOCATION
0201	8F	R(F).0 -> D	PUT EVENT COUNTER IN D
0202	3A	IF D .NE. 0 THEN GOTO 020A	
0203	0A		
0205	7F		LINES 0202-0207 CHECK FOR
0204	F8	7F -> D	DIVIDE BY ZERO, IF TRUE A LARGE
0206	AD	D -> R(D).1	VALUE IS PUT IN THE RESULT
0207	BD	D -> R(D).0	
0208	30	GOTO 0231	GOTO THE SUBROUTINE
0209	31		RETURN SET-UP
020A	E2	X -> R(2)	R(2) IS MEM POINTER
020B	9E	R(E).1 -> D	
020C	FE	MSB -> DF	
020D	33	IF DF=1 THEN GOTO 0221	DIVIDE A NEG. NO.
020E	21		
020F	8E	R(E).0 -> D	
0210	73	D -> M(R(2)), R(2)-1	
0211	9E	R(E).1 -> D	
0212	52	D -> M(R(2))	LINES 020F-021E
0213	60	R(2)+1	DIVIDE A POS. NO.
0214	1D	R(D)+1	
0215	8F	R(F).0 -> D	
0216	F5	M(R(2))-D -> D, DF	
0217	73	D -> M(R(2)), R(2)-1	
0218	9F	R(F).1 -> D	
0219	75	M(R(2))-D-(NOT DF) -> D, DF	
021A	52	D -> M(R(2))	
021B	60	R(2)+1	
021C	FE	MSB -> DF	
021D	3B	IF DF=0 THEN GOTO 0214	REPEAT UNTIL SIGN
021E	14		CHANGES
021F	30	GOTO 0231	
0220	31		
0221	8E	R(E).0 -> D	
0222	73	D -> M(R(2)), R(2)-1	
0223	9E	R(E).1 -> D	
0224	52	D -> M(R(2))	LINES 0221-0230 DIVIDE
0225	60	R(2)+1	A NEGATIVE NUMBER
0226	2D	R(D)-1	
0227	8F	R(F).0 -> D	
0228	F4	M(R(2))+D -> D, DF	

0229	73	D -> M(R(2)), R(2)-1	
022A	9F	R(F).1 -> D	
022B	74	M(R(2))+D+DF -> D, DF	
022C	52	D -> M(R(2))	
022D	60	R(2)+1	
022E	FE	MSB -> DF	
022F	33	IF DF=1 THEN GOTO 0226	REPEAT UNTIL SIGN
0230	26		CHANGES

LINES 0231-0233 SET UP
 THE RETURN TO THE CALLING
 LOCATION

0231	E2	X -> R(2)	R(2) IS MEM POINTER
0232	60	R(2)+1	
0233	30	GOTO 0200	GOTO THE RETURN
0234	00		INSTRUCTION

```

c          program curvel
c
c          programmed by:
c                      Dennis L. Lundberg
c
c          Program to convert raw current meter data to current velocity
c          for each of 6 current meters. The data is then edited for
c          wild points and for spikes caused by a reversal in direction
c          during a 1 second sampling period. The data are then passed
c          through a low pass filter and stored on disk for further analysis.
c
c
c          real cv(1000,6),raw(1000,6),rev(2,6),fwd(2,6)
c          real ave,y2,co,f0,c1,a(41),c(41),c2
c          integer n,i,j,r(1000,6),k,m,q,f
c          character*10, infil,outfil
c          character*4, pre
c          character*1,ans
c          data (fwd(1,i),i=1,6)/.107,.087,.124,.116,.098,.098/
c          data (fwd(2,i),i=1,6)/.03,0.0,.06,.02,.03,.03/
c          data (rev(1,i),i=1,6)/.097,.089,.104,.113,.086,.086/
c          data (rev(2,i),i=1,6)/.05,0.0,.06,.02,.02,.02/
c          data pi/3.1415927/
c          f=0
c          write(6,*) 'enter the input filename'
c          read(5,'(a9)') infil
c          open(1,file=infil,status='old')
c
c          reading the input file
c
c          do 100 i=1,1000
c              read(1,fmt=102,end=101) (r(i,j),j=1,6)
100      continue
101      n=i-1
c          close(1)
102      format (2x,6(i6,2x))
c          write(6,*) 'no. of data pts.=',n
c          do 103 i=1,n
c              write(6,104) (r(i,j),j=1,6)
c 103      continue
c 104      format(2x,6(i6))
c          convert integer data to real data
c
c          do 110 i=1,n
c              do 110 j=1,6
c                  raw(i,j)=real(r(i,j))
110      continue
c
c          transform raw data to current velocity
c
c 111      continue
c          do 120 i=1,n
c              do 120 j=1,6

```

```

        if (abs(raw(i,j)) .gt. 4096.) then
            cv(i,j)=0.0
        else if (raw(i,j) .lt. 0.0) then
            y2=abs(1/raw(i,j))
            cv(i,j)=-1.*(4.*(y2/fwd(1,j))+fwd(2,j))
        else if (raw(i,j) .gt. 0.0) then
            y2=1/raw(i,j)
            cv(i,j)=4*(y2/rev(1,j))+rev(2,j)
        endif
120    continue
c
c    end of the section to convert raw data to velocity
c
c    begin the routine to remove wild points
c
        co=3.
c    cut-off velocity is 3 m/sec for pass 1
c    pass 1 removes obvious wild points and replaces them with
c    the average of the two adjacent points.
        do 130 i=2,n-1
            do 130 j=1,6
                ave=(cv(i-1,j)+cv(i+1,j))/2.
                if(abs(cv(i,j)) .ge. co) then
                    cv(i,j)=ave
                endif
130    continue
c
c    pass 2 looks for more subtle errors assoc. with a change in
c    direction during the 1 sec sampling interval. if it finds a
c    value greater >= 20 cm/sec and the adjacent points have opp.
c    signs, then it is replaced by the ave of the two adjacent
c    points.
        do 135 i=2,n-1
            do 135 j=1,6
                ave=(cv(i-1,j)+cv(i+1,j))/2.
                if (abs(cv(i,j)) .lt. .2) then
                    goto 135
                else if (cv(i-1,j) .le. 0.0 .and. cv(i+1,j) .ge. 0.0) then
                    cv(i,j)=ave
                else if (cv(i-1,j) .ge. 0.0 .and. cv(i+1,j) .le. 0.0) then
                    cv(i,j)=ave
                endif
135    continue
c
c    end of the editing for wild point routine
c
c    convert from m/sec to cm/sec
c
        do 140 i=1,n
            do 140 j=1,6
                cv(i,j)=100.*cv(i,j)
140    continue
c

```

```

c      write(6,*) 'do you want to filter the data (y/n)'
c      read(5,*) ans
c      if(ans .eq. 'n') then
c          goto 145
c      endif
c  this section calculates the weights for a low pass filter
c  and passes the data through the filter
      f=1
c      write(6,*) 'how many weights for the filter (odd)?'
c      read(5,*) m
      m=25
      f0=.45
      c1=2.*pi*f0
c  calculate the raw weights
      a(1)=2.*f0
      do 141 i=2,m+1
          c2=real(i)-1.
          a(i)=(sin(c1*c2))/(pi*c2)
141      continue
c  calculate the smoothed weights
      do 142 i=1,m+1
          c2=real(i)
          c(i)=(1-abs(c2)/(m+1))*a(i)
142      continue
c
c  now pass the data through the filter
      q=n-m-1
      do 144 j=1,6
          do 144 i=m+1,q
              cv(i,j)=c(1)*cv(i,j)
              do 143 k=2,m+1
                  cv(i,j)=cv(i,j)+c(k)*(cv(i+k-1,j)+cv(i-k+1,j))
143          continue
144      continue
c
c  write the final transformed data to disk
c
145      if (f .eq. 1) then
          pre='fcur'
          outfil=pre//infil(4:)
      else
          pre='cur'
          m=1
          q=n
          outfil=pre(:3)//infil(4:)
      endif
      open(1,file=outfil,form='formatted',status='new')
      do 150 i=m+1,q
          write(1,1000) (cv(i,j), j=1,6)
150      continue
      close(1)
1000      format(2x,6(f8.3,2x))
      stop
      end

```

```

10  THIS IS A NON-LINEAR CURVE FITTING PROGRAM DESIGNED TO
20  FIT THE PENDULUM DATA TO DECAYED SINUSOIDAL OSCILLATION.
30
40  PROGRAMMED BY:
50  DENNIS L. LUNDBERG
60
70  LAST UPDATE: 30APR86
80
90
100 OPTION BASE 1
110 DIM TIM(1000),TADC(1000),YFIT(1000),A(2),DELTA(2)
120 DIM PEAKS(200),TPEAK(200),PFIT(1000)
130
140 TIM ----- ARRAY FOR THE TIME
150 TADC ----- ARRAY OF ANGULAR POSITION
160 YFIT ----- FITTED DATA
170 PEAKS ----- ARRAY OF THE PEAKS OF THE DATA
180 C ----- NUMBER OF PEAKS FOUND
190 PFIT ----- FITTED PEAK DATA
200 TPEAK ----- TIME OF EACH PEAK
210 A ----- THE PARAMETERS TO BE FIT
220      ELEMENT #1 IS THE DECAY CONSTANT
230      ELEMENT #2 IS THE PERIOD IN SECONDS
240 DELTA ----- AMOUNT EACH PARAMETER IS INCREMENTED
250 NTERMS ----- NUMBER OF TERMS OR PARAMETERS TO FIT
260 AMAX ----- MAXIMUM ANGLE i.e. THE STARTING ANGLE
270 FSUMSQ ----- SUMS OF THE SQUARE OF THE DEVIATIONS
280 NPTS ----- NUMBER OF DATA POINTS IN THE TADC ARRAY
290 TCHOP ----- TIME CORRECTION TO THE TO C.M. DATA TO COMPENSATE
300      FOR THE DATA 'CHOPPED' FROM THE ADC DATA
310
320 NPTS=0
330 M$="D700"
340 GOSUB Read_data ! SUBROUTINE TO READ ANGULAR POSITION DATA FROM DISK
350 AMAX=TADC(1)
360 NTERMS=2
370 GOSUB Peak_seek
380 DISP "ENTER THE START-UP VALUE FOR THE DECAY CONSTANT"
390 INPUT A(1)
400 DISP "ENTER THE START-UP VALUE FOR THE PERIOD"
410 INPUT A(2)
420 DELTA(1)=.001
430 DELTA(2)=.02
440 FOR Q=1 TO NTERMS
450   GOSUB Fit
460 NEXT Q
470 ! THE FOLLOWING LOOP GENERATES THE FINAL DECAY CURVE DATA
480 U=NPTS
490 GOSUB Fit_dat
500 DISP
510 DISP
520 GOSUB Sum_Sq
530 DISP
540 DISP
550 DISP
560 DISP "THE FINAL VALUES ARE:"
570 DISP "      DECAY CONSTANT      ";A(1)
580 DISP "      PERIOD              ";A(2)
590 DISP "THE SUM OF THE SQUARE OF THE DEVIATIONS IS:";FSUMSQ
600 L=LEN (M$)
610 E$=M$(L-2,L)
620 A$="CONST"
630 FLE$=A$&E$&M$
640 CREATE FLE$,1,S6
650 ASSIGN# 2 TO FLE$
660 PRINT# 2 : A(1),A(2),CHOP,TCHOP,NPTS,FSUMSQ
670 ASSIGN# 2 TO *
680 END
690 *****

```



```

700 ! *****
710 Read_data: ! *** SUBROUTINE TO READ INPUT DATA AND GENERATE TIME ARRAY ***
720 DISP "INPUTTING DATA FROM DISK"
730 CHOP=0
740 DISP "ENTER THE INPUT DATA FILE NAME"
750 INPUT FILE$
760 ASSIGN# 1 TO FILE$%Msus$
770 READ# 1 ; NPTS@ NPTS=NPTS-6
780 FOR I=1 TO NPTS
790   READ# 1 ; TADC(I)
800   PRINT I,TADC(I)
810 NEXT I
820 ASSIGN# 1 TO *
830 ! A LOOP TO DISPLAY FIRST 50 DATA POINTS FOR CHOPPING
840 TIM(1)=0 @ DT=1/8
850 FOR I=1 TO 50
860   DISP I,TADC(I)
870 NEXT I
880 DISP "DO YOU WANT TO CHOP ANY OF THIS DATA (Y/N)"
890 INPUT ANS$
900 IF ANS$="N" THEN 980
910 DISP "ENTER THE NUMBER OF PIECES TO CHOP"
920 INPUT CHOP
930 NPTS=NPTS-CHOP
940 FOR J=1 TO NPTS
950   TADC(J)=TADC(J+CHOP)
960 NEXT J
970 TCHOP=(CHOP-1)*DT
980 FOR I=2 TO NPTS
990   TIM(I)=TIM(I-1)+DT
1000 NEXT I
1010 RETURN
1020 ! *****
1030 ! *****
1040 Peak_seek: ! SUBROUTINE TO FIND THE PEAKS IN THE PENDULUM DATA
1050 DISP "SEARCHING FOR PEAKS"
1060 TPEAK(1)=TIM(1)
1070 PEAKS(1)=TADC(1)
1080 C=1
1090 FOR I=2 TO NPTS-1
1100   IF NOT (TADC(I)-TADC(I-1)>0 AND TADC(I+1)-TADC(I)<= 0) THEN 1150
1110   IF TADC(I)<0 THEN 1150 ! WANT ONLY 'POSITIVE PEAKS'
1120   IF TADC(I)<1 THEN 1160 ! STOP WHEN MAXIMUM AMPLITUDE LESS THAN 1 DEG
1130   C=C+1
1140   PEAKS(C)=TADC(I) @ TPEAK(C)=TIM(I)
1150 NEXT I
1160 NPTS=I ! SET UPPER LIMIT OF DATA ANALYZED
1170 PRINTER IS 701
1180 FOR J=1 TO C
1190   PRINT TPEAK(J),PEAKS(J)
1200 NEXT J
1210 PRINTER IS 1
1220 DISP "PRESS THE 'CONT' BUTTON TO CONTINUE"
1230 PAUSE
1240 RETURN
1250 ! *****

```

```

1260 ! *****164
1270 Sum_Sq: SUBROUTINE TO GENERATE THE SUMS OF THE SQUARES OF THE DEV.
1280 FSUMSQ=0
1290 IF Q=1 THEN 1340
1300 FOR S=1 TO U
1310 FSUMSQ=FSUMSQ+(TACC(S)-YFIT(S))^2
1320 NEXT S
1330 GOTO 1370
1340 FOR S=1 TO U
1350 FSUMSQ=FSUMSQ+(PEAKS(S)-PFIT(S))^2
1360 NEXT S
1370 RETURN
1380 ! *****
1390 ! *****
1400 Fit: SUBROUTINE TO FIT THE DATA
1410 DISP "ENTERING THE FITTING SUBROUTINE"
1420 DISP "FITTING TERM NO.:";Q
1430 SSD1=0 @ SSD2=0 @ SSD3=0
1440 IF Q=1 THEN U=C ELSE U=NPTS
1450 IF Q=1 THEN GOSUB Decay ELSE GOSUB Fit_dat
1460 GOSUB Sum_Sq
1470 SSD1=FSUMSQ
1480 DEL=DELTA(Q)
1490 A(Q)=A(Q)+DEL
1500 IF Q=1 THEN GOSUB Decay ELSE GOSUB Fit_dat
1510 GOSUB Sum_Sq
1520 SSD2=FSUMSQ
1530 DIF=SSD1-SSD2
1540 IF DIF=0 THEN 1490
1550 IF DIF>0 THEN 1610
1560 DISP "REVERSING DIRECTION"
1570 DEL=-DEL
1580 A(Q)=A(Q)+DEL
1590 IF Q=1 THEN GOSUB Decay ELSE GOSUB Fit_dat
1600 SAV=SSD1 @ SSD1=SSD2 @ SSD2=SAV
1610 A(Q)=A(Q)+DEL
1620 IF Q=1 THEN GOSUB Decay ELSE GOSUB Fit_dat
1630 GOSUB Sum_Sq
1640 SSD3=FSUMSQ
1650 IF SSD2-SSD3<0 THEN 1670
1660 SSD1=SSD2 @ SSD2=SSD3 @ GOTO 1610
1670 ! THE NEXT LINE IS A PARABOLIC INTERPOLATION
1680 DEL=DEL*(1/(1+(SSD1-SSD2)/(SSD3-SSD2))+.5)
1690 A(Q)=A(Q)-DEL
1700 RETURN
1710 ! *****
1720 ! *****
1730 Decay: SUBROUTINE TO GENERATE ESTIMATED DECAY CURVE DATA
1740 FOR F=1 TO U
1750 PFIT(F)=AMAX/(1+AMAX*TPEAK(F)*A(1))
1760 NEXT F
1770 RETURN
1780 ! *****
1790 ! *****
1800 Fit_dat: SUBROUTINE TO GENERATE ESTIMATED DAMPED PENDULUM DATA
1810 W=2*PI/A(2)
1820 FOR F=1 TO U
1830 YFIT(F)=AMAX*CCS (W*TIM(F))/(1+AMAX*TIM(F)*A(1))
1840 NEXT F
1850 RETURN

```

```

10 :      THIS PROGRAM IS DESIGNED TO CALCULATE THE GAIN AND PHASE LAG
20 :      OF THE DUCTED IMPELLOR CURRENT METERS
30 :
40 :      DATE LAST MODIFIED:
50 :      28JUN85
60 :
70 :      PROGRAM NAME:
80 :      CALIB
90 :
100 :
110 OPTION BASE 1
120 DEG
130 DIM ET(1000),RT(1000),FU(300),BU(300),VF(100),VB(100),TADC(1000),TME(1000)
140 DIM PO(100),CO(100),DEL(100),MAXAMP(100)
150 INTEGER FCM(250),BCM(250)
160 DT=1/8
170 C=1 @ C1=1 @ C2=1 @ PNPTS=1
180 ! C --- COUNTER FOR THE NUMBER OF CURRENT METER DATA POINTS
190 ! C1 -- COUNTER FOR THE NUMBER OF ZERO CROSSINGS IN THE CURRENT METER DATA
200 ! C2 -- COUNTER FOR THE NUMBER OF ZERO CROSSINGS IN THE PENDULUM DATA
210 MSUS$=":D700"
220 DISP "ENTER THE FILE NAME FOR THE CM DATA (NAME:D70_)"
230 INPUT CFILE$
240 ASSIGN# 1 TO CFILE$
250 ON ERROR GOTO 320
260 READ# 1 ; R,E
270 IF R=0 THEN 260
280 RT(C)=R/64.002
290 ET(C)=E
300 C=C+1
310 GOTO 260
320 IF ERRN <> 72 THEN DISP ERRN ,ERRL
330 OFF ERROR
340 C=C-1
350 DISP "THERE ARE";C;"DATA POINTS"
360 DISP "ENTER THE FILE NAME FOR THE ADC DATA (EG TC1A0:D701)"
370 INPUT ADC$
380 E$=ADC$(3,5)
390 L=LEN (ADC$) @ MS$=ADC$(L-4,L)
400 FLE$="CONST"&E$&MS$
410 ASSIGN# 2 TO FLE$
420 READ# 2 ; A(1),A(2),CHOP,TCHOP
430 ASSIGN# 2 TO *
440 ASSIGN# 3 TO ADC$
450 ON ERROR GOTO 490
460 READ# 3 ; TADC(PNPTS)
470 PNPTS=PNPTS+1
480 GOTO 460
490 IF ERRN <> 72 THEN DISP ERRN ,ERRL @ PAUSE
500 PNPTS=PNPTS-1
510 OFF ERROR

```

```

10 :      THIS PROGRAM IS DESIGNED TO CALCULATE THE GAIN AND PHASE LAG
20 :      OF THE DUCTED IMPELLOR CURRENT METERS
30 :
40 :      DATE LAST MODIFIED:
50 :      28JUN85
60 :
70 :      PROGRAM NAME:
80 :      CALIB
90 :
100 :
110 OPTION BASE 1
120 DEG
130 DIM ET(1000),RT(1000),FU(300),BU(300),VF(100),VB(100),TADC(1000),TME(1000)
140 DIM PO(100),CO(100),DEL(100),MAXAMP(100)
150 INTEGER FCM(250),BCM(250)
160 DT=1/8
170 C=1 @ C1=1 @ C2=1 @ PNPTS=1
180 ! C --- COUNTER FOR THE NUMBER OF CURRENT METER DATA POINTS
190 ! C1 -- COUNTER FOR THE NUMBER OF ZERO CROSSINGS IN THE CURRENT METER DATA
200 ! C2 -- COUNTER FOR THE NUMBER OF ZERO CROSSINGS IN THE PENDULUM DATA
210 M$us$="D700"
220 DISP "ENTER THE FILE NAME FOR THE CM DATA (NAME:D70_)"
230 INPUT CFILE$
240 ASSIGN# 1 TO CFILE$
250 ON ERROR GOTO 320
260 READ# 1 ; R,E
270 IF R=0 THEN 260
280 RT(C)=R/64.002
290 ET(C)=E
300 C=C+1
310 GOTO 260
320 IF ERRN <> 72 THEN DISP ERRN ,ERRL
330 OFF ERROR
340 C=C-1
350 DISP "THERE ARE";C;"DATA POINTS"
360 DISP "ENTER THE FILE NAME FOR THE ADC DATA (EG TC1A0:D701)"
370 INPUT ADC$
380 E$=ADC$(3,5)
390 L=LEN(ADC$) @ MS$=ADC$(L-4,L)
400 FLE$="CONST"&E$&MS$
410 ASSIGN# 2 TO FLE$
420 READ# 2 ; A(1),A(2),CHOP,TCHOP
430 ASSIGN# 2 TO *
440 ASSIGN# 3 TO ADC$
450 ON ERROR GOTO 490
460 READ# 3 ; TADC(PNPTS)
470 PNPTS=PNPTS+1
480 GOTO 460
490 IF ERRN <> 72 THEN DISP ERRN ,ERRL @ PAUSE
500 PNPTS=PNPTS-1
510 OFF ERROR

```

```

520 FNPTS=FNPTS-CHOP
530 FOR J=1 TO FNPTS
540   TADC(J)=TADC(J+CHOP)
550 NEXT J
560 TME(1)=0
570 FOR I=2 TO FNPTS
580   TME(I)=TME(I-1)+DT
590 NEXT I
600 ASSIGN# 3 TO *
610 FOR I=1 TO C -
620   RT(I)=RT(I)-TCHOP
630 NEXT I
640 DISP "ENTER THE TITLE FOR THE GRAPHICS"
650 INPUT TITLE$
660 GOSUB Max_cm
670 GOSUB Gain
680 GOSUB Phase
690 GOSUB Plot_G
700 END
710 ! *****
720 ! *****
730 Max_cm: ! SUBROUTINE TO FIND THE MAX CM OUTPUT (ie THE MINIMUM COUNT)
740 !         FOR BOTH THE FORWARD AND BACKWARD MOTIONS.
750 !
760 DISP "SEARCHING FOR PEAKS AND VALLEYS OF C. M. DATA."
770 !
780 FMIN=1 @ BMIN=1
790 FOR I=2 TO C-1
800   MID=ABS (ET(I)) @ BEF=ABS (ET(I-1)) @ AFT=ABS (ET(I+1))
810   IF NOT (MID-BEF<= 0 AND AFT-MID>0) THEN 850
820   IF ET(I)<0 THEN 840
830   FCM(FMIN)=I @ FMIN=FMIN+1 @ GOTO 850
840   BCM(BMIN)=I @ BMIN=BMIN+1
850 NEXT I
860 FMIN=FMIN-1 @ BMIN=BMIN-1
870 PRINTER IS 701
880 PRINT @ PRINT @ PRINT "PEAKS AND VALLEYS;";TITLE$
890 PRINT FMIN
900 FOR I=1 TO FMIN
910   PRINT RT(FCM(I));ET(FCM(I))
920 NEXT I
930 PRINT BMIN
940 FOR J=1 TO BMIN
950   PRINT RT(BCM(J));ET(BCM(J))
960 NEXT J
970 RETURN
980 ! *****
990 ! *****
1000 Gain: ! SUBROUTINE TO CALCULATE THE GAIN OF THE CURRENT METER BY
1010 !        DOING A LINEAR FIT OF THE CM DATA TO THE CALCULATED TRUE
1020 !        VELOCITY.
1030 !
1040 DISP "CALCULATING THE GAIN."
1050 !
1060 L=4.058 ! LENGTH OF THE PENDULUM ARM IN METERS
1070 AMAX=TADC(1)
1080 RA=PI /180
1090 W=2*PI /A(C)
1100 FOR I=1 TO FMIN
1110   T=RT(FCM(I))
1120   FU(I)=L*W*(AMAX/(1+AMAX*T*A(1)))*RA
1130 NEXT I
1140 FOR J=1 TO BMIN
1150   T=RT(BCM(J))
1160   BU(J)=L*W*(AMAX/(1+AMAX*T*A(1)))*RA
1170 NEXT J

```

```

1180
1190 FOR F=1 TO 2
1200 SUM(F)=0 @ SUMX(F)=0 @ SUMY(F)=0 @ SUMX2(F)=0 @ SUMXY(F)=0 @ SUMY2(F)=0
1210 IF F=2 THEN Back
1220 ! FORWARD CALIBRATION
1230 FOR I=1 TO FMIN
1240 VF(I)=1/ET(FCM(I))
1250 SUM(F)=SUM(F)+1
1260 SUMX(F)=SUMX(F)+FU(I)
1270 SUMY(F)=SUMY(F)+VF(I)
1280 SUMX2(F)=SUMX2(F)+FU(I)^2
1290 SUMXY(F)=SUMXY(F)+VF(I)*FU(I)
1300 SUMY2(F)=SUMY2(F)+VF(I)^2
1310 NEXT I
1320 GOTO Coef
1330 Back: ! BACKWARDS CALIBRATION
1340 FOR J=1 TO BMIN
1350 VB(J)=1/ABS(ET(BCM(J)))
1360 SUM(F)=SUM(F)+1
1370 SUMX(F)=SUMX(F)+BU(J)
1380 SUMY(F)=SUMY(F)+VB(J)
1390 SUMX2(F)=SUMX2(F)+BU(J)^2
1400 SUMXY(F)=SUMXY(F)+VB(J)*BU(J)
1410 SUMY2(F)=SUMY2(F)+VB(J)^2
1420 NEXT J
1430 Coef: ! CALCULATION OF THE LINEAR FITTING COEFFICIENTS
1440 DELTA=SUM(F)*SUMX2(F)-SUMX(F)^2
1450 A1(F)=(SUMX2(F)*SUMY(F)-SUMX(F)*SUMXY(F))/DELTA
1460 B(F)=(SUMXY(F)*SUM(F)-SUMX(F)*SUMY(F))/DELTA
1470 IF F=1 THEN DF=FMIN-2 ELSE DF=BMIN-2
1480 VAR=(SUMY2(F)+SUM(F)*A1(F)^2+SUMX2(F)*B(F)^2-2*(A1(F)*SUMY(F)+B(F)*SUMXY(
F)-A1(F)*B(F)*SUMX(F)))/DF
1490 SIGMAA(F)=SQR(VAR*SUMX2(F)/DELTA)
1500 SIGMAB(F)=SQR(VAR*SUM(F)/DELTA)
1510 R(F)=(SUM(F)*SUMXY(F)-SUMX(F)*SUMY(F))/SQR(DELTA*(SUM(F)*SUMY2(F)-SUMY(F)^
2))
1520 NEXT F
1530 RETURN
1540 ! *****
1550 ! *****
1560 Plot_G: ! SUBROUTINE TO PLOT THE FITTED CURVE AND THE DATA FOR THE GAIN
1570 DISP "PRESS THE 'CONT' TO CONTINUE"
1580 PAUSE
1590 GCLEAR
1600 GRAPH
1610 LINE TYPE 1
1620 LOCATE 15,125,10,90
1630 FRAME
1640 SCALE 0,1.2,0,.12
1650 CSIZE 5
1660 PEN 1
1670 AXES .02,.01,0,0,5,3,4
1680 LOG 5
1690 CSIZE 3
1700 FOR X=0 TO 1.2 STEP .1
1710 MOVE X,-.005 @ LABEL X
1720 NEXT X
1730 LOG 4
1740 MOVE .5,-.01
1750 LABEL "VELOCITY AMPLITUDE (M/SEC)"
1760 LOG 8
1770 FOR Y=0 TO .12 STEP .03
1780 MOVE 0,Y @ LABEL Y
1790 NEXT Y
1800 LOIR 90
1810 MOVE -.1,.06

```

```

1820 LONG 4
1830 LABEL '1/COUNT'
1840 LDIR 0
1850 MOVE 0,A1(1)
1860 DRAW FU(1),A1(1)+B(1)*FU(1)
1870 LINE TYPE 4
1880 PEN 2
1890 MOVE 0,A1(2)
1900 DRAW BU(1),A1(2)+B(2)*BU(1)
1910 MOVE 0,0
1920 C$="*" @ L$="+"
1930 CSIZE 2
1940 LONG 5
1950 PEN 1
1960 FOR I=1 TO FMIN
1970   MOVE FU(I),VF(I)
1980   LABEL C$ @ PLOT FU(I),VF(I)
1990 NEXT I
2000 PEN 2
2010 FOR I=1 TO BMIN
2020   MOVE BU(I),VB(I)
2030   LABEL L$ @ PLOT BU(I),VB(I)
2040 NEXT I
2050 LINE TYPE 5
2060 ! PEN 1
2070 ! NA=A1(1)-SIGMAA(1) @ PA=A1(1)+SIGMAA(1)
2080 ! NB=B(1)-SIGMAB(1) @ PB=B(1)+SIGMAB(1)
2090 ! MOVE 0,PA
2100 ! DRAW FU(1),PA+PB*FU(1)
2110 ! MOVE 0,NA
2120 ! DRAW FU(1),NA+NB*FU(1)
2130 ! MOVE 0,0
2140 CSIZE 4
2150 MOVE .7,.03
2160 DRAW .8,.03
2170 MOVE .85,.03
2180 LONG 2 @ PEN 2
2190 LABEL "REVERSE"
2200 LINE TYPE 1 @ PEN 1
2210 MOVE .7,.025 @ DRAW .8,.025
2220 MOVE .85,.025
2230 LABEL "FORWARD"
2240 MOVE .7,.02 @ LABEL "FWD SLOPE :";B(1)
2250 MOVE .7,.015 @ LABEL "REV SLOPE :";B(2)
2260 LONG 5
2270 MOVE .6,.11
2280 LABEL "GAIN "&TITLE$
2290 RETURN
2300 ! *****
2310 ! *****
2320 Phase: ! SUBROUTINE TO CALCULATE AND PLOT THE PHASE LAG OF THE CURRENT
2330 !       METERS
2340 DISP "CALCULATING THE PHASE LAG."
2350 !
2360 FOR I=1 TO FNPTS
2370   IF TADC(I)=0 THEN PO(C2)=TME(I) @ C2=C2+1
2380   A=SGN (TADC(I)) @ B=SGN (TADC(I+1))
2390   IF A=B THEN 2420
2400   DELTA_t=-(1*DT*TADC(I)/(TADC(I+1)-TADC(I)))
2410   PO(C2)=TME(I)+DELTA_t @ C2=C2+1
2420 NEXT I
2430 ! *** THIS LOOP FINDS ZERO CROSSINGS OF THE CURRENT METER DATA ***
2440 ! FOR I=1 TO C
2450 !   ET(I)=1/ET(I)
2460 ! NEXT I
2470 FOR I=1 TO C-1

```

```

2480 A=SGN (ET(I)) @ B=SGN (ET(I+1))
2490 IF A=B THEN 2550
2500 DELE=ET(I+1)-ET(I)
2510 E1=ABS (ET(I+1))/1024*1.5 @ E=ABS (ET(I))/1024*1.5
2520 DELT=RT(I+1)-E1-(RT(I)-E)
2530 DELTA_t=-(1*ET(I)*DELT/DELE)
2540 CO(C1)=RT(I)+DELTA_t
2550 C1=C1+1
2560 NEXT I
2570 IF C1<= C THEN UL=C1 ELSE UL=C
2580 AMAX=TADC(1)
2590 RA=PI /180
2600 W=2*PI /A(2)
2610 FOR I=1 TO UL-1
2620 T=CO(I)
2630 DEL(I)=T-PO(I)-A(2)/4
2640 MAXAMP(I)=L*W*(AMAX/(1+AMAX*PO(I)*A(1)))*RA
2650 NEXT I
2660 PRINT @ PRINT @ PRINT "PHASE LAG FOR";TITLE$
2670 PRINT "PENDULUM","CM","LAG"
2680 FOR K=1 TO UL-1
2690 PRINT PO(K),CO(K),DEL(K)
2700 NEXT K
2710 GCLEAR
2720 GRAPH
2730 LOCATE 15,125,10,90
2740 PEN 1
2750 FRAME
2760 SCALE 0,1.2,0,1
2770 AXES .02,.01,0,0,5,5,4
2780 LORG 5
2790 CSIZE 3
2800 FOR X=0 TO 1.2 STEP .1
2810 MOVE X,-.05 @ LABEL X
2820 NEXT X
2830 LORG 6
2840 MOVE .6,-.1
2850 LABEL "VELOCITY AMPLITUDE (M/SEC)"
2860 LORG 8
2870 FOR Y=0 TO 1 STEP .1
2880 MOVE 0,Y @ LABEL Y
2890 NEXT Y
2900 MOVE -.05,.5
2910 LDIR 90
2920 LORG 4
2930 LABEL "SEC"
2940 LDIR 0
2950 CSIZE 4
2960 C$="*"
2970 LORG 5
2980 FOR I=1 TO UL
2990 IF PO(I)>60 THEN 3030
3000 MOVE MAXAMP(I),DEL(I)
3010 LABEL C$
3020 NEXT I
3030 CSIZE 4
3040 MOVE .6,.7 @ LABEL "PHASE LAG "&TITLE$
3050 MOVE 1,.05
3060 RETURN
3070 ! *****
3080 ! *****

```



```

10 ! THIS IS THE MODIFIED DUMP PROGRAM FOR THE CALIBRATION DATA
20 ! MODIFIED: 03MAY85
30 !
40 OPTION BASE 1
50 DIM ADC(2000),RT(3000),ET(3000),ETime(1000),RTime(1000)
60 C=0 @ C1=0 @ C2=0
70 CONTROL 4,4 ; 0
80 CONTROL 4,3 ; 1
90 DISP "TO BEGIN THE DATA DUMP TYPE 'CONT'"
100 DISP "AND PRESS 'END LINE' KEY"
110 PAUSE
120 C=C+1
130 IF C1=5 THEN 210
140 ENTER 4 USING "#,B" ; ADC(C)
150 ! DISP C,ADC(C),DTH$ (ADC(C))
160 IF ADC(C)=255 THEN C1=C1+1
170 GOTO 120
180 !
190 ! BEGIN THE LOOP TO ENTER THE TIME DATA
200 !
210 C2=C2+1
220 ENTER 4 USING "#,B" ; LB
230 ENTER 4 USING "#,B" ; UB
240 IF LB=255 AND UB=255 THEN 315
250 LB$=DTH$ (LB) @ UB$=DTH$ (UB) @ B$=UB$(3,4)&LB$(3,4)
260 RT(C2)=HTD (B$)
270 ENTER 4 USING "#,B" ; EL
280 ENTER 4 USING "#,B" ; EU
290 EL$=DTH$ (EL) @ EU$=DTH$ (EU) @ C$=EU$(3,4)&EL$(3,4)
300 ET(C2)=HTD (C$)
310 GOTO 210
315 IMAGE 3X,DDD.DDD,4X,MDDDD.D,12X,5D
316 PRINT " Time(sec.) Event Time(msec) Event Time(counts)"
320 FOR I=1 TO C2-1
330 RTIME(I)=RT(I)/64.002
340 IF ET(I)>= 0 THEN 360
350 ET(I)=ABS (ET(I))-32768
360 ETime(I)=ET(I)/1024.032
370 PRINT USING 315 ; RTime(I),ETime(I)*1000,ET(I)
380 NEXT I
385 IMAGE 3X,3D,4X,3D,4X,3D,4X,3D
390 FOR J=1 TO C-1 STEP 4
400 PRINT USING 385 ; ADC(J),ADC(J+1),ADC(J+2),ADC(J+3)
410 NEXT J
430 DISP "DO YOU WANT TO STORE THIS DATA ON DISK (Y/N)"
440 INPUT ANS$
450 IF ANS$="N" THEN 620
460 DISP "ENTER THE FILE NAME FOR THE ADC DATA"
470 INPUT ADC$
480 DISP "ENTER THE FILE NAME FOR THE TIME DATA"
490 INPUT DAT$
500 DISP "WHAT DISK DRIVE DO YOU WANT TO USE"
510 INPUT M$US$
520 CREATE ADC$&M$US$,1,8*C
530 CREATE DAT$&M$US$,1,16*C2
540 ASSIGN# 1 TO ADC$&M$US$
550 ASSIGN# 2 TO DAT$&M$US$
560 FOR I=1 TO C-1
570 PRINT# 1 ; ADC(I)
580 NEXT I
585 ASSIGN# 1 TO *
590 FOR I=1 TO C2-1
600 PRINT# 2 ; RT(I),ET(I)
610 NEXT I
615 ASSIGN# 2 TO *
620 END

```

AUTOBIOGRAPHICAL STATEMENT

Dennis L. Lundberg

Born:

June 22, 1949. Ludington, Michigan

Education:

B.S. December 1972, The University of Michigan

Honors:

Phi Kappa Phi, 1984

Appointments and Positions:

U.S. Navy. Commissioned as Ensign in December, 1972, resigned as Lieutenant in March, 1976.

Old Dominion University. Teaching/Research Assistant. 1978-1980.

Planning Systems Inc. Senior Scientist. November, 1980 to May, 1983.

Old Dominion University. Teaching/Research Assistant 1983-1985.

U.S. Navy Reserve. Staff Oceanographer. January, 1978-Present.

Professional Membership:

American Geophysical Union